



NAVAL POSTGRADUATE SCHOOL

MONTEREY, CALIFORNIA

THESIS

**DIRECT OBSERVATION OF TWO PHASE FLOW
GENERATED BY AN ALUMINA SEEDED GRAIN IN
HIGH ASPECT RATIO CHANNELS**

by

Keith B. Fahlenkamp

June 2010

Thesis Advisor:
Second Reader:

Christopher Brophy
Anthony Gannon

Approved for public release; distribution is unlimited

THIS PAGE INTENTIONALLY LEFT BLANK

REPORT DOCUMENTATION PAGE			<i>Form Approved OMB No. 0704-0188</i>	
Public reporting burden for this collection of information is estimated to average 1 hour per response, including the time for reviewing instruction, searching existing data sources, gathering and maintaining the data needed, and completing and reviewing the collection of information. Send comments regarding this burden estimate or any other aspect of this collection of information, including suggestions for reducing this burden, to Washington headquarters Services, Directorate for Information Operations and Reports, 1215 Jefferson Davis Highway, Suite 1204, Arlington, VA 22202-4302, and to the Office of Management and Budget, Paperwork Reduction Project (0704-0188) Washington DC 20503.				
1. AGENCY USE ONLY (Leave blank)		2. REPORT DATE June 2010	3. REPORT TYPE AND DATES COVERED Master's Thesis	
4. TITLE AND SUBTITLE Direct Observation of Two Phase Flow Generated by an Alumina Seeded Grain in High Aspect Ratio Channels			5. FUNDING NUMBERS	
6. AUTHOR Keith B. Fahlenkamp				
7. PERFORMING ORGANIZATION NAME(S) AND ADDRESS(ES) Naval Postgraduate School Monterey, CA 93943-5000			8. PERFORMING ORGANIZATION REPORT NUMBER	
9. SPONSORING /MONITORING AGENCY NAME(S) AND ADDRESS(ES) ATK Thiokol			10. SPONSORING/MONITORING AGENCY REPORT NUMBER	
11. SUPPLEMENTARY NOTES The views expressed in this thesis are those of the author and do not reflect the official policy or position of the Department of Defense or the U.S. Government. IRB Protocol number ____N/A____.				
12a. DISTRIBUTION / AVAILABILITY STATEMENT Approved for public release; distribution is unlimited			12b. DISTRIBUTION CODE A	
13. ABSTRACT (maximum 200 words) Adding appropriate amounts of aluminum to solid rocket propellant improves energy performance by increasing both the specific impulse and propellant energy density. However, as the propellant combusts, the aluminum is oxidized into alumina (Al ₂ O ₃) which tends to agglomerate into relatively large molten droplets under the right flow conditions, and may cause significant two-phase flow losses, potentially catastrophic nozzle erosion, and a potentially increased burn rate as a result of erosive burning. Significant research has been conducted regarding agglomerate formation at the propellant surface and agglomerate impact on nozzle erosion, but little is known about agglomerate behavior within high aspect ratio regions of advanced propellant grain designs and how this behavior affects flow through the combustion chamber and impacts erosive burning. An experiment was designed to image agglomerate behavior within these regions. The experimental method was validated using an inert calibration grain containing known alumina particulates. The primary goal of this thesis was to establish a working experimental setup and method that can be used to evaluate agglomerate flow for actual propellant samples.				
14. SUBJECT TERMS Solid Rocket Propellant, Two Phase Flow, Erosive Burning, Alumina Agglomeration, Laser Imaging			15. NUMBER OF PAGES 109	
			16. PRICE CODE	
17. SECURITY CLASSIFICATION OF REPORT Unclassified	18. SECURITY CLASSIFICATION OF THIS PAGE Unclassified	19. SECURITY CLASSIFICATION OF ABSTRACT Unclassified	20. LIMITATION OF ABSTRACT UU	

NSN 7540-01-280-5500

Standard Form 298 (Rev. 2-89)
Prescribed by ANSI Std. Z39-18

THIS PAGE INTENTIONALLY LEFT BLANK

Approved for public release; distribution is unlimited

**DIRECT OBSERVATION OF TWO PHASE FLOW GENERATED BY AN
ALUMINA SEEDED GRAIN IN HIGH ASPECT RATIO CHANNELS**

Keith B. Fahlenkamp
Lieutenant Commander, United States Navy
B.S., Washington State University, 1999

Submitted in partial fulfillment of the
requirements for the degrees of

**MECHANICAL ENGINEER
and
MASTERS OF SCIENCE IN MECHANICAL ENGINEERING**

from the

**NAVAL POSTGRADUATE SCHOOL
June 2010**

Author: Keith B. Fahlenkamp

Approved by: Dr. Christopher Brophy
Thesis Advisor

Dr. Anthony Gannon
Second Reader

Dr. Knox Milsaps
Chairman, Department of Mechanical and Aerospace Engineering

THIS PAGE INTENTIONALLY LEFT BLANK

ABSTRACT

Adding appropriate amounts of aluminum to solid rocket propellant improves energy performance by increasing both the specific impulse and propellant energy density. However, as the propellant combusts, the aluminum is oxidized into alumina (Al_2O_3) which tends to agglomerate into relatively large molten droplets under the right flow conditions, and may cause significant two-phase flow losses, potentially catastrophic nozzle erosion, and a potentially increased burn rate as a result of erosive burning. Significant research has been conducted regarding agglomerate formation at the propellant surface and agglomerate impact on nozzle erosion, but little is known about agglomerate behavior within high aspect ratio regions of advanced propellant grain designs and how this behavior affects flow through the combustion chamber and impacts erosive burning. An experiment was designed to image agglomerate behavior within these regions. The experimental method was validated using an inert calibration grain containing known alumina particulates. The primary goal of this thesis was to establish a working experimental setup and method that can be used to evaluate agglomerate flow for actual propellant samples.

THIS PAGE INTENTIONALLY LEFT BLANK

TABLE OF CONTENTS

I.	INTRODUCTION.....	1
II.	BACKGROUND	5
A.	ALUMINA CHARACTERISTICS	5
1.	Melting Point and Boiling Point	5
2.	Surface Tension.....	5
B.	PROPELLANT CHARACTERISTICS	8
III.	EXPERIMENTAL SETUP	11
A.	EXPERIMENTAL DESIGN.....	11
1.	Laser.....	12
2.	Camera.....	13
a.	<i>Camera Calibration.....</i>	<i>14</i>
3.	Ignition Torch.....	15
4.	Gas Generator	15
a.	<i>Calibration Propellant Mixing</i>	<i>16</i>
5.	2-D Slab Burner	17
a.	<i>Slab Burner Propellant Housing.....</i>	<i>20</i>
b.	<i>Slab Burner Cap.....</i>	<i>25</i>
c.	<i>Slab Burner Nozzle</i>	<i>26</i>
d.	<i>Slab Burner View Window Assembly.....</i>	<i>27</i>
6.	Test Cell Setup.....	29
a.	<i>Gas Header.....</i>	<i>30</i>
b.	<i>Valve Board.....</i>	<i>31</i>
7	Control Software.....	32
IV.	ANALYSIS AND RESULTS	35
A.	ANALYTICAL PROJECTIONS	35
1.	Weber Number Calculations	35
a.	<i>Gas Velocity (u_g).....</i>	<i>36</i>
b.	<i>Agglomerate Diameter (d_{ag}).....</i>	<i>38</i>
c.	<i>Agglomerate Velocity (u_{ag}).....</i>	<i>39</i>
2.	Weber Number Results	40
a.	<i>Agglomerates Forming in Region A</i>	<i>41</i>
b.	<i>Agglomerates Forming in Region B</i>	<i>42</i>
c.	<i>Agglomerates Forming in Region C</i>	<i>42</i>
B.	RESULTS	43
V.	SUMMARY AND CONCLUSIONS	45
APPENDIX A:	STANDARD OPERATING PROCEDURE.....	47
APPENDIX B:	ENGINEERING DRAWINGS	51
APPENDIX C:	LABVIEW SOFTWARE CODE.....	77

A.	ER 3000 CONTROL.....	77
1.	Block Diagram.....	77
2.	ER 3000 Control.vi Explanation.....	78
B.	VALVE CONTROL	80
1.	Block Diagram.....	80
2.	Valve Control.vi Explanation	81
APPENDIX D: TEST CELL PHOTOGRAPHS		83
LIST OF REFERENCES		87
INITIAL DISTRIBUTION LIST		89

LIST OF FIGURES

Figure 1.	Effect of Aluminum Addition on Specific Impulse (I_{sp})	2
Figure 2.	Depiction of Narrow Passages in 8-Point Hybrid Star / Finocyl Grain Configurations.....	3
Figure 3.	Alumina Surface Tension for Three Temperature Variability Estimates	7
Figure 4.	Overall Setup	11
Figure 5.	Flat Burner Assembly with Data Acquisition.....	12
Figure 6.	Camera Calibration Sequence.....	14
Figure 7.	Inert Propellant Mixing.....	16
Figure 8.	2-D Slab Burner Assembly	17
Figure 9.	Slab Burner Propellant Housing	20
Figure 10.	Average von Mises Stress with 6.9 MPa (1000 psia) internal pressure.....	21
Figure 11.	Transient Thermal Analysis of Slab Burner Propellant Housing	24
Figure 12.	Slab Burner Cap.....	25
Figure 13.	Slab Burner Nozzle	26
Figure 14.	Window Holder.....	27
Figure 15.	Inert Gas Distribution Ring.....	28
Figure 16.	Viewing Assembly Detail	29
Figure 17.	Outside Gas Header	30
Figure 18.	Universal Test Cell Gas Supply Design.....	31
Figure 19.	Photograph of Common Valve Board.....	32
Figure 20.	ER 3000 Control Virtual Instrument Front Panel	33
Figure 21.	Valve Control Virtual Instrument Front Panel.....	34
Figure 22.	Flat Burner Bottom with Propellant Strands.....	36
Figure 23.	Detail of Propellant Region in Flat Burner Showing Decrease in Mass Flux with Burn Time.....	36
Figure 24.	Regional Flat Burner Combustion Gas Velocities vs. Time.....	37
Figure 25.	Combustion Surface Agglomerate Size Distribution [From 8]	38
Figure 26.	Weber Number vs. Velocity Difference for Various Agglomerate Diameters	40
Figure 27.	Maximum Weber Number Variability.....	41
Figure 28.	Calibration Grain Photographs	44
Figure 29.	Flat Burner Bottom Sheet 1 of 6.....	51
Figure 30.	Flat Burner Bottom Sheet 2 of 6.....	52
Figure 31.	Flat Burner Bottom Sheet 3 of 6.....	53
Figure 32.	Flat Burner Bottom Sheet 4 of 6.....	54
Figure 33.	Flat Burner Bottom Sheet 5 of 6.....	55
Figure 34.	Flat Burner Bottom Sheet 6 of 6.....	56
Figure 35.	Flat Burner Top Sheet 1 of 5.....	57
Figure 36.	Flat Burner Top Sheet 2 of 5.....	58
Figure 37.	Flat Burner Top Sheet 3 of 5.....	59
Figure 38.	Flat Burner Top Sheet 4 of 5.....	60

Figure 39.	Flat Burner Top Sheet 5 of 5.....	61
Figure 40.	Flat Burner Nozzle Sheet 1 of 2.....	62
Figure 41.	Flat Burner Nozzle Sheet 2 of 2.....	63
Figure 42.	Window Holder Sheet 1 of 2	64
Figure 43.	Window Holder Sheet 2 of 2	65
Figure 44.	Nitrogen Distribution Port Sheet 1 of 1	66
Figure 45.	Gas Generator Nozzle Sheet 1 of 1	67
Figure 46.	Propellant Blank Sheet 1 of 1	68
Figure 48.	Regulator Mounting Bracket Sheet 2 of 3 (Base)	70
Figure 49.	Regulator Mounting Bracket Sheet 3 of 3 (Stem)	71
Figure 50.	Slab Burner Support Sheet 1 of 4	72
Figure 51.	Slab Burner Support Sheet 2 of 4 (Top)	73
Figure 52.	Slab Burner Support Sheet 3 of 4 (Right Leg).....	74
Figure 53.	Slab Burner Support Sheet 4 of 4 (Left Leg).....	75
Figure 54.	ER 3000 Control.vi Block Diagram.....	77
Figure 55.	Valve Control.vi Block Diagram	80
Figure 56.	Experimental Setup	83
Figure 57.	Oxford Copper Vapor Laser	84
Figure 58.	National Instruments Control Cabinet	85

LIST OF TABLES

Table 1.	Surface Tension Temperature Variability for Common Metals [After 7]	6
Table 2.	Propellant Composition [From 8]	9
Table 3.	Propellant Properties From CEQUEL in Combustion Chamber (3.45 MPa) ..	10
Table 4.	Propellant Properties From CEQUEL for Optimum Expansion to 1 ATM.....	10
Table 5.	304 Stainless Steel Mechanical Properties [After 9]	18
Table 6.	304 Stainless Steel Composition [After 9].....	19

THIS PAGE INTENTIONALLY LEFT BLANK

EXECUTIVE SUMMARY

The addition of aluminum to solid rocket propellant can boost propellant performance, but also introduces negative aspects such as two phase flow. As the aluminum combusts, it forms aluminum oxide (Al_2O_3), which is also known as alumina. The melting temperature of alumina is 2327 K and the boiling point is higher than 4500 K. Alumina, therefore, exists as a liquid in the combustion chamber of solid rocket propellant, resulting in two phase bulk fluid flow. Two phase flow lowers propulsive efficiency by exerting drag on the combustion gasses, can cause nozzle erosion and subsequent non-axial thrust, and can cause an increased propellant burn rate due to erosive burning.

Considerable research has been conducted to understand how alumina agglomerates form at the propellant surface. Research has also been conducted regarding agglomerate interaction at the nozzle. The focus of this research is to characterize agglomerate flow within the propellant grain channels. This research is relevant because modern grain design continues to reduce the area of propellant grain channels in an effort to increase the propellant volume fraction. The smaller propellant grain channels result in higher combustion gas velocity within the channels and an increased risk of erosive burning. It is important to understand how agglomerate behavior within the propellant grain channels impacts erosive burning so grain designers can properly account for erosive burning.

Analytical predictions of alumina flow within the propellant grain channel are difficult due to the nature of two phase flow. The random formation of various sized agglomerates and the potential interaction between agglomerates makes the problem extremely challenging. Theory predicts that agglomerates will either remain intact or shear apart based on the Weber number. Analytical projections have been made based on this theory for individual agglomerates, but experimental observation will be required to fully characterize agglomerate interaction.

An experiment was designed to image agglomerate flow in a slab burner. In particular, two small propellant samples will be ignited inside of the slab burner and high

speed photography will be used to image the event. As the propellant burns, a copper vapor laser will be pulsed at 10 kHz to illuminate the combustion channel. The high-speed camera photographs the combustion channel at a shutter speed of 1000 frames per second and an exposure time of 2 μ sec. The camera observed field of view is 3.5 mm in diameter, and the camera resolution is 3.5 pixels per μ m, with a detector size of 1024 x 1280 pixels. The camera is capable of imaging particles larger than 30 μ m with sufficient resolution.

The experimental setup was used to image a calibration grain. Calibration grains consisting of 122 μ m alumina particles, HTPB, and a curative agent were made to fit inside of a gas generator. A hydrogen/air torch was used to burn the calibration grain and the combustion products were transferred into the slab burner for imaging. At the image port, the combustion gas velocity was 180 m/sec and the alumina particle velocity was approximately 50 m/sec. The alumina particles, which remained in solid state throughout the event, were successfully imaged under these circumstances. The calibration grain test proves the validity of the experimental setup; however, testing of actual propellant samples has not been conducted at the time of this writing.


LIST OF ACRONYMS, ABBREVIATIONS, AND SYMBOLS

ACRONYMS

AP	Ammonium Perchlorate
CCD	Charge Couple Device
HTPB	hydroxyl-terminated polybutadiene
psia	pounds force per square inch absolute
psig	pounds force per square inch gage
vi	Virtual Instrument

ABBREVIATIONS

A	Area	[m ²]	(in ²)
Ac	Cross Sectional Area	[m ²]	(in ²)
Al	Aluminum		
ATM	Atmosphere (pressure)		
C*	Characteristic Exhaust Velocity	[m/sec]	
C _D	Drag Coefficient	[1]	
d _{ag}	agglomerate diameter	[m ²]	(in ²)
D _h	Hydraulic Diameter	[m]	(in)
f	friction factor	[1]	
h	convection coefficient	[W/m ² *K]	
Hz	Hertz		
I _{sp}	Specific Impulse	[sec]	
k	thermal conductivity	[W/m*K]	
L	characteristic length	[m]	(in)
\dot{m}	mass flow rate	[kg/sec]	
mol	mole		
Nu	Nusselt Number	[1]	
P	Pressure or Perimeter	[Pa or m]	(psi or in)

Pa	Pascal		
Pr	Prandtl Number	[1]	
	burn rate	[m/sec]	(in/sec)
Re	Reynolds Number	[1]	
sec	Second		
T	Temperature	[K or C]	
u	velocity	[m/sec]	
W	Watt		
We	Weber Number	[1]	

SYMBOLS

μ	dynamic viscosity	[Poise]
ρ	density	[kg/m ³]
σ	surface tension or mechanical stress	[N/m or Pa]

ACKNOWLEDGMENTS

The author wishes to recognize the support of Professor Chris Brophy for his guidance and assistance throughout the design and validation of this thesis work. Additionally, Mr. George Hageman and Mr. Dave Dausen provided instrumental technical expertise during the experimental setup. Considerable machine shop work was conducted by Mr. Doug Learned and his team at Inter-City Manufacturing and by Mr. John Mobley of the Naval Postgraduate School Mechanical and Aeronautical Engineering machine shop. Without their expert craftsmanship, the research would not have been possible. This work was motivated by and initially supported through a research grant from ATK Thiokol. Finally, I would like to thank my wife, Karen, for her support throughout the entire process.

THIS PAGE INTENTIONALLY LEFT BLANK

I. INTRODUCTION

Aluminum based propellants are widely used for solid rocket propulsion. Conventional composite propellants usually contain between 60% and 72% ammonium perchlorate as a crystalline oxidizer, up to 22% aluminum powder as a metal fuel, and 8% to 16% of elastomeric binder including its plasticizer (composition in mass percent). The addition of an energetic nitramine such as HMX or RDX can be added in place of some of the ammonium perchlorate to boost performance and increase propellant density. The aluminum portion of the propellant consists of small spherical particles, typically ranging from 5 to 60 μm in diameter [1]. During propellant combustion, the aluminum particles are oxidized into alumina (Al_2O_3), which is in liquid form in the combustion chamber. The liquid alumina particles tend to agglomerate into larger particles during combustion.

The addition of aluminum boosts propellant performance by increasing propellant density, combustion temperature, and the heat of combustion. Unfortunately, the aluminum addition results in the formation of molten alumina agglomerates that cause two phase flow losses in the combustion chamber and the rocket nozzle. These agglomerates lower the propulsive efficiency of the exhaust flow because the agglomerates do not expand in the nozzle and also introduce a drag force on the flow. This causes energy to be expended by the combustion gasses in order to accelerate the alumina agglomerates to the speed of the bulk flow. Depending on the aluminum particle size and mixture percentage, two phase flow losses can reduce the propellant specific impulse by as much as 6% [2]. Figure 1 demonstrates the advantages of aluminum addition. For a propellant consisting of ammonium perchlorate, HTPB, and aluminum, the peak specific impulse typically occurs when the mass content of aluminum is approximately 18%.

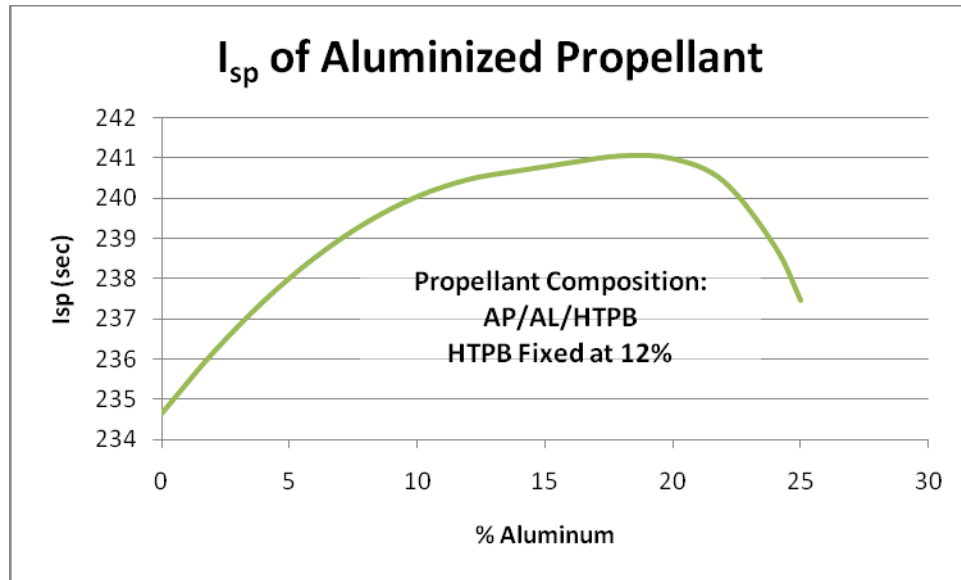


Figure 1. Effect of Aluminum Addition on Specific Impulse (I_{sp})

Alumina agglomerate formation has been extensively studied for more than 40 years. Research has primarily focused on the size and flux density of agglomerate formation when using various concentrations of aluminum, various aluminum particulate sizes, and various combustion conditions. Several models have been developed that strive to predict agglomerate formation based on these parameters [3], [4], [5]. Today's models can predict agglomerate formation at the combustion surface with good accuracy; however, experimental analysis is still required to confirm the model results.

Currently, there are no validated models available that predict agglomerate flow or transformation as the agglomerates travel through narrow passages of web channels or down the combustion chamber. The ever-present demand to increase propellant volume fraction in the combustion chamber is leading to creative grain geometries with small combustion channels. In particular, finocyl configurations, anchor formations, and star grains with many points are often utilized and continually improve solid rocket motor design. In some cases, unexpected levels of erosive burning at the propellant grain surface has been detected. Additional understanding of agglomerate behavior through the narrow combustion channels will help aid grain designers to properly account for erosive burning in future propellant grain configurations.

**Area of High Velocity
and Potential
for Erosive Burning**

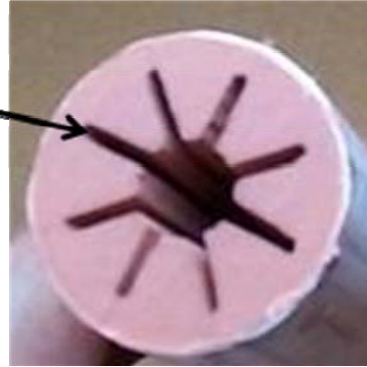


Figure 2. Depiction of Narrow Passages in 8-Point Hybrid Star / Finocyl Grain Configurations

Nozzle design can also be impacted by agglomerate flow. Rocket nozzles are subjected to extremely violent conditions. The combustion products that travel through nozzles do so at very high temperature. The pressure gradient across a rocket nozzle is tremendous, often dropping over one hundred atmospheres in just a few inches of travel. Finally, combustion products acceleration through a rocket nozzle is very high. The combustion products typically enter the nozzle around Mach 0.2, reach Mach 1 (sonic) at the throat, and exit at high supersonic velocities. Alumina agglomerate impingement on the rocket nozzle under these conditions can have disastrous consequences. The molten alumina has a tendency to stick to the rocket nozzle, which can transfer a tremendous amount of heat to the nozzle. In some cases, the alumina can solidify on the nozzle and further restrict the flow. Although most modern rocket nozzles are designed to erode as the rocket engine burns, alumina agglomerate interaction on the nozzle surface can hasten this erosion or cause uneven erosion. Unplanned nozzle erosion can lead to non-axial thrust beyond the control capability of onboard attitude control systems, and ultimately lead to in-flight abortion.

The research conducted as part of this research seeks to investigate alumina agglomerate flow in the combustion chamber. In particular, alumina agglomerates will be observed not at the propellant grain surface, but in the center of the propellant grain web channels. Specifically, the agglomerates will be observed at their highest velocity as they exit the propellant grain channel and enter the combustion chamber. It is expected

that the results of this research will serve as a baseline in understanding bulk fluid agglomerate flow. The results will allow grain designers to better predict the internal ballistics of metalized solid rocket motors and the impact on erosive burning as a result of agglomerate flow.

II. BACKGROUND

A. ALUMINA CHARACTERISTICS

A great deal of testing has been conducted on alumina because of its prevalence in solid rocket motor combustion gases. The violence of the combustion environment makes it extremely difficult to precisely measure the physical properties of alumina in a practical combustion environment. This has resulted in much of the available data being for “pure” alumina, Al_2O_3 , not the “dirty” alumina that agglomerates in combustion gasses and may contain other combustion products.

1. Melting Point and Boiling Point

The melting point of alumina, 2327 K, is well agreed upon. The boiling point of alumina is not as clear. According to Reed and Calia [6], it is not clear that alumina exists in the gaseous state. Instead, the boiling point is commonly reported as a temperature at which a huge enthalpy increase occurs due to the onset of dissociation to Al, AlO, Al_2O , O, and O_2 . For this reason the boiling point has been erroneously reported as 3200 K at 1 ATM. Instead, Reed and Calia suggest using the equation $T_b = 250.365 \ln(P) + 876.84$ where T_b is in Kelvin and P is in Pascals. At a pressure of 3.45 MPa (500 psia), the boiling point is 4645.6 K.

It should also be noted that the melting point of pure aluminum is 933 K and the boiling point is 2793 K [7].

2. Surface Tension

Surface tension is a property of a material commonly measured by researchers and then reported for the conditions under which the measurement was made. If the conditions change, then the surface tension also changes. One of the largest contributors to surface tension variability is the temperature of the liquid being measured. As the temperature increases, the surface tension decreases. The surface tension for many common metals is well known and is reported in two parts. The first part is the surface

tension at a particular temperature and the second part is the surface temperature variability with temperature. For example, the surface tension (σ) of aluminum at 933 K (the melting point) is 914 mN/m with a temperature variability $\left(\frac{d\sigma}{dT}\right)$ of -0.35 mN/(m*K).

The surface tension of alumina has been measured at the melting point by several researchers; however, the temperature variability is not well known. According to Smithells [7], the surface tension of alumina at 2327 K is 690 mN/m. Reed and Calia [6] report a surface tension of 650 mN/m at the same temperature. The surface tension temperature variability of alumina is unknown, so the surface tension of alumina at the temperatures expected in the combustion chamber is not directly known. For the purpose of this research, the surface tension temperature variability was approximated using surface tension temperature variabilities of known substances.

Table 1. Surface Tension Temperature Variability for Common Metals [After 7]

Metal	Surface Tension $\left(\frac{mN}{m}\right)$	$\frac{d\sigma}{dT} \left(\frac{mN}{m \cdot K}\right)$
Silver	903	-0.16
Aluminum	914	-0.35
Gold	1140	-0.52
Tin	544	-0.07
Cadmium	570	-0.26
Iron	1872	-0.49
Lead	468	-0.13

Table 1 shows that surface tension temperature variability can vary from -0.07 mN/m*K for tin to -0.52 mN/m*K for gold. Aluminum is near the median at -0.35 mN/m*K. The average of the common surface tension temperature variabilities is -0.28 mN/m*K. It is understood that error will be introduced because the true surface tension temperature variability of alumina is not known. It is believed that correcting the alumina surface tension using an approximated surface temperature variability will yield less error than simply using the melt point surface tension at all temperatures. The

surface tension of alumina will therefore be approximated as

$$\sigma = \sigma_o + (T - T_o) \left(\frac{d\sigma}{dT} \right)$$

where $\sigma_o = 690$ mN/m, $T_o = 2327$ K, and $\frac{d\sigma}{dT} = -0.3 \left(\frac{\text{mN}}{\text{meter} \cdot \text{K}} \right)$.

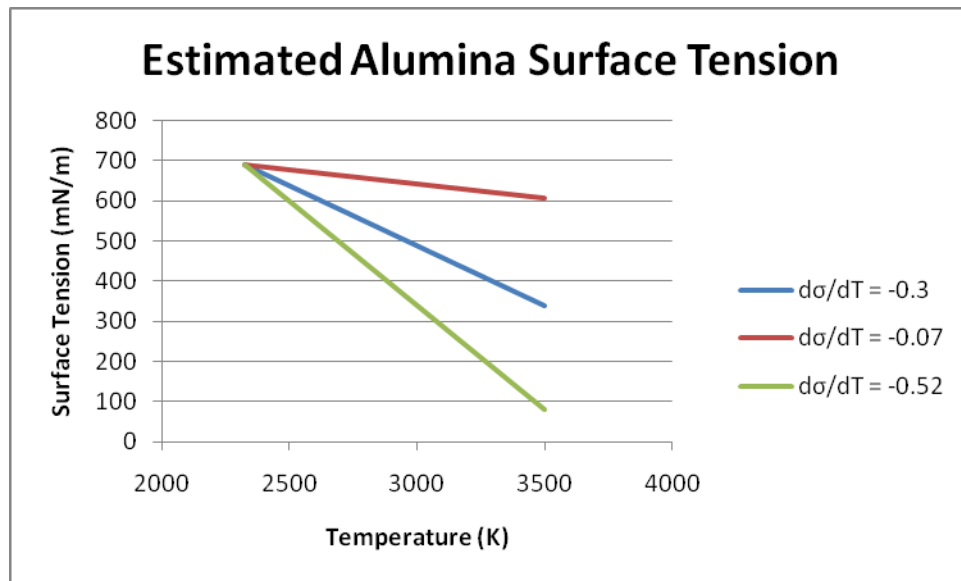


Figure 3. Alumina Surface Tension for Three Temperature Variability Estimates

Figure 3 shows the approximated alumina surface tension for the estimated temperature variability of $-0.3 \left(\frac{\text{mN}}{\text{m}} \right)$ as well as for a temperature variability of $-0.07 \left(\frac{\text{mN}}{\text{m}} \right)$ and $-0.52 \left(\frac{\text{mN}}{\text{m}} \right)$, which correspond to tin and gold, respectively. It is highly likely that the true surface tension of alumina lies within this range.

B. PROPELLANT CHARACTERISTICS

This experiment has been designed so that it can be repeated for any solid rocket propellant; however testing will begin using propellant strands with known agglomerate formation characteristics. Specifically, propellant strands identical to those characterized by Christopher R. DeSena at the Naval Postgraduate School Rocket Lab in 2006 [8] will be the focus of this research. DeSena's thesis tested propellant strands in a combustion bomb utilizing a similar laser imaging system to capture agglomerate formation at the propellant surface. The propellant, manufactured by ATK Thiokol, has a theoretical specific impulse of 274 seconds. The burn rate at 3.45 MPa (500 psia) was reported as 10.16 mm/sec. The propellant density is approximately 1.8 g/cm^3 . The propellant strands to be ignited measure 6.35 mm x 25.4 mm x 50.8 mm (1/4 inch x 1 inch x 2 inches). Two propellant strands are simultaneously ignited and the burn area remains constant at 6.35 mm x 50.8 mm x 2 strands (645.16 mm^2 or 1 in^2) throughout the combustion event. The propellant composition is shown in Table 2.

Table 2. Propellant Composition [From 8]

Material	Percentage of Total Mass (%)
200 um AP	45.50
60 um Al	20.00
3 um RDX	17.00
R45M	8.15
3um AP	6.00
DOA	2.00
IPDI	0.58
Iron Oxide	0.50
HX 752	0.27

Using the propellant composition with a chamber pressure of 3.45 MPa (500 psia), additional characteristics were obtained using the chemical equilibrium code CEQUEL. The properties in the combustion chamber and when exhausted to atmosphere are shown in Table 3 and Table 4, respectively.

Table 3. Propellant Properties From CEQUEL in Combustion Chamber (3.45 MPa)

Characteristic	Value
Combustion Temperature	3466 K
Combustion Gas Density (ρ_g)	3.466 kg/m ³
Molecular Weight (M)	28.98 g/mol
Specific Heat Ratio (γ)	1.274
Sonic Velocity (a)	1060 m/sec

Table 4. Propellant Properties From CEQUEL for Optimum Expansion to 1 ATM

Characteristic	Value
Isp (Vacuum)	272 sec
Combustion Gas Density (ρ_g)	0.1555 kg/m ³
Molecular Weight (M)	28.98 g/mol
Specific Heat Ratio (γ)	1.292
Sonic Velocity (a)	867 m/sec
Characteristic Exhaust Velocity (C*)	1571 m/sec

III. EXPERIMENTAL SETUP

A. EXPERIMENTAL DESIGN

The experimental objective of this research is to observe alumina agglomerates as they accelerate in a combustion chamber. Realizing the objective requires a system that is capable of capturing images of agglomerate particles as small as $50\text{ }\mu\text{m}$ in diameter in a smoky combustion environment as they travel at speeds up to 100 m/sec . The primary components of the system designed to achieve this objective are shown in Figures 4 and 5.

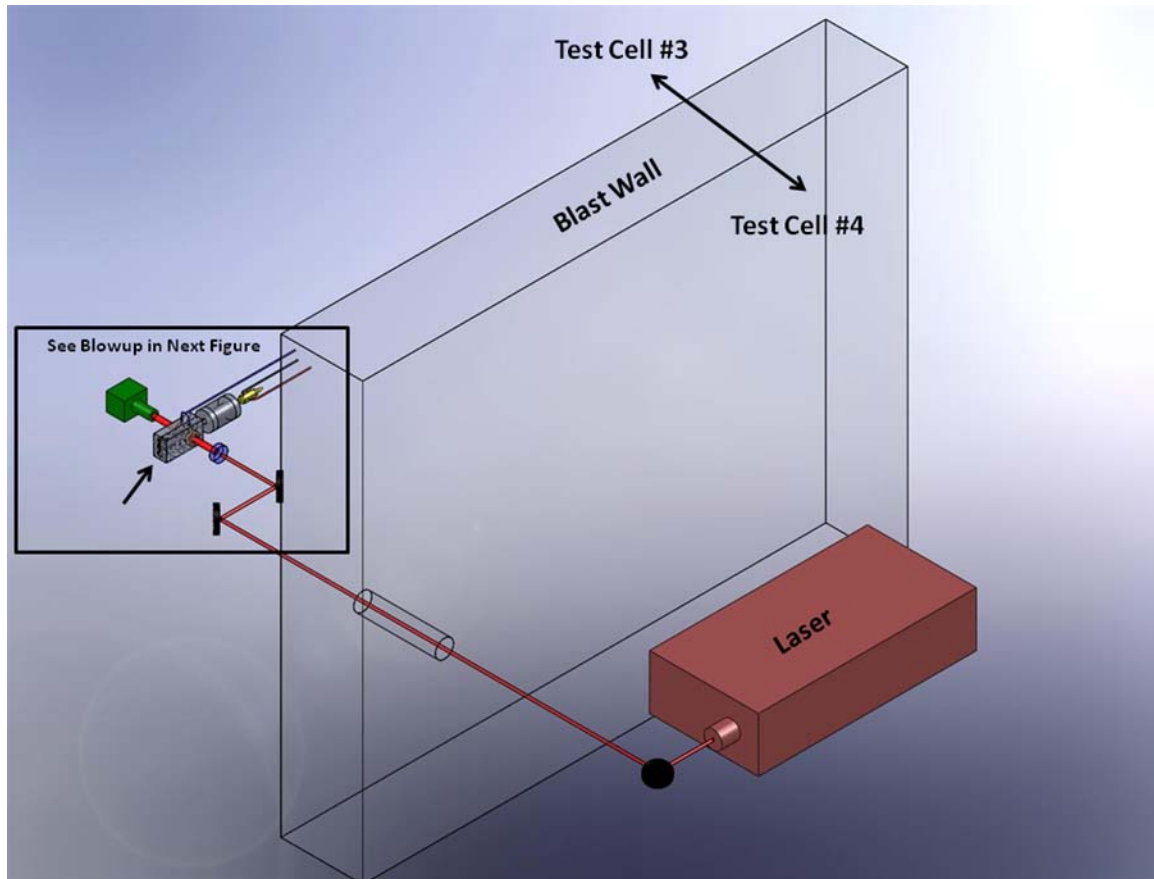


Figure 4. Overall Setup

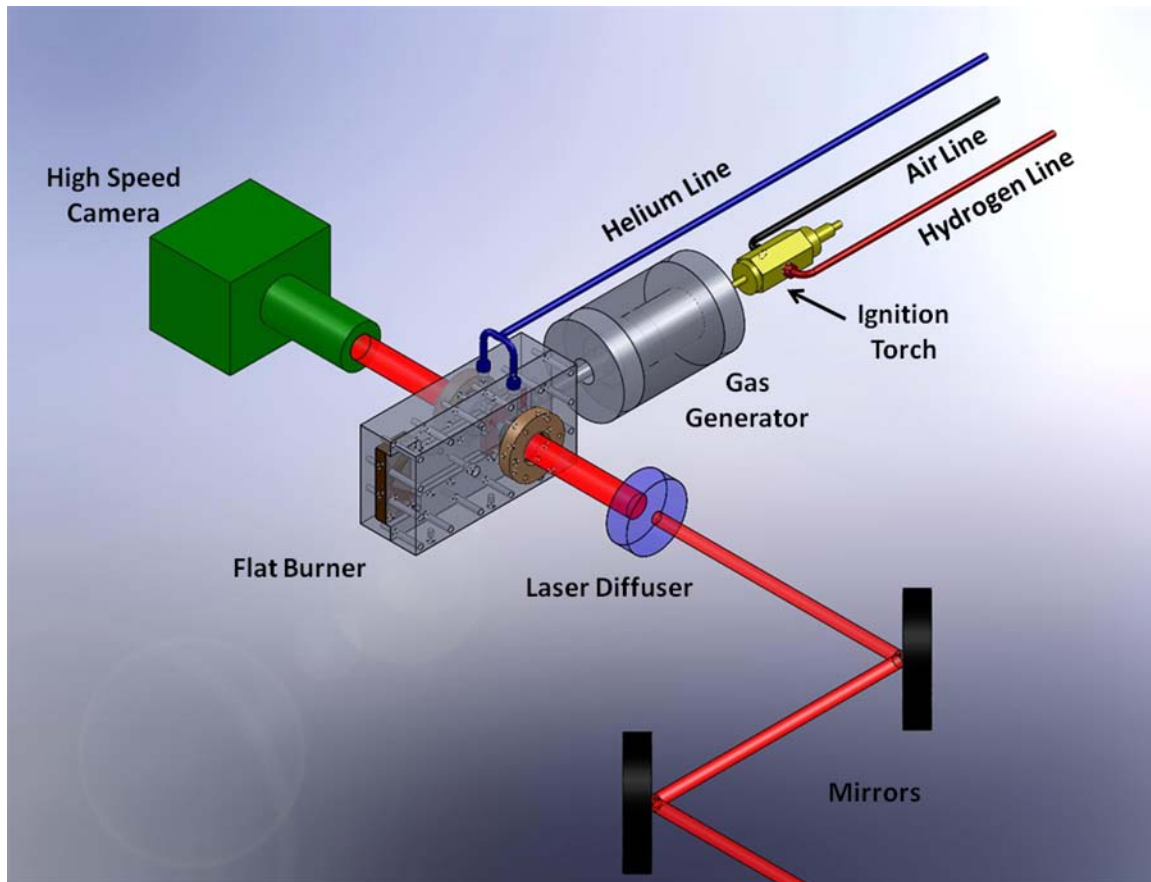


Figure 5. Flat Burner Assembly with Data Acquisition

1. Laser

The light source for the project was a water cooled Oxford model LS 20-10 copper vapor laser. This laser delivered pulses ranging from 5 to 60 nanoseconds at wavelengths of 510.6 and 578.2 nanometers. The laser provided a 20 W output.

The laser's dichromatic circular beam has a diameter of 25.4 cm (1 inch). The beam was redirected using two-axis steering mirrors and diffused using a frosted window as shown in Figure 5. The beam was used to illuminate the combustion products as they traveled through the propellant grain channel. The laser was synchronized with the camera system so that one laser pulse was provided each time the camera shutter opened. For future testing it may be advantageous to provide multiple pulses per camera shutter operation so that agglomerate velocity can be directly measured.

2. Camera

The propellant grain channel was imaged by a DRS Lightning RDT camera that utilized the MiDAS 2.0 software package. The camera was focused on the centerline of the propellant grain channel through the window diametrically opposite of the laser illumination. A dedicated computer was used for the camera system and software. The camera has a variable frame rate, exposure time, and shutter speed. For the scope of this project, a frame rate of 1000 frames per second was used with an exposure time of 2 μ sec. Future testing may require variance of these parameters.

The digital camera was equipped with a Nikkor 35 - 105 mm lens attached to a 30.48 cm (12 inch) extension tube. The extension tube was incorporated to increase the magnification level. The circular field of view of was 3.5 mm. The camera has a 1280 x 1024 CCD sensor and a resolution of 3.5 μ m per pixel.

A 20 nm bandwidth filter centered at 520 nm was attached to the front of the camera lens. This was done to limit the effects of the natural broadband luminosity. However, this also filtered out the 578.2 nm component of the beam provided by the laser.

a. Camera Calibration

The camera was initially calibrated using the Air Force Calibration Tool and ultimately verified using 122 μm alumina particles.

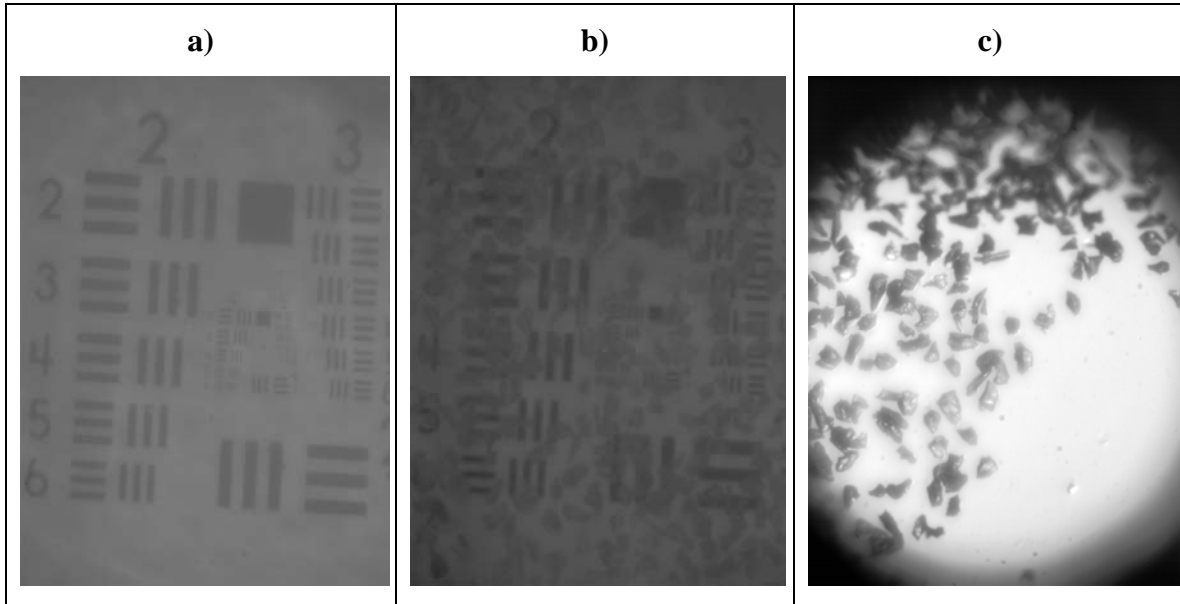


Figure 6. Camera Calibration Sequence

Figure 6 shows the results of the camera calibration. All photographs in Figure 6 were taken using a work light, not laser illumination. Figure 6 a and b were taken of the Air Force Calibration Tool outside of the slab burner assembly. Figure 6 a was taken to show the camera resolution. Block 4 step 3 is 124 μm square, which is roughly the resolution required to clearly see the 122 μm alumina targets. The lines on target 5, step 3 can be easily resolved. Target 5, step 3 is 62 μm long. The solid black square representing target 6, step 2 can be recognized. This target is 34.8 μm square, which gives confidence that agglomerates as small as 50 μm as will be detected by the imaging system. A simple piece of clear scotch tape was sprinkled with 122 μm alumina and photographed in Figure 6 b. The alumina particles can be clearly seen, and are approximately the size of target 4 step 3.

Figure 6 c is a simple piece of clear scotch tape sprinkled with 122 μm alumina particles. The tape was placed inside of the slab burner assembly and centered in the propellant grain channel. A work light was used to provide backlight. The alumina particles can be clearly distinguished inside of the slab burner.

3. Ignition Torch

Propellant ignition was performed by a hydrogen / air torch. Pressure regulated hydrogen and air were independently supplied through 12.7 mm ($\frac{1}{2}$ inch) pneumatically operated ball valves, 6.35 mm ($\frac{1}{4}$ inch) pneumatically operated ball valves, 6.35 mm ($\frac{1}{4}$ inch) solenoid operated valves, and a 6.35 mm ($\frac{1}{4}$ inch) check valves. Flow was further controlled using a physical choke between the final solenoid valve and the check valve. Calculations show that stoichiometric conditions exist for a mixture of 3% hydrogen / 97% air by mass. The expected combustion temperature for this mixture ratio is 2443 K. A 3% hydrogen / 97% air mixture was achieved by installing a 0.3429 mm (0.0135 inch) diameter choke with a 3.07 MPa (445 psig) backpressure in the hydrogen line and a 0.74168 mm (0.0292 inch) diameter choke with an 5.52 MPa (800 psig) backpressure in the air supply line. Labview software was used regulate pressure and control valve operation timing. As the final solenoid valve opened, hydrogen and were ported into the ignition torch body and a spark plug ignited the torch.

4. Gas Generator

The gas generator will not be required when burning actual propellant strands in the slab burner, but was used for this research to prove the experimental setup before actual propellant strands are burned. The gas generator was designed to house cylindrical propellant grains measuring two inches in diameter and two inches in length. In this case, a calibration grain consisting of alumina blended into HTPB was installed in the gas generator. The ignition torch was hot enough to force the HTPB to burn, although the HTPB did not continue to burn when the ignition torch was secured. As the ignition torch combustion products forced the HTPB to burn, the alumina particulates were entrained in the combustion gasses. The gasses traveled out of the gas generator and into

the slab burner where they were imaged much like agglomerates would be imaged during an actual combustion event. During actual propellant combustion inside of the slab burner, the gas generator will be removed from the system and the ignition torch will be connected directly to the slab burner.

a. Calibration Propellant Mixing

A calibration propellant consisting of HTPB, PAPI, and 122 μm alumina particulates was made for experimental validation. The mixture consisted of 67% HTPB, 8% PAPI, and 25% alumina. Six inert grains were created for use inside of the gas generator.



Figure 7. Inert Propellant Mixing

5. 2-D Slab Burner

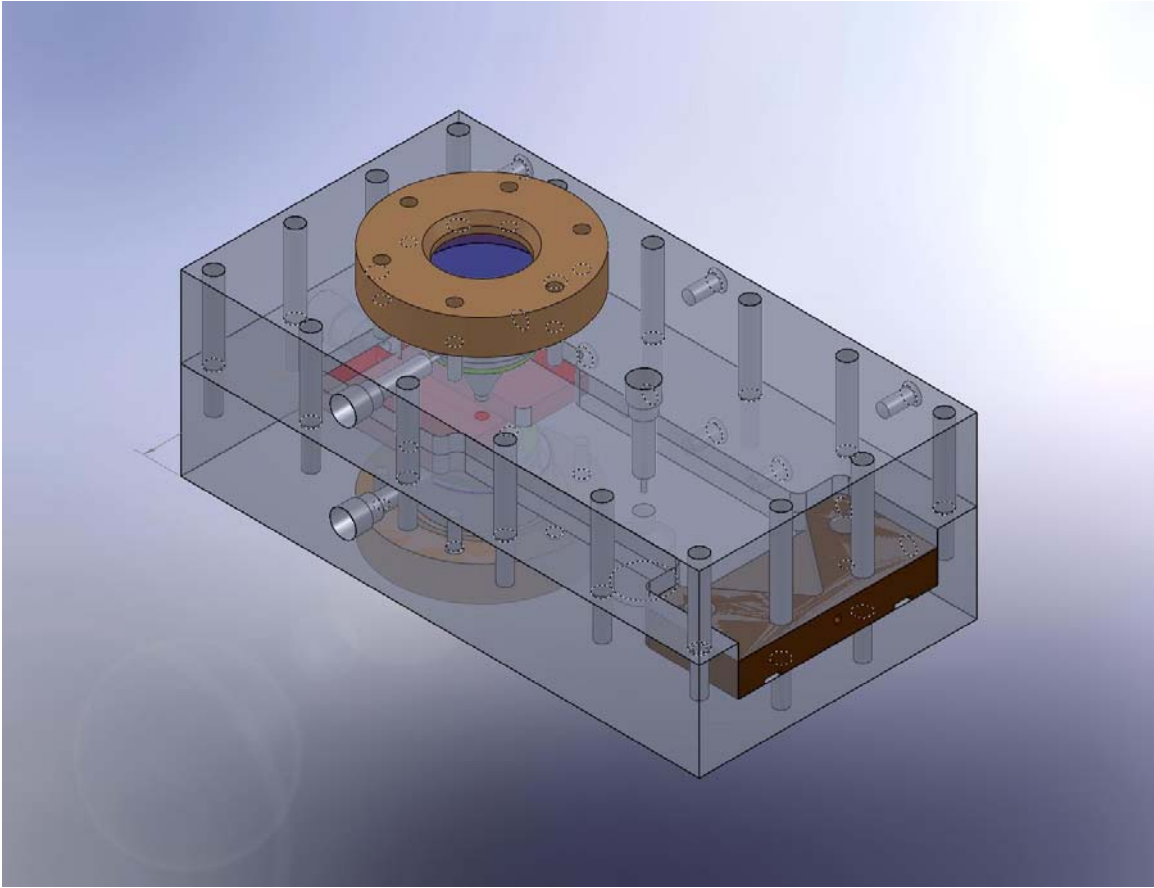


Figure 8. 2-D Slab Burner Assembly

The slab burner was the primary test article of the experiment. It was designed to house the test propellant strands and contain the combustion event. Incorporation of a modular nozzle allows for simple combustion chamber pressure adjustment by varying exit area. Two windows are located on the sides of the slab burner. One window was designed to deliver diffuse laser light to illuminate the region of interest. The other window is a view window that allows the high speed camera to capture images of the flow field. The slab burner has access ports to allow for torch ignition, pressure sensing, overpressure relief, and nitrogen or helium transfer to the view ports. The slab burner was designed to withstand a 3500 K combustion event at a pressure of 6.9 MPa (1000 psia) for a period of 2.5 seconds with a factor of safety exceeding 6.

With the exception of the glass windows, the entire slab burner assembly is constructed of 304 stainless steel. This material is well suited to house the high combustion temperatures and pressures. One drawback of 304 stainless steel is its machining difficulty. Designing the slab burner assembly required significant consideration for the machining process. For example, interior corners were designed to have a 6.35 mm (1/4 inch) fillet so that a relatively large bit could be employed to make the initial cut during fabrication. Additionally, extra large entry port holes were designed for the nitrogen ports and pressure sensing ports because small drill bits could not penetrate the depth of the slab burner wall.

Table 5. 304 Stainless Steel Mechanical Properties [After 9]

Temperature (C)	Yield Strength (MPa)
Room	241
400	159
600	134
800	114
1000	96.5

Table 6. 304 Stainless Steel Composition [After 9]

Element	Composition Percentage
Carbon	<0.08
Manganese	<2
Phosphorous	<0.045
Sulfur	<0.03
Silicon	<0.75
Chromium	18-20
Nickel	8-12
Nitrogen	<0.1
Iron	Balance

a. *Slab Burner Propellant Housing*

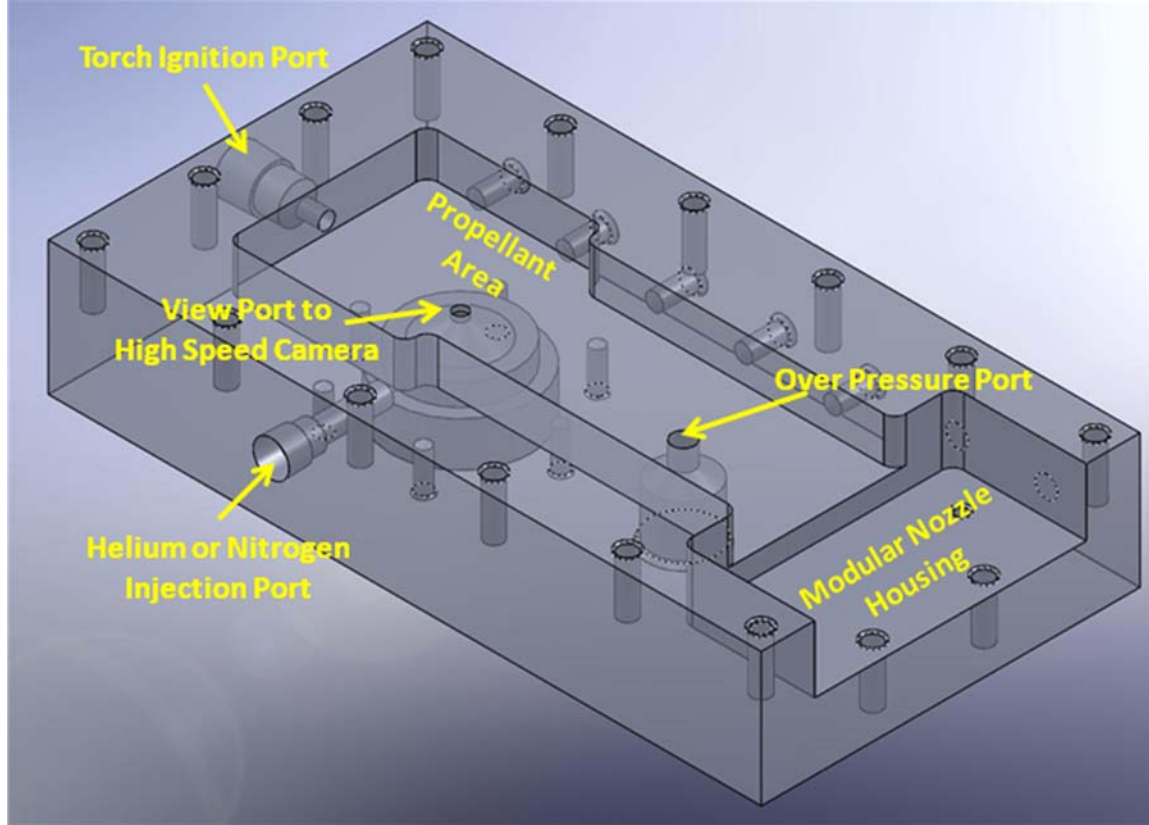


Figure 9. Slab Burner Propellant Housing

The slab burner propellant housing is shown in Figure 9. The ignition torch port hole can be used as a hydrogen/air ignition system or can be used to transfer in gasses generated outside the slab burner. This feature can be used for initial instrument calibration to provide confidence in actual test results when the agglomerate size is unknown and so that actual propellant test strands will not be wasted in a faulty experimental setup. The helium or nitrogen port allows for the inert gasses to be distributed between the view window and the combustion chamber. The addition of inert gas to this plenum prevents combustion gasses from forming a film on the view window that would prevent light transmission and image capture during combustion.

The propellant housing is mechanically stressed during the combustion event because it must contain the heat and pressure associated with the event. It has been

designed to withstand a pressure of 6.9 MPa (1000 psig) at a temperature of 3500 K for a period of 2.5 seconds with a minimum safety factor of 6. An over pressure port with a burst disk set to rupture at 7 MPa (1021 psig) has been added to the slab burner propellant housing for safety.

Significant study has been conducted to ensure the slab burner propellant housing design is sound. First, static structural analysis was performed using ANSYS to determine the expected mechanical stress distribution within the slab burner propellant housing body. A 6.9 MPa (1000 psig) pressure was placed on the inside of the slab burner propellant housing. One corner was fixed while the remainder of the component was allowed to flex. Finally, the average von Mises stress was plotted throughout the body.

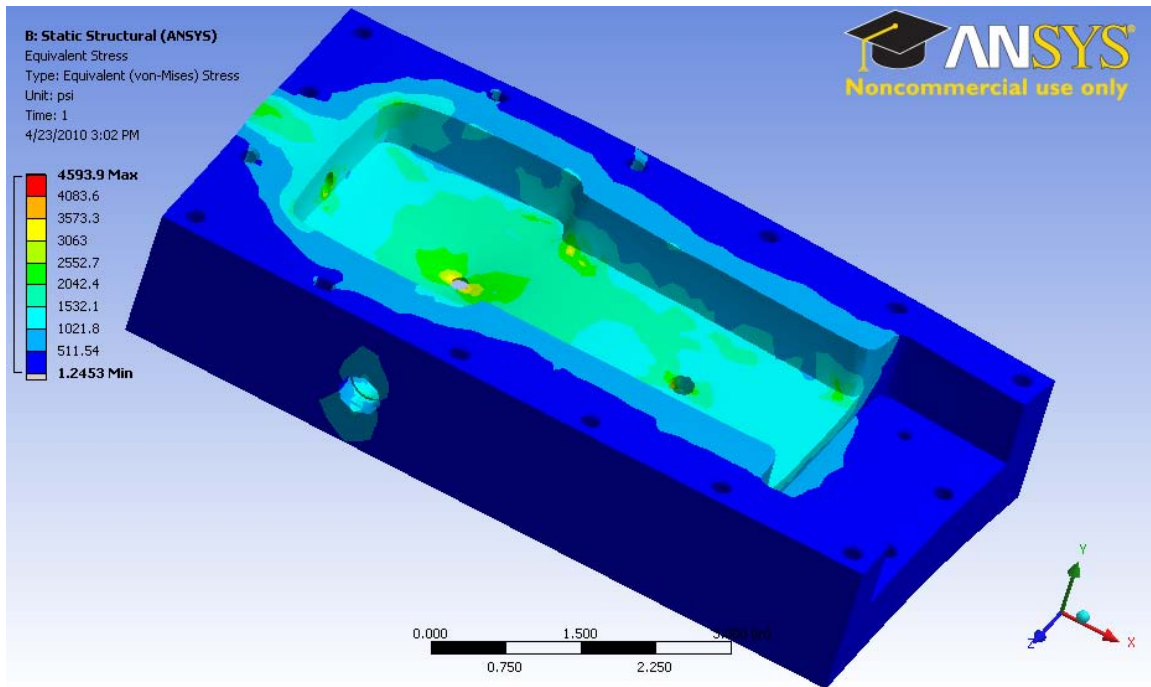


Figure 10. Average von Mises Stress with 6.9 MPa (1000 psia) internal pressure

In the von Mises theory, failure occurs when, at any point in the body, the distortion energy per unit volume in a state of combined stress becomes equal to that associated with the yielding in a simple tension test. Using principal stresses

$$(\sigma_1 - \sigma_2)^2 + (\sigma_2 - \sigma_3)^2 + (\sigma_3 - \sigma_1)^2 = 2\sigma_{\text{vMises}}^2 \quad [10]$$

The ANSYS simulation, shown in Figure 10, shows that the maximum expected average von Mises stress is 30.3 MPa (4593.9 psia), and that it occurs at the view window port. In order to ensure a factor of safety of at least six, the material yield strength must be higher than 6*30.3 or 181.8 MPa. Since the material yield strength is a function of temperature, thermal analysis of the slab burner propellant housing is also required.

Heat transfer inside of the slab burner propellant housing is convective in nature. The convection coefficient, h , has been found using the procedure found in [11]. First, because the slab burner is not cylindrical in nature, an effective hydraulic diameter must be calculated.

$$D_h = \frac{4A_c}{P}$$

A_c and P are the cross sectional flow area and perimeter, respectively. The hydraulic diameter is 11.1 mm. Next, the Reynolds number is calculated.

$$Re_D = \frac{\rho u D_h}{\mu}$$

Where ρ is the combustion gas density, u is the combustion gas velocity, and μ is the combustion gas dynamic viscosity. Using CEQUEL at a chamber pressure of 6.9 MPa (1000 psia), the combustion gas density and viscosity were found to be 6.85 kg/m³ and 1.00 mPoise, respectively. Note that 1 Poise is equivalent to 1g/cm*sec. The combustion gas velocity is calculated using the continuity equation as follows.

$$u = \frac{\dot{V} \rho_{\text{propellant}} A_{\text{burn}}}{\rho_{\text{gas}} A_{\text{chamber}}}$$

The combustion gas velocity in the combustion chamber is 12.1 m/sec, and the Reynolds number is 4628. It should be noted that Reynolds flow is considered turbulent for Reynolds numbers higher than 2300, although most equations to calculate

the Nusselt number are only valid for Reynolds numbers higher than 10,000. For that reason, Gnielinski's equation for the Nusselt number was used. It is valid for Reynolds numbers higher than 3000.

$$Nu_D = \frac{\left(\frac{f}{8}\right)(Re_D - 1000)Pr}{1 + 12.7\left(\frac{f}{8}\right)^{0.2}\left(Pr^{\frac{2}{3}} - 1\right)}$$

where

$$f = (0.79 \ln Re_D - 1.64)^{-2}$$

The friction factor, f , is 0.0397. The Prandtl Number, found using CEQUEL at a combustion pressure of 6.9 MPa, is 0.298. The Prandtl Number for equilibrium flow was used because the long resident time in the combustion chamber will allow the combustion products to reach chemical equilibrium. A similar assumption was made for the combustion gas thermal conductivity. The Nusselt number is 10.58. Finally, the convection coefficient can be found.

$$h = \frac{Nu_D k_{gas}}{L}$$

The conduction coefficient, k_{gas} , found using CEQUEL at a combustion pressure of 6.9 MPa is 12.5 mW/m*K, and the characteristic length is 44.45 mm. Finally, the convection coefficient is calculated to be 298 W/m²*K. Incropera and Dewitt note that errors up to 10% should be expected, so a conservative estimate of 330 W/m²*K was used for ANSYS simulations.

Transient thermal analysis of the slab burner propellant housing was conducted in ANSYS with a convection coefficient of 330 W/m²*K and a combustion temperature of 3500 K.

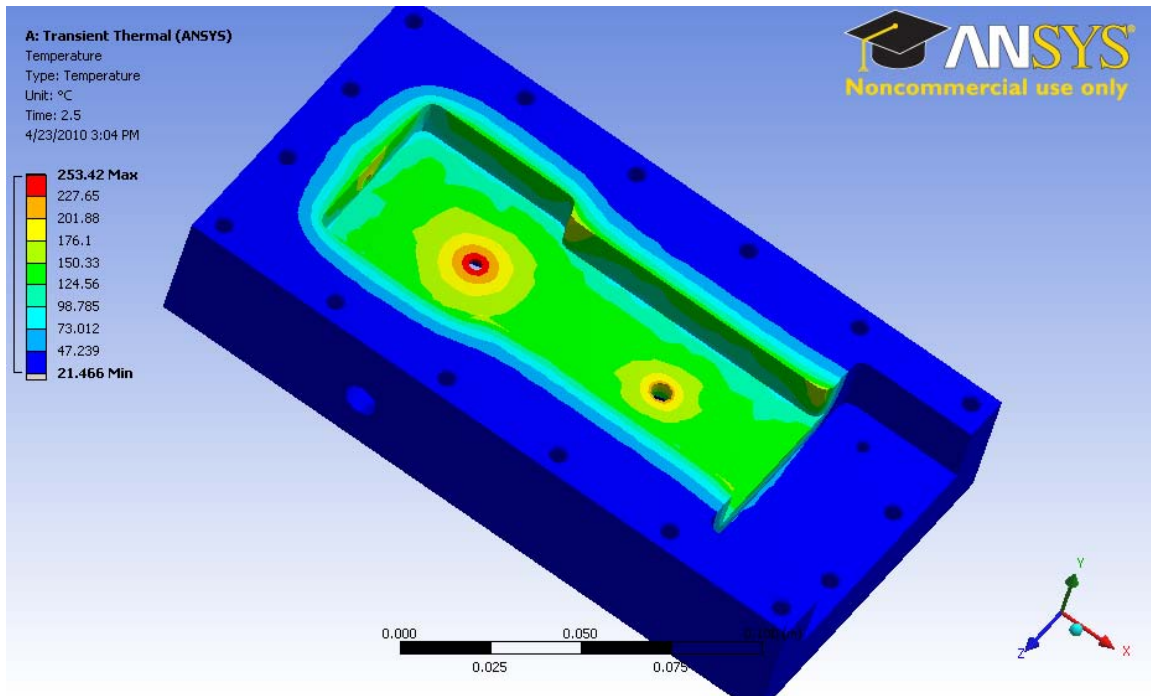


Figure 11. Transient Thermal Analysis of Slab Burner Propellant Housing

The results show a maximum expected temperature of 253.42 C after a 2.5 second propellant burn time. The highest temperature is experienced at the view window port, which coincides with the area of predicted maximum stress. Using linear interpolation, the yield stress of 304 Stainless Steel at 253 C is 192.5 MPa. With a maximum expected stress of 30.3 MPa, the safety factor is 6.35.

b. Slab Burner Cap

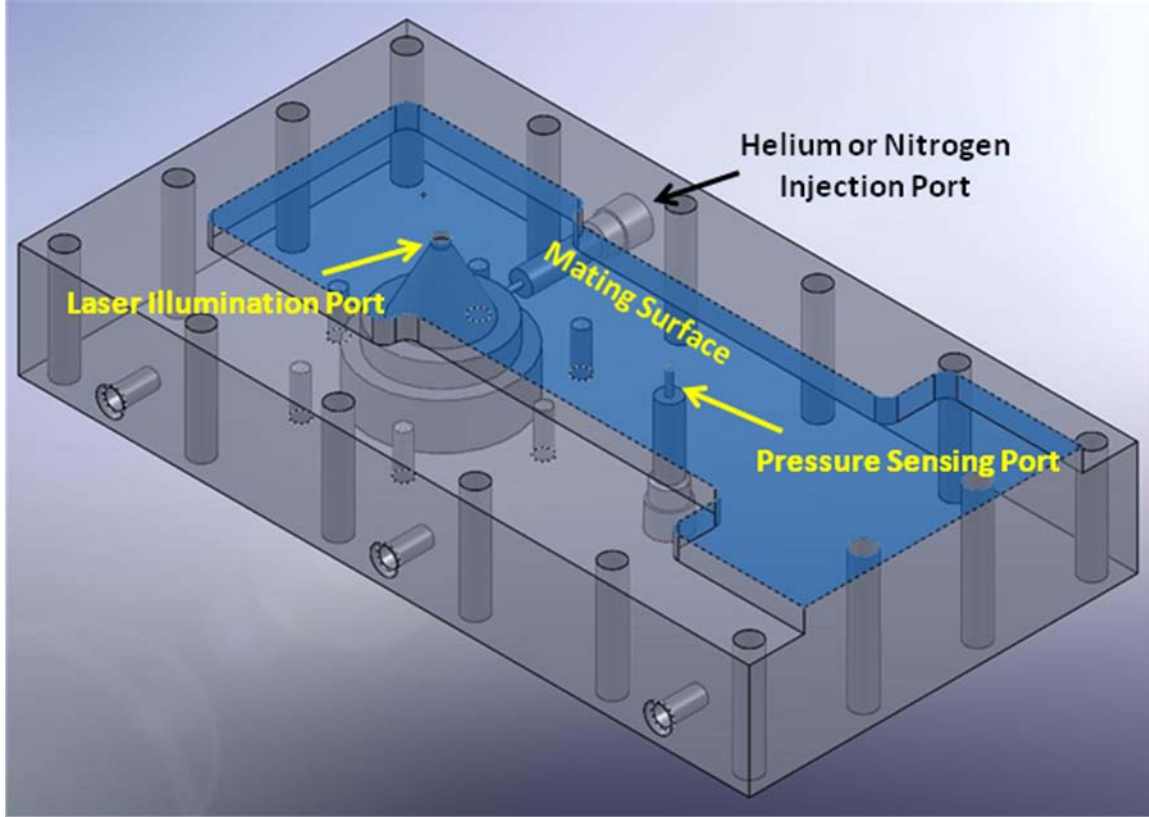


Figure 12. Slab Burner Cap

The slab burner cap is the second half of the primary assembly and fastens to the slab burner propellant housing with 16 1/4"-20 fasteners. The mating surface projects from the cap base and snugly fits into the propellant housing. The snug fit accompanied by flat gasket material around the outer border provides an adequate seal for the combustion gasses. There are three penetration ports in the slab burner cap. A pressure transducer is connected to the pressure sensing port for data collection during combustion. The laser illumination port allows laser light to illuminate agglomerates during combustion. The helium or nitrogen injection port ensures that the laser window remains clear of combustion products that would block illumination light.

c. *Slab Burner Nozzle*

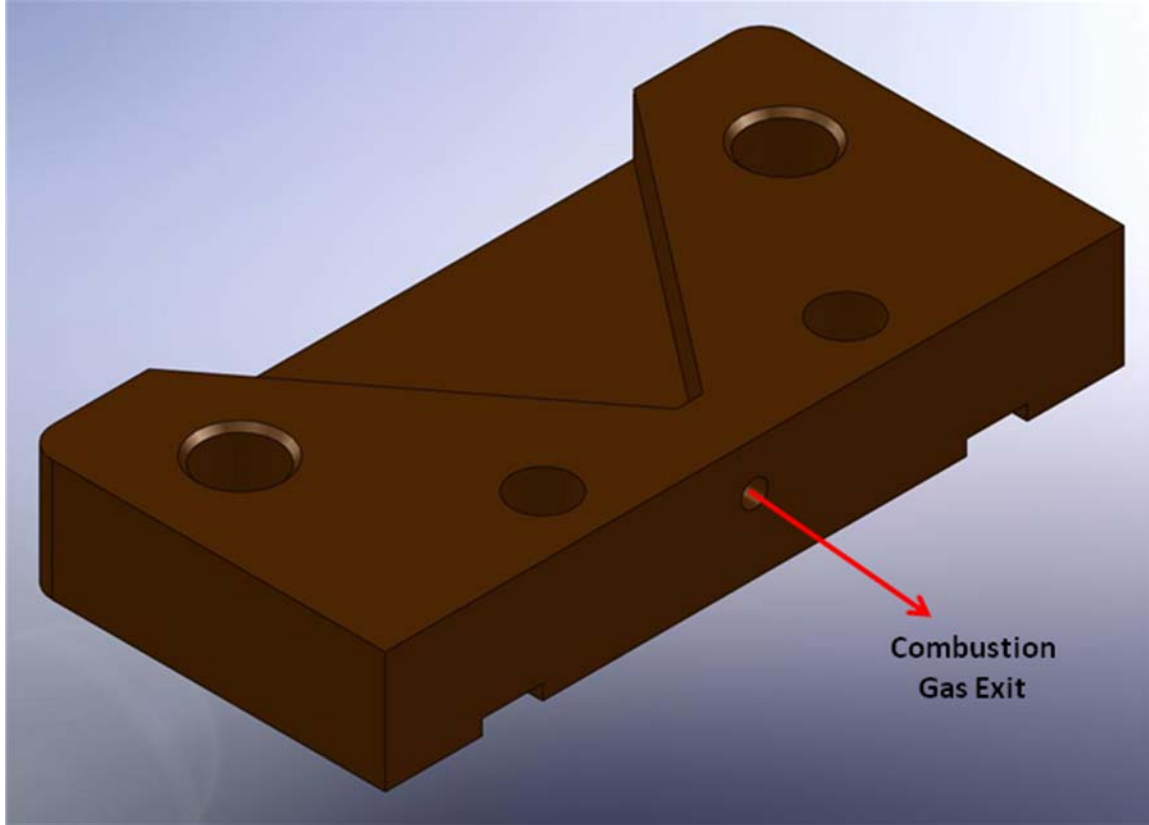


Figure 13. Slab Burner Nozzle

The slab burner nozzle was designed for simple fabrication. It is a convergent-only nozzle because nozzle performance is not of concern for this research. In essence, the nozzle is simply used to control combustion chamber pressure. The nozzle is modular in nature and is fastened directly to the propellant housing using two counter sunk 10-32 fasteners and held in place with two more 1/4"-20 fasteners that penetrate from the slab burner cap to the propellant housing. Reliefs were added to the bottom to facilitate nozzle removal.

For this thesis, the nozzle throat area was sized to produce an internal pressure of approximately 3.45 MPa (500 psia). The throat area was calculated using

$$A_{th} = \frac{\dot{m} C^*}{P_c} \text{ where } \dot{m} = \dot{r} \rho_{\text{propellant}} A_{\text{burn}}$$

From Cequel, C^* is 1571 m/sec. The required throat area is 5.37 mm², which corresponds to a throat diameter of 2.62 mm. In order to standardize the throat size, the nozzle was drilled with a 7/64 inch diameter, which corresponds to 2.79 mm.

d. Slab Burner View Window Assembly

From the laser to the camera, the imaging light travels through the first of two 19.05 mm (3/4 inch) thick, 38.1 mm (1.5 inch) diameter glass windows, a cavity that is purged with helium or nitrogen, the combustion chamber, a second helium or nitrogen cavity, and finally, the second glass window as shown in Figure 16. The windows are held in place with a window holder. The window holder has been designed to prevent glass to metal contact. The inner O-ring groove is cut shallower than required so that the glass only contacts the O-ring. Because the inner wall of the window holder is subjected to combustion pressure, two O-rings are required to provide a complete seal. The Window holder is secured to the slab burner using six 10-32 fasteners.

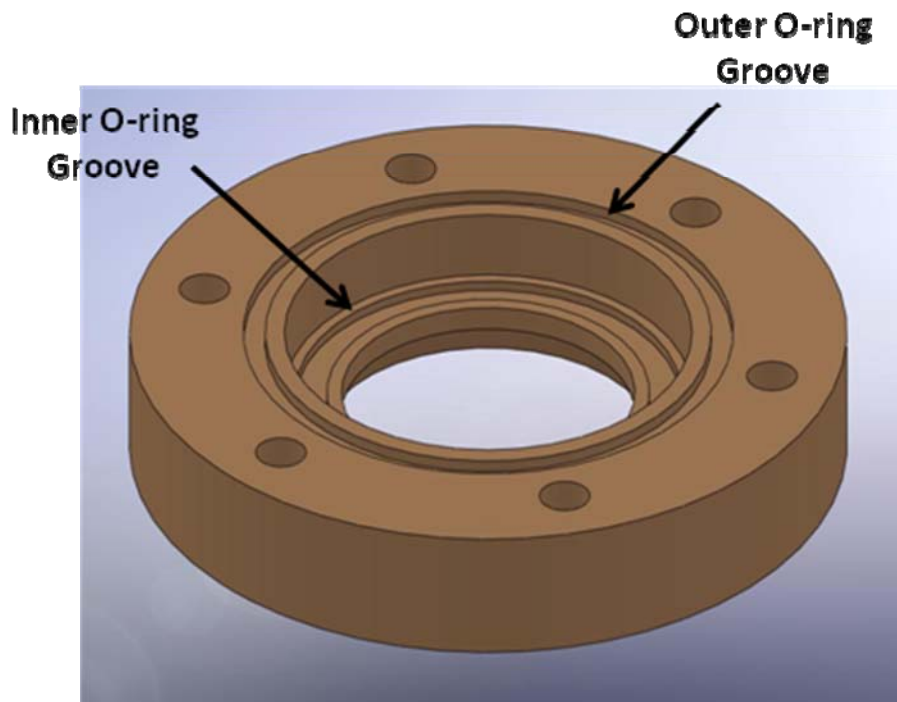


Figure 14. Window Holder

To capture clean images, it is essential to keep the view glass clean. This is accomplished by porting either nitrogen or helium into the cavity on the combustion side of the glass. For initial testing nitrogen was used because of its low cost; however, for final imaging and data collection helium will be used. Helium is more expensive, but its low molecular weight minimizes purge gas/combustion gas interference. In order to evenly distribute the nitrogen or helium in throughout the cavity, a distribution ring was designed. Inert gas is provided through the Nitrogen or Helium Injection ports and is distributed around the cavity using 12 smaller holes.

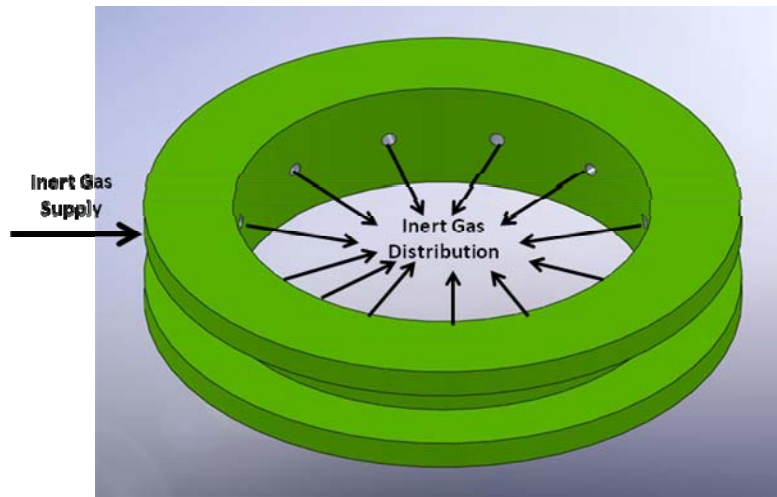


Figure 15. Inert Gas Distribution Ring

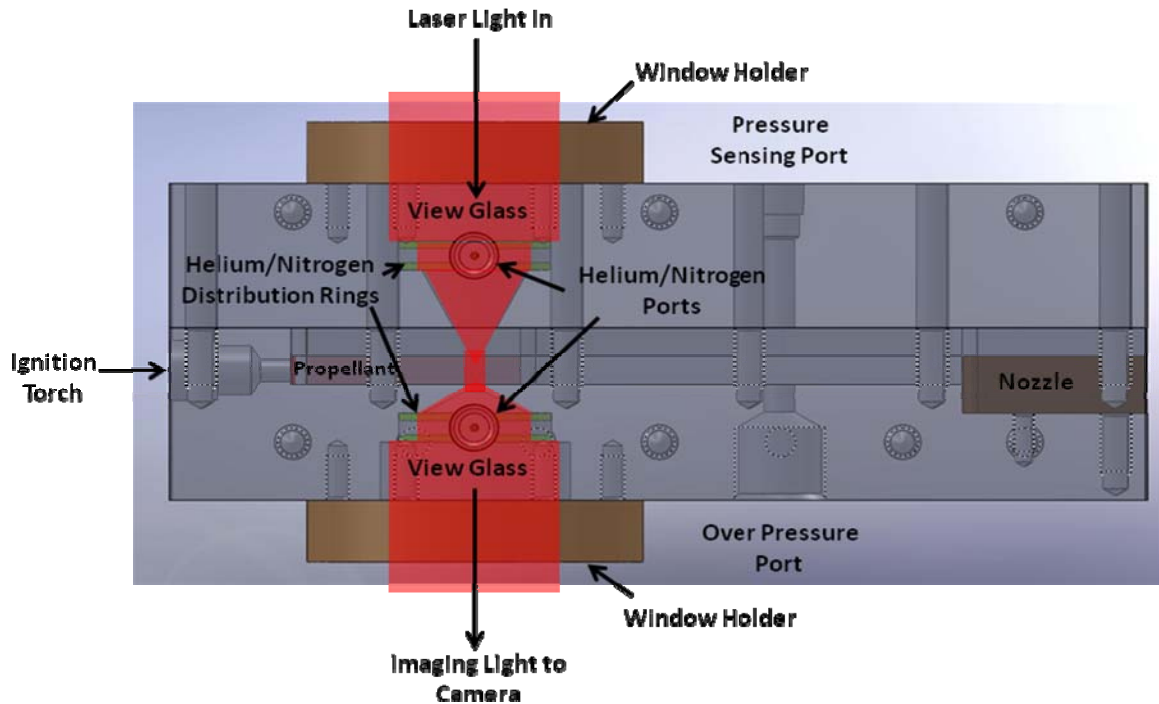


Figure 16. Viewing Assembly Detail

6. Test Cell Setup

The mechanical hardware and electrical sensing equipment of test cell #3 at the Naval Postgraduate School Rocket Lab was upgraded in order to conduct the research associated with this thesis. The cell had not been utilized for solid or liquid rocket testing for several years and required significant modernization. In the course of planning and executing the update, a strong effort was made to ensure the basic test cell layout is applicable to a myriad of future testing including solid propellant, liquid fuel, and air breathing applications.

a. Gas Header

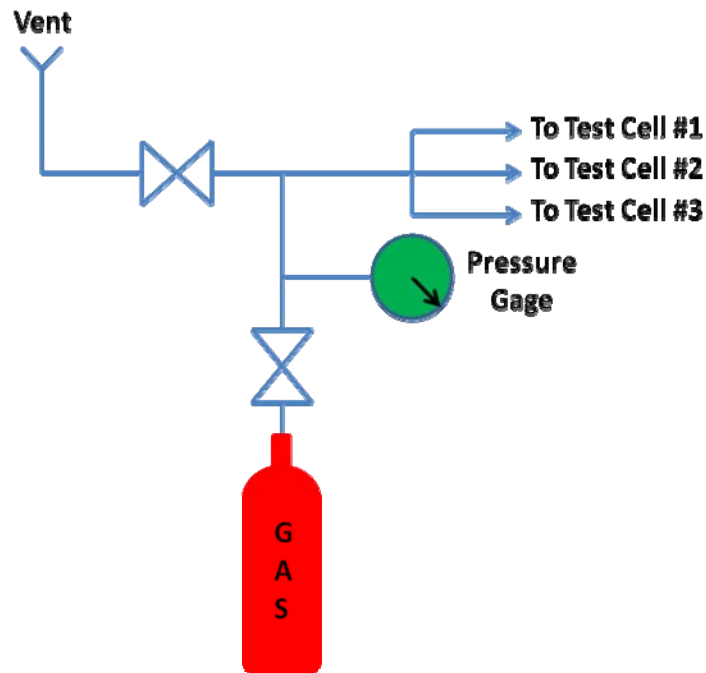


Figure 17. Outside Gas Header

A gas header was constructed on the roof of the building which facilitated improved gas delivery to all three active test cells at the Naval Postgraduate School rocket lab. This header provides four 12.7 mm (1/2 inch) diameter tubes to all three of the active test cells. Nominally, these tubes consist of an oxygen line, nitrogen line, hydrogen line, and a special fuel such as ethane or ethylene. For this thesis work, only the hydrogen line was required.

The gas header largely eliminates the need to locate pressurized gas or fuel bottles inside of the test cells. This allows maximum versatility and convenience since multiple test cells can now be served from common gas banks. Additionally, safety is improved by locating bulk fuels and oxidizers outside of the test cells in which research is conducted. The lineup from a common gas bank into a test cell for one of the four gas headers is shown in Figure 17.

b. Valve Board

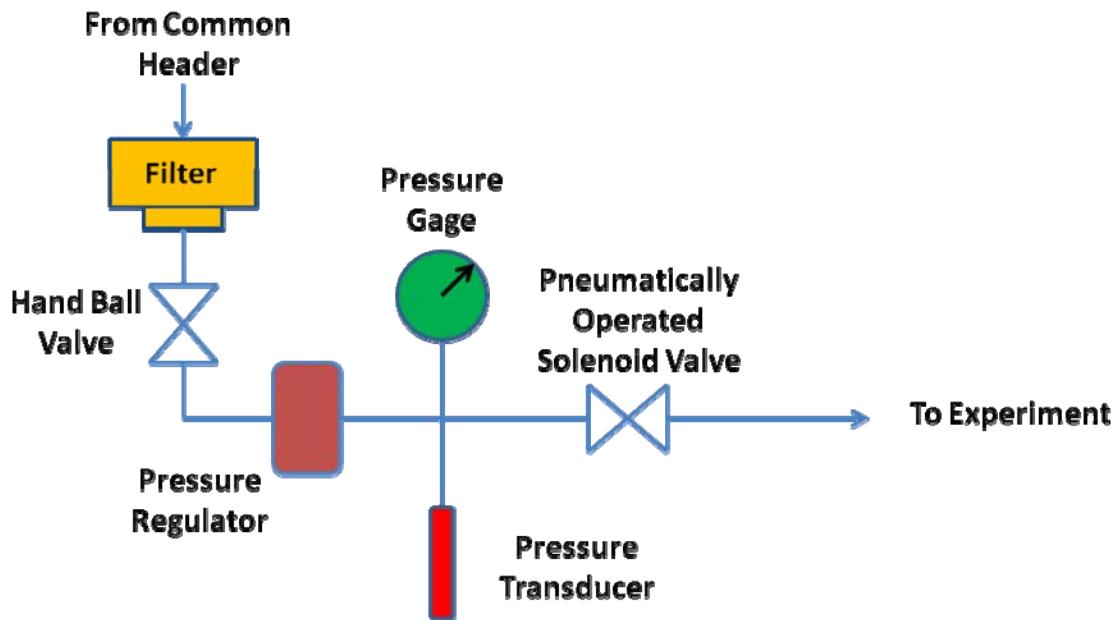


Figure 18. Universal Test Cell Gas Supply Design

A common valve board was designed that provides maximum convenience and versatility. The valve board base is an aluminum plate that measures 0.00635 m x 0.9144 m x 1.2191 m (1/4 inch x 36 inches x 48 inches). The size of the plate was chosen to provide ample space for the regulators, pressure transducers, pressure gages, and pneumatically operated ball valves associated with the four gas lines from the roof header. Identical copies of the valve board will be constructed for use in the other two test cells at the Naval Postgraduate School Rocket Lab due to its versatility. The configuration located within the test cell for one of the four available gas headers is shown in Figure 18 and an actual photograph of the valve board is shown in Figure 19.



Figure 19. Photograph of Common Valve Board

7 Control Software

Labview software was used to control valve operation and pressure regulation for the experiment. Two separate virtual instruments, which were operated simultaneously, were designed to accomplish this task. The first virtual instrument (vi), ER 3000 Control, was used to regulate nitrogen/helium and hydrogen line pressure. This vi reads the analog voltage input from the nitrogen/helium and hydrogen pressure transducers shown in Figure 18. The transducer voltages are then sent to the pressure regulator as a feedback signal. A setpoint signal is also sent to the pressure regulator. The setpoint signal is generated by the user input on the front window of the vi. Pressure regulator comparison of the setpoint and feedback signals ensures accurate nitrogen/helium and hydrogen pressures are provided to the test equipment. The ER 3000 Control vi also reads the input from the pressure transducer located on the slab burner. This pressure is

displayed on the front window of the vi and the pressure data can be recorded into a text file for post experimental analysis. The ER 3000 Control vi continues to regulate pressures throughout the combustion event and is secured when the test is complete by pressing the stop button.

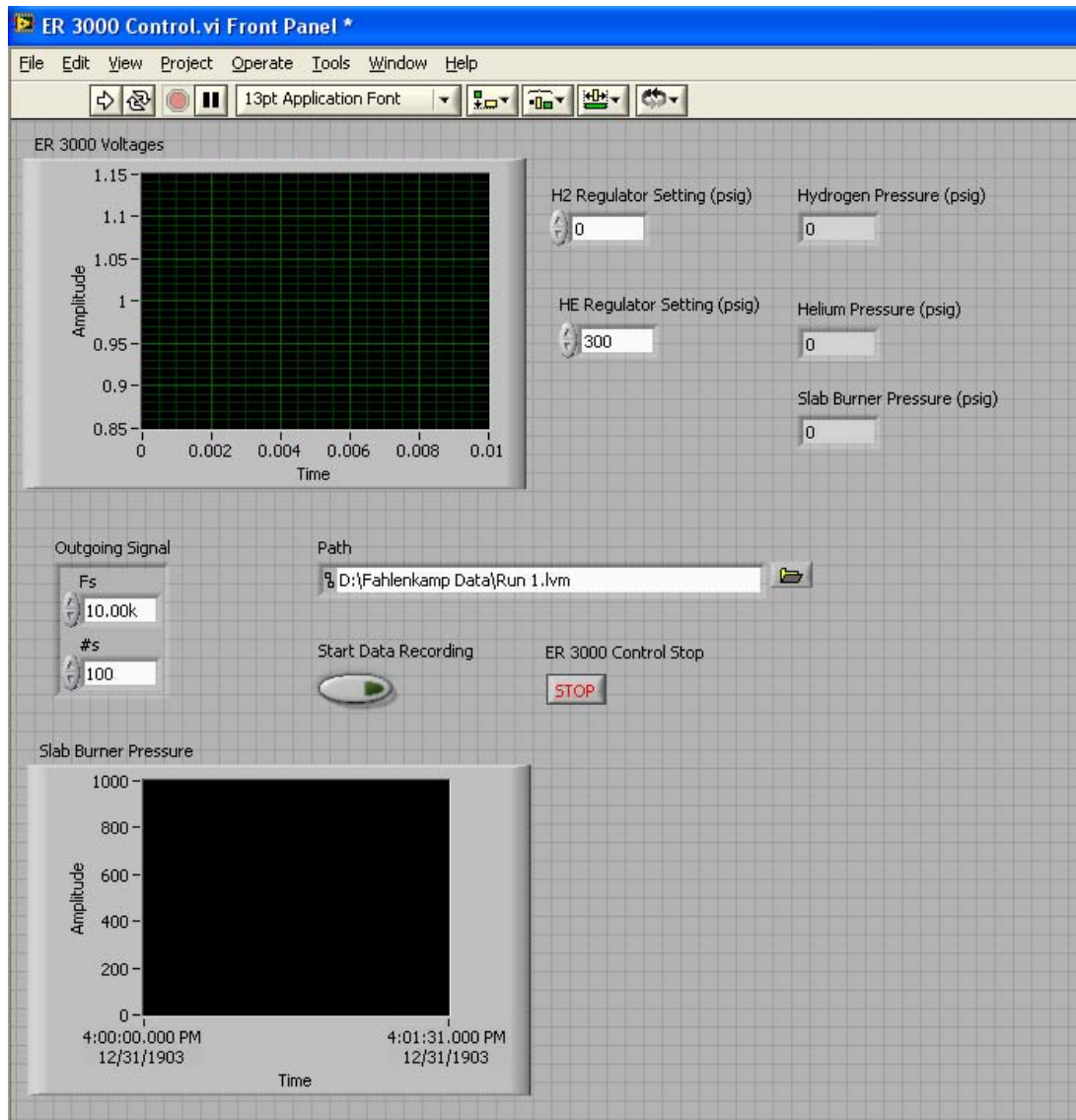


Figure 20. ER 3000 Control Virtual Instrument Front Panel

A second vi was used for valve control. The valve control vi sends a digital signal to the pneumatically operated ball valves and solenoid valves that opens or shuts the valves in the correct sequence and at the correct time. The user can adjust the amount of time the ignition torch remains lit on the front panel. When the start button is pressed, the nitrogen/helium and hydrogen 12.7 mm (1/2 inch) ball valves open after a short delay. This provides purge gas to the slab burner windows and pressurizes the hydrogen line on the test table. The 6.35 mm (1/4 inch) hydrogen and air ball valves open on the table after a one second delay, then the 6.35 mm (1/4 inch) hydrogen and air solenoid valves open after another one second delay. At this time, the spark plug is also energized, which ignites the torch. The sequence is reversed after the torch has burned for the user specified time interval. Shutting the valves secures gasses from the test equipment.

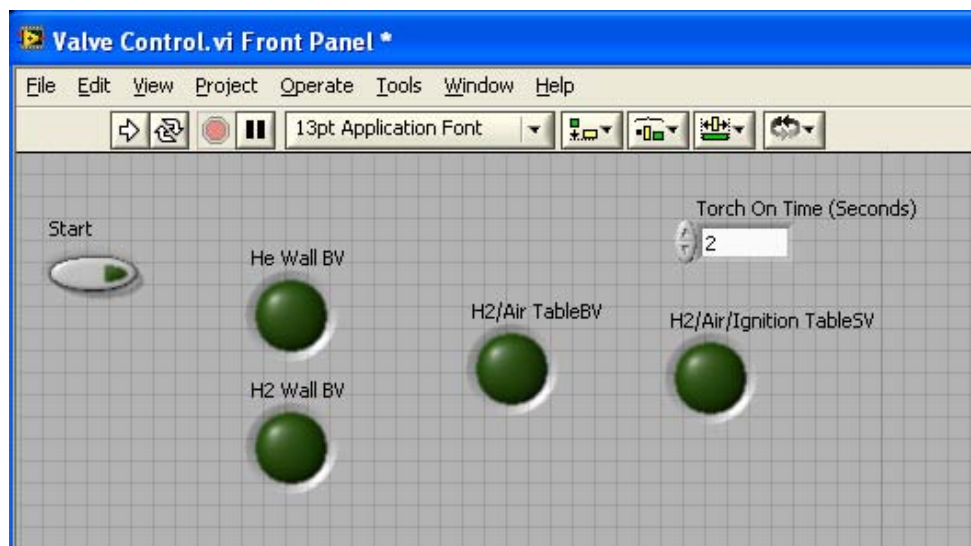


Figure 21. Valve Control Virtual Instrument Front Panel

IV. ANALYSIS AND RESULTS

A. ANALYTICAL PROJECTIONS

Research conducted by Caveny and Gany [12] shows a correlation between the Weber number and alumina agglomerate breakup. Below Weber numbers of 4, droplets are essentially spherical. Their research shows that agglomerates begin to distort at Weber numbers higher than 4 and that agglomerate breakup can occur at Weber numbers between 12 and 20. Agglomerate breakup is almost certain for Weber numbers higher than 20. Agglomerate behavior was predicted for this thesis using the Caveny and Gany criteria.

1. Weber Number Calculations

The Weber number is a dimensionless number that is typically used in fluid flow where there is an interface between two different fluids. In this case it will be applied to the multiphase flow between the combustion gasses and the alumina agglomerates. In general it is a measure of the relative importance of the fluid's inertia compared to its surface tension. The Weber number for agglomerates is calculated using

$W_g = \frac{d_{ag}\rho_g(u_g - u_{ag})}{\sigma}$, where d_{ag} is the agglomerate diameter, ρ_g is the combustion gas density, u_g is the combustion gas velocity, u_{ag} is the agglomerate velocity, and σ is the agglomerate surface tension.

For this research, the combustion gas density, ρ_g , is constant. Using CEQUEL it was found to be 3.466 kg/m³.

The surface tension, σ , is calculated using $\sigma = \sigma_o + (T - T_o)\left(\frac{d\sigma}{dT}\right)$, where $\sigma_o = 690$ mN/meter, $T_o = 2327$ K, and $\frac{d\sigma}{dT} = -0.3 \left(\frac{\text{mN}}{\text{meter-K}}\right)$. At a combustion temperature, T , of 3466 K, the expected surface tension is 348.3 mN/m.

a. *Gas Velocity (u_g)*

The gas velocity between the propellant slabs in the combustion chamber is not constant.

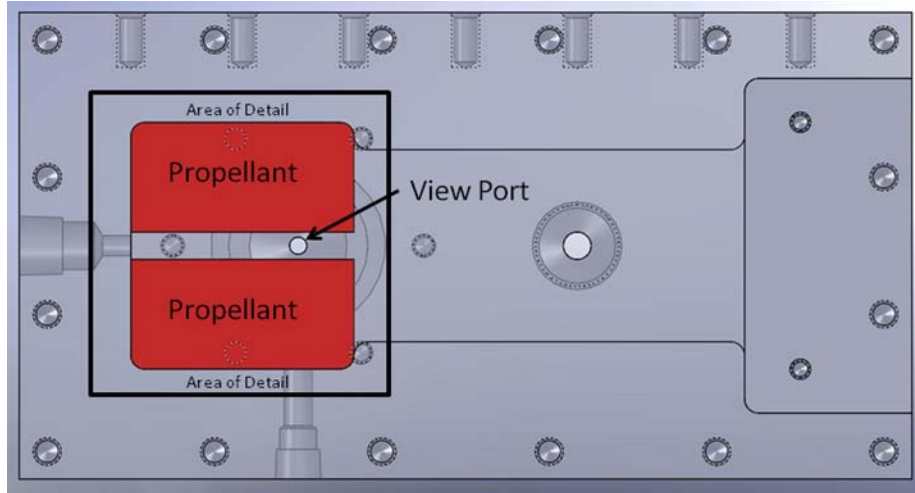


Figure 22. Flat Burner Bottom with Propellant Strands

First, the mass flow rate increases from the back of the propellant to the front of the propellant as more combustion products enter the channel. Second, as the propellant burns, the channel area increases due to the natural regression of the grain. The increased area slows the combustion gas velocity.

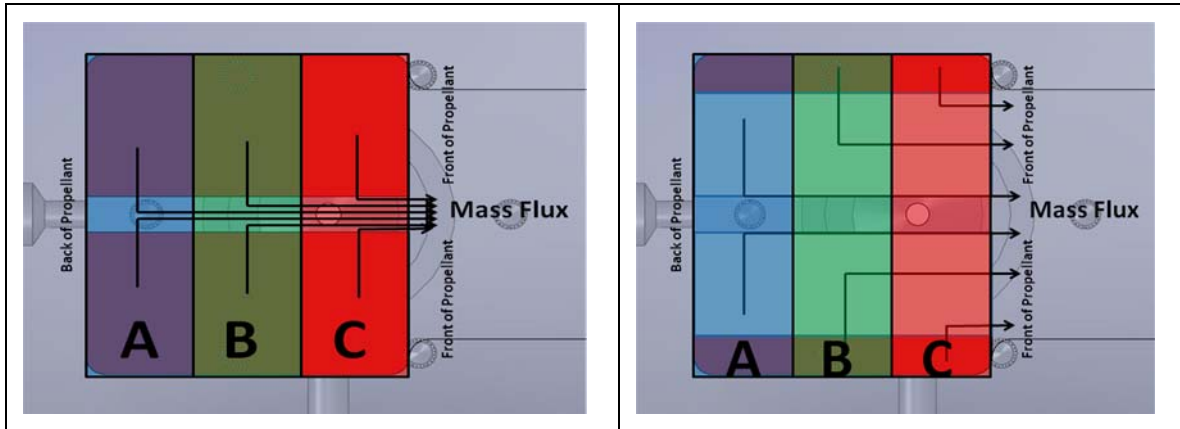


Figure 23. Detail of Propellant Region in Flat Burner Showing Decrease in Mass Flux with Burn Time

As an example, the initial gas velocity at the propellant strand outlet can be calculated using the continuity equation.

$$\dot{m} = \rho_{gas} u_{gas} A_{chamber} = \dot{V} \rho_{propellant} A_{burn}$$

SO

$$u_{gas} = \frac{\dot{V} \rho_{propellant} A_{burn}}{\rho_{gas} A_{chamber}} =$$

$$\frac{0.4 \text{ in}}{\text{sec}} * \frac{1.8 \text{ g}}{\text{cm}^3} * \frac{1 \text{ in}^2}{1} \frac{\text{m}^3}{3.466 \text{ kg}} * \frac{1}{0.25^2 \text{ in}^2} * \frac{\text{kg}}{1000 \text{ g}} * \frac{100^3 \text{ cm}^3}{\text{m}^3} \frac{2.54 \text{ cm}}{\text{in}} \frac{\text{m}}{100 \text{ cm}} = 84.42 \frac{\text{m}}{\text{sec}}$$

Referring to Figure 23, the velocity at the right-hand side of point C at time zero is 84.42 m/sec. As the burn progresses, the chamber area increases until the propellant has burned a distance of 19.05 mm (0.75 inches), corresponding to a burn time of 1.875 seconds. At this time, the chamber area has increased to 6.35 mm x 19.05 mm (0.25 inch x 1.75 inches) and the associated combustion gas velocity drops to 12.06 m/sec and remains constant for the remaining 0.625 seconds of the burn. Figure 24 shows the combustion gas velocities as a function of time associated with the regions depicted in Figure 23.

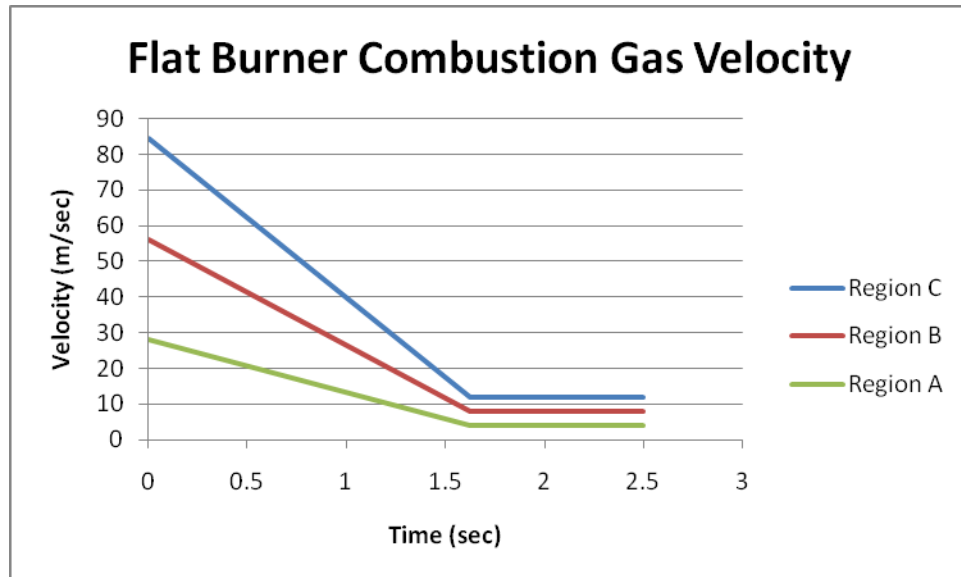


Figure 24. Regional Flat Burner Combustion Gas Velocities vs. Time

At the right-hand side of region B, the initial and final velocities can be similarly calculated. The mass flux at the right-hand side of region B is only 2/3 that at point C, so the initial velocity is 56.28 m/sec and the final velocity is 8.04 m/sec. The initial and final velocities at the right-hand side of region A are 28.14 m/sec and 4.02 m/sec, respectively. Figure 24 shows the regional velocity variation as a function of burn time.

b. Agglomerate Diameter (d_{ag})

The agglomerate diameter, d_{ag} , varies over a wide range. The results of DeSena's research are shown in the Figure 25 for the propellant mixture described in Table 2.

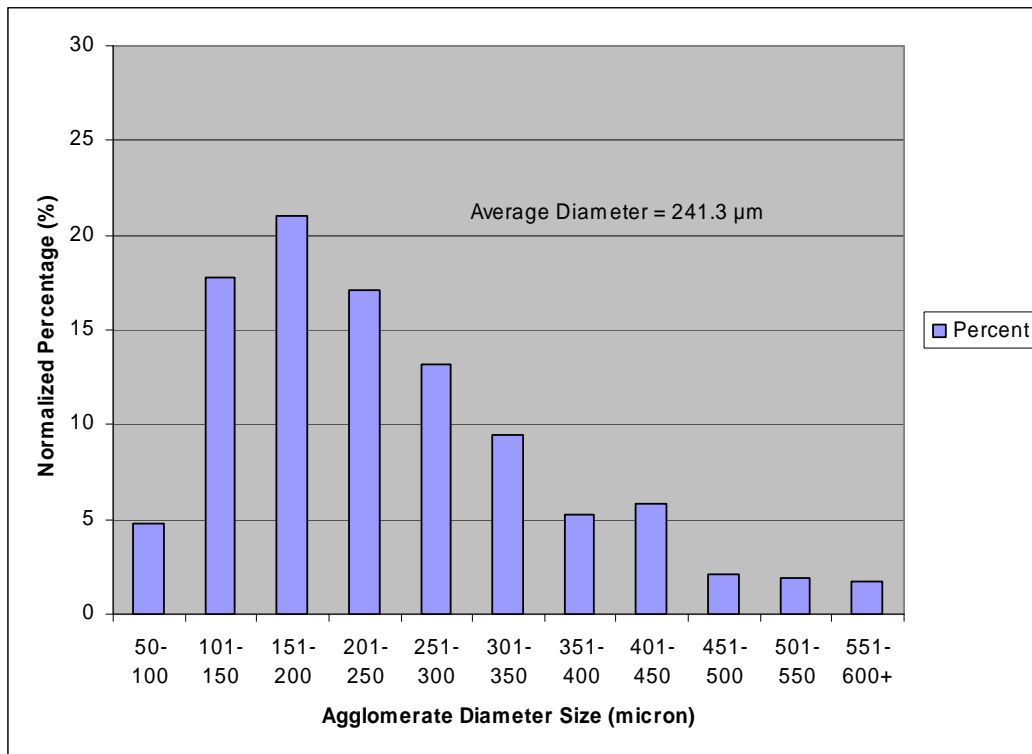


Figure 25. Combustion Surface Agglomerate Size Distribution [From 8]

Agglomerate size at the combustion surface varies from 50 μm to more than 600 μm , with most agglomerates falling in the 100 to 350 μm range. The average agglomerate diameter was 241.3 μm .

c. Agglomerate Velocity (u_{ag})

The agglomerate velocity (u_{ag}) will be left as an unknown. It has been shown that multiple agglomerate diameters are possible and that the agglomerates will experience a wide range of relative velocity with the combustion gasses depending upon the location along the propellant strand at which they form. The agglomerate acceleration is based on the drag force placed on the agglomerate by the combustion gasses and the velocity of course is the integral of the acceleration. The drag force can be calculated using $F = 0.5 C_D \rho_g (u_g - u_{ag})^2 \left(\frac{\pi}{4}\right) d_{ag}^2$ where C_D is a function of the Reynolds Number. Due to the high variance in agglomerate diameter and the unknown agglomerate velocity, the Weber number will be simply plotted against a velocity difference, ($u_g - u_{ag}$).

2. Weber Number Results

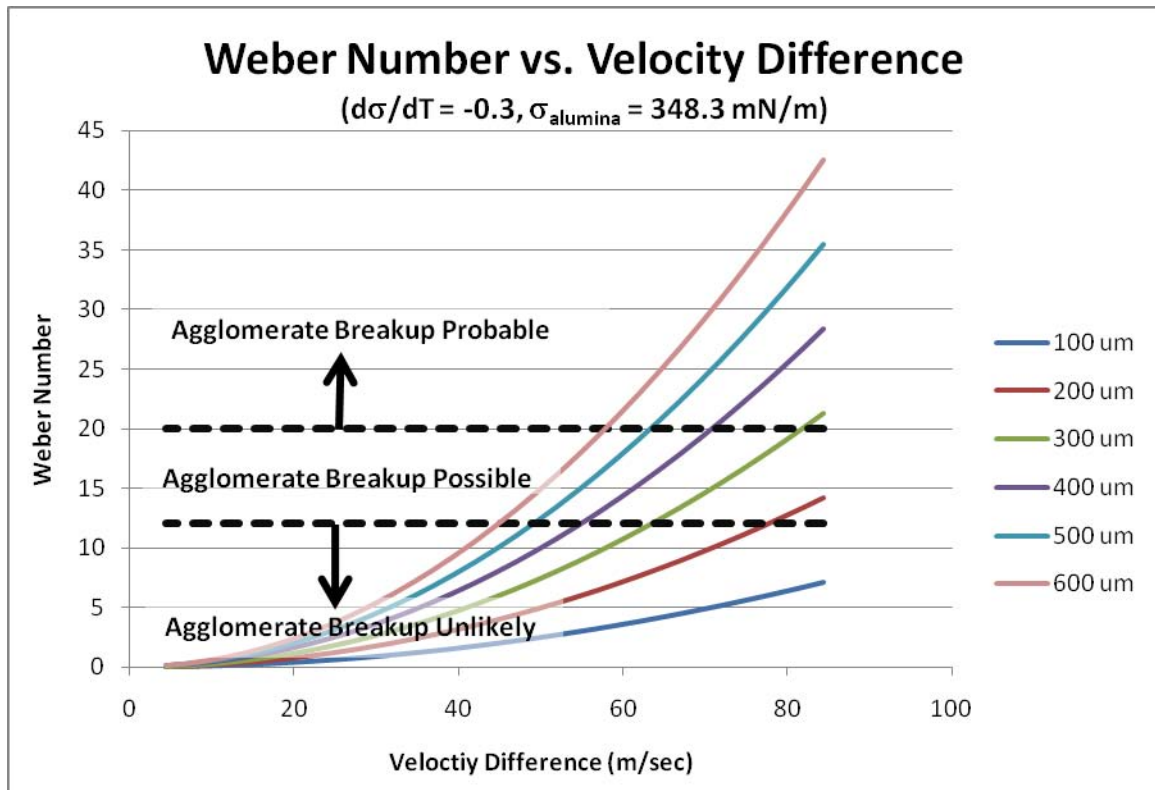


Figure 26. Weber Number vs. Velocity Difference for Various Agglomerate Diameters

Figure 26 shows the Weber numbers for various agglomerate diameters based on a surface tension of 348.3 mN/m. This surface tension has been calculated based on the known surface tension of alumina at the melt point and the projected surface tension temperature variance of -0.3 mN/m*K. Considerable error could be introduced by the surface temperature variance projection. Figure 27 shows the projected upper and lower Weber number bounds based on surface tension variabilities of -0.07 mN/meter*K and -0.52 mN/meter*K that are based on Tin and Gold.

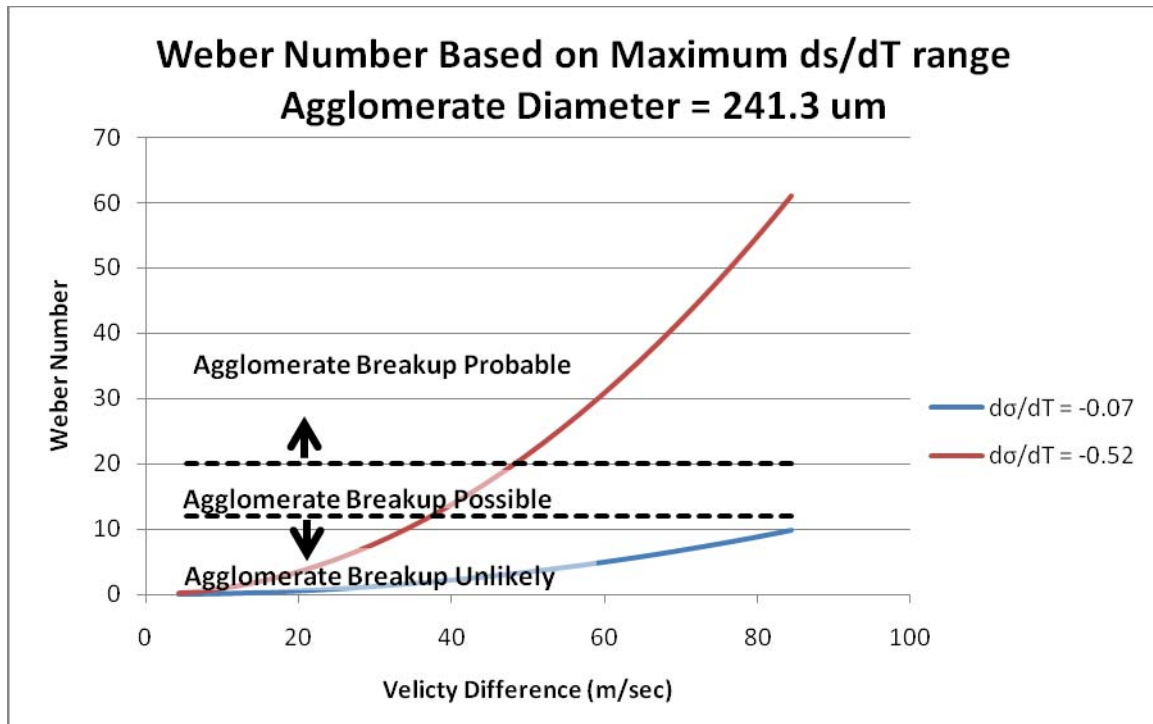


Figure 27. Maximum Weber Number Variability

Based on the Weber calculations and the position of the view window, several agglomerate sizes are predicted to be photographed.

a. Agglomerates Forming in Region A

The agglomerates that form in region A encounter a maximum velocity differential of 28.14 m/sec at ignition. Figure 26 predicts that all agglomerate sizes will survive under these conditions. It is likely that agglomerates forming in region A will acquire sufficient velocity to maintain a velocity differential below the Weber number threshold for breakup. Therefore, all agglomerate sizes originating in region A are expected to be seen in the view window.

Although DeSena's research shows that agglomerate size at formation was generally smaller than 500 μm , it is possible that agglomerates forming in region A could join together to form much larger agglomerates. The Weber number calculations suggest that agglomerates 1000 μm or larger could survive in region A. If they accelerate

through the combustion chamber, it would be possible for the large agglomerates to survive in regions B and C as well due to lower differential velocities based on the preceding acceleration.

b. Agglomerates Forming in Region B

The agglomerates forming in region B will experience a maximum velocity differential of 56.28 m/sec. Under these conditions, the Weber number graph predicts that agglomerates larger than 600 μm will most likely break up. Agglomerates ranging from 400–500 μm will possibly break up and agglomerates 300 μm and less will likely survive. As propellant burning increases the chamber area, however, the velocity differential for newly forming agglomerates drops to just 8.04 m/sec and all agglomerates are once again predicted to survive.

Agglomerate flow, breakup, and/or further agglomeration in region B could be significantly impacted by the entrance of region A agglomerates. The agglomerates forming in region A could have significant velocity when they enter region B. Experimentation is required to observe the outcome of this interaction.

c. Agglomerates Forming in Region C

The view window is located in region C. The agglomerates forming in region C will experience a maximum velocity differential of 84.42 m/sec at ignition. Under these conditions the Weber number graph indicates that only 100 μm agglomerates will survive. Still, agglomerates that formed in regions A and B could have accelerated to the point that their relatively low velocity differential has allowed them to survive. Therefore, even shortly after ignition, it is possible to see large agglomerates in the view window.

As the propellant strand burns and the chamber area increases, larger agglomerate sizes can form and survive in region C. After only 0.5 seconds agglomerates less than 300 μm are predicted to survive, and after 1 second agglomerates smaller than 600 μm can survive. Agglomerate flow from upstream will likely have a significant

impact in region C. It is expected that the large agglomerates of region A will have significant velocity at region C. Experimentation observation will show how the relatively slow moving agglomerates in region C interact with the large and fast moving agglomerates originating in region A and B.

B. RESULTS

The calibration grain was tested using the experimental setup and procedure described in this thesis. During the calibration run, the laser was pulsed at 10,000 Hz. The camera shutter speed was set at 1000 frames per second with a 2 μ sec exposure time. The ignition torch was lit using a mixture of 3% hydrogen and 97% air, which provides a combustion temperature of 2443 K. The ignition torch on time was varied from two to four seconds during a total of four calibration runs. Hydrogen and air mass flow rates were set to provide a slab burner chamber pressure of 1.38 MPA (200 psia). Figure 28 shows still photographs captured during the calibration grain burn. The 122 μ m alumina particles can be clearly distinguished.

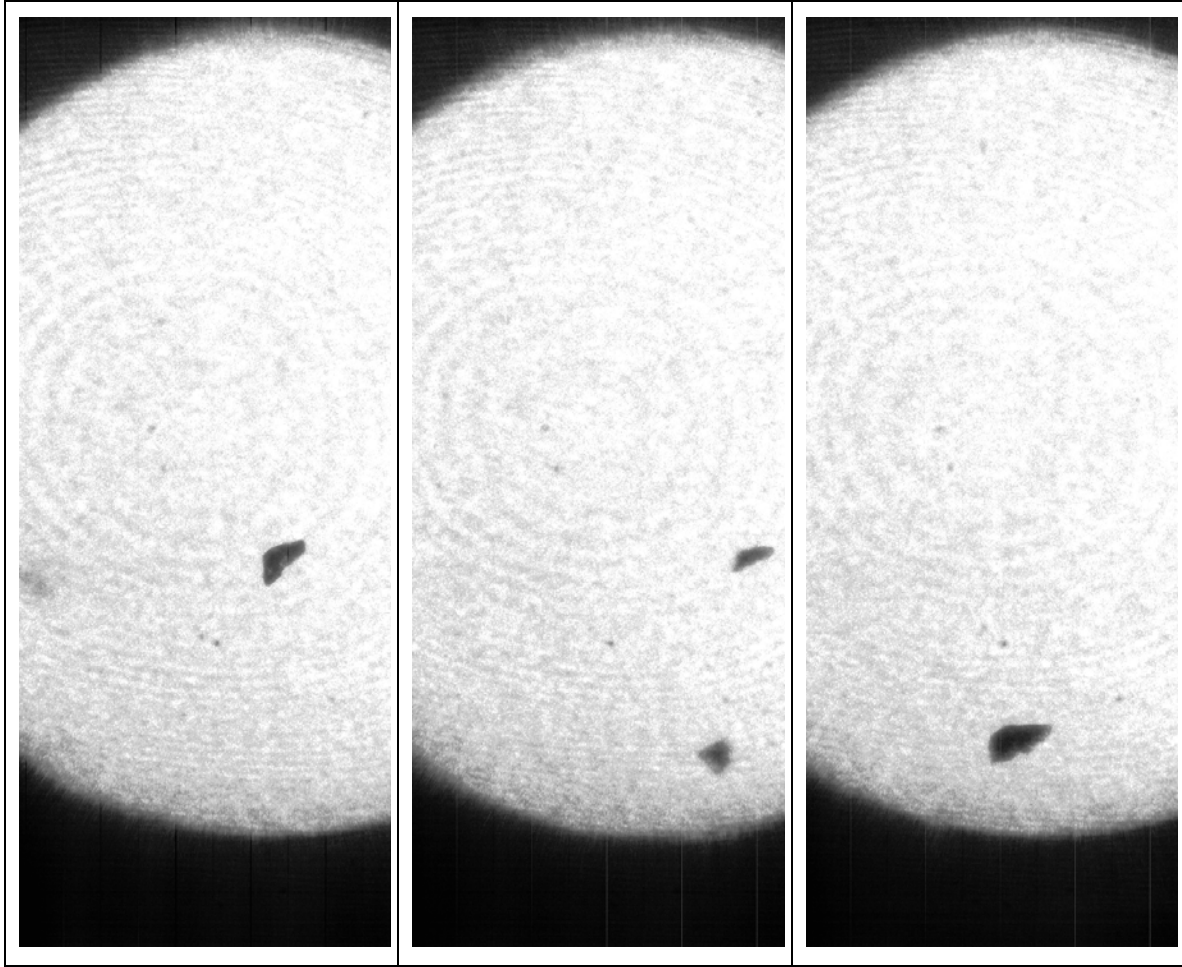


Figure 28. Calibration Grain Photographs

Using the continuity equation, the velocity of the gas from the ignition torch during the calibration runs was calculated to be 180 m/sec at the view window where the torch gas mass flow rate is 6×10^{-3} kg/sec, the torch gas density at 1.38 MPA (200 psia) is 0.8185 kg/m³, and the cross sectional area is 40 mm² (0.25 x 0.25 inches). The resulting Reynolds number is 1160, so the drag coefficient can be calculated using $C_D = 0.271 Re_D^{0.217}$. The drag coefficient on the alumina particles is 1.25 and the resulting force can be calculated using $F = 0.5 C_D \rho_g (u_g - u_{alumina})^2 \left(\frac{\pi}{4} \right) d_{alumina}^2$. The resulting force is 2×10^{-4} N. Applying dynamic equations of motion, the alumina velocity at the view window can be estimated at 50 m/sec.

V. SUMMARY AND CONCLUSIONS

Due to the difficulties in modeling two phase flow and the unpredictability of agglomerate size formation, it is extremely difficult to analytically predict what will happen during actual propellant combustion. The potential for agglomerate interaction further complicates this problem. Basic predictions have been made during this thesis research, but many questions remain. In particular, any error in the assumptions used to estimate the surface tension temperature variability of alumina will have an impact on Weber number calculations. This could cause significant variation between the predicted and actual results from propellant testing. Observation of actual agglomerate behavior through propellant testing is required to fully characterize agglomerate behavior in the combustion channel.

The experimental method and experimental setup developed by this thesis is capable of imaging alumina agglomerate flow in a combustion channel. Imaging of a calibration grain was successfully conducted. Specifically, 122 μm alumina particles were photographed in the slab burner assembly in a smoky environment at a velocity of 50 m/sec. The results of camera calibration suggest that agglomerates as small as 30 μm will be detectable in the combustion chamber. Based on the expected agglomerate size as reported in DeSena's thesis the capabilities of the experimental assembly are adequate to provide quality agglomerate imaging during actual propellant testing.

THIS PAGE INTENTIONALLY LEFT BLANK

APPENDIX A: STANDARD OPERATING PROCEDURE

Standard Operating Procedure (25 May 2010)

Test Cell #3

Slab Burner Solid Propellant Testing

Facility Open Procedure (Start of the Day)

1. Lab Personnel and Golf Course (x2167 ext #1): NOTIFY OF LIVE TEST
2. Control Console: TURN ON AND ENERGIZE YELLOW WARNING LIGHTS
3. Test Cell #3 table power kill switch located in control room: VERIFY OFF
4. Labview Control Program "TestCell3Control": OPEN ON TC #3 PC
5. Cell Phones or devices producing static electricity: LEAVE IN CONTROL ROOM IN DESIGNATED AREA
6. Class 1.3 Propellant: FOLLOW SOP FOR PROPELLANT REMOVAL FROM GOLAN 5 STORAGE UNIT
7. Copper Vapor Laser: PREPARE LASER FOR OPERATION. ENSURE SHUTTER REMAINS DOWN TO PREVENT EXTERNAL LASING. USE LASER SOP IN TC #4.

Testing Set Up

8. Hydrogen Supply: VERIFY SHUTOFF VALVE AT GAS BOTTLE SHUT
9. Helium Supply Bottle: VERIFY SHUTOFF VALVE AT GAS BOTTLE SHUT
10. Node 4 air: VERIFY TC #3 N4-1 SHUT
11. Shop Air: VERIFY TC #3 SA-1 SHUT
12. Gas manifold in TC #3: VERIFY TC #3 HBV-1, TC #3 HBV-2, TC #3 HBV-3, and TC #3 HBV-4 SHUT
13. NI cabinet power: SWITCH TC #3 NI-1 ON
14. ER 3000 and Transducer Power: SWITCH TC #3 NI-2 ON
15. Pressure Transducers: VERIFY HYDROGEN AND HELIUM PRESSURE TRANSDUCERS ARE ELECTRICALLY CONNECTED
16. Laser Mirrors: VERIFY ALIGNMENT AND CLEANLINESS
17. Propellant Transportation: VERIFY CLEAR TRANSPORTATION PATH BETWEEN GOLAN 5 AND TC #3.

WARNING: SOLID ROCKET MOTORS CAN IGNITE WITH MINIMAL SPARK

18. Solid Rocket Propellant: TRANSPORT TWO PROPELLANT SLABS FROM THE GOLAN 5 TO TEST CELL #3.
19. Solid Rocket Propellant: INSTALL TWO PROPELLANT SLABS INTO THE FORWARD RECESS OF THE SLAB BURNER.

a. Trim edges as necessary to ensure snug fit. Use propellant blanks as a template.

b. Apply RTV along bottom and edges to control propellant burn area

20. Slab Burner: REASSEMBLE SLAB BURNER

a. Window Assembly: USE SIZE 10 ALLEN HEAD TORQUE WRENCH TO INSTALL WINDOW ASSEMBLY. APPLY 10 IN-LBF OF TORQUE USING A STAR TORQUE PATTERN.

b. Main Assembly: USE 1/4"-20 DRIVER TO SECURE FASTENERS

c. Pressure Transducer: INSTALL HARDWARE AND ELECTRICALLY CONNECT.

d. Helium Purge Lines: MECHANICALLY CONNECT HELIUM SUPPLY TO 2 PORTS

e. Burst Disc: MECHANICALLY CONNECT BURST DISC ASSEMBLY. ENSURE BURST DISC IS RATED TO 1015 PSI.

WARNING: TO PREVENT INADVERTANT IGNITION DO NOT ELECTRICALLY CONNECT IGNITION TORCH!

f. Ignition Torch: MECHANICALLY CONNECT IGNITION TORCH

21. Node-4 Air: OPEN TC #3 N4-1

22. Shop Air: OPEN TC #3 SA-1

23. Hydrogen Supply: OPEN SHUTOFF VALVE AT GAS BOTTLE

24. Helium Supply: OPEN SHUTOFF VALVE AT GAS BOTTLE

25. Hydrogen Supply: OPEN TC #3 HBV-3

26. Leak Check: SNOOP FOR LEAKS. PAY PARTICULAR ATTENTION TO DISTURBED CONNECTIONS.

27. High Speed Camera: VERIFY IMAGE IS DISPLAYED ON CONTROL ROOM MONITOR

28. Non-essential lab personnel: MOVE BEHIND BLAST DOORS

Testing

29. Lab Personnel: CONDUCT HEAD COUNT AND SECURE ENTRY GATE

30. Test Cell #3 Table Power Kill Switch: VERIFY BUTTON IS PRESSED IN.

*******WARNING*******

TEST IS IMMINENT BEYOND THIS STEP

31. Ignition Torch: CONNECT ELECTRICAL POWER

WARNING: USE LASER EYE PROTECTION. LASER LIGHT IS HAZARDOUS TO THE EYES

32. Laser: OPEN LASER SHUTTER AND VERIFY BEAM PATH IS ACCEPTABLE
33. Labview Program "Path": SELECT TARGET FOR OUTPUT FILE
34. Labview Program "H2 Regulator Setting": ADJUST H2 PRESSURE TO APPROPRIATE VALUE
35. Labview Program "HE Regulator Setting": ADJUST HELIUM PRESSURE TO APPROPRIATE VALUE
36. Labview Program "Outgoing Signal": SET Fs (SAMPLE RATE) TO 1000 (HZ) AND SET #s (NUMBER OF SAMPLES) TO 9900.
37. Labview Program Torch On Time (Seconds): SET TORCH ON TIME TO APPROPRIATE VALUE.
38. Golf Course: VERIFY CLEAR
39. Flashing Yellow Light: VERIFY ON
40. Siren and red perimeter/alley warning lights: SWITCH ON
41. Test Cell #3 table power kill switch: SWITCH ON
42. Labview Program: RUN
43. Labview Program "Enable Cell" Switch: MOVE TO ON
44. Labview Program "H2 Supply WBV": MOVE TO ON
45. Labview Program "HE Supply WBV": MOVE TO ON

**WARNING: THE FOLLOWING STEP WILL COMMENCE AN AUTOMATED
IGNITION SEQUENCE**

46. Labview Program "Start" Button: MOVE TO ON.

Test Complete

WARNING: METAL COMPONENTS MAY BE HOT

47. Test Cell #3 table power kill switch: OFF
48. Siren: OFF
49. Laser: PLACE BEAM STOP CLOSED
50. Ignition Torch: DISCONNECT POWER SUPPLY
51. High Speed Camera: POWER OFF
52. Hydrogen Supply: SHUT TC#3 HBV-3
53. Helium Supply: SHUT SHUTOFF VALVE AT GAS BOTTLE
54. Hydrogen Supply: SHUT SHUTOFF VALVE AT GAS BOTTLE
55. Node-4 Air: SHUT TC#3 N4-1
56. Shop Air: SHUT TC#3 SA-1
57. Residual Line Pressure: ENSURE LINES ARE BLED THROUGH VENT LINES

THIS PAGE INTENTIONALLY LEFT BLANK

APPENDIX B: ENGINEERING DRAWINGS

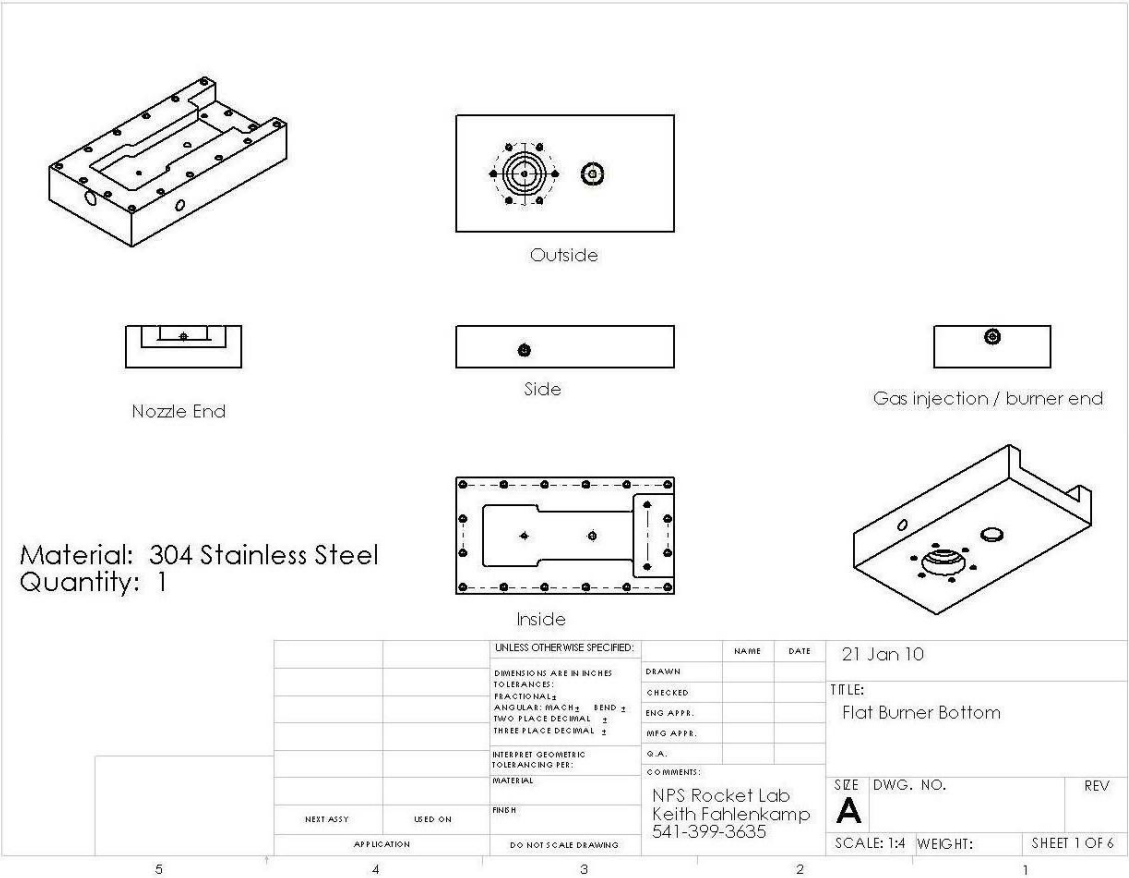


Figure 29. Flat Burner Bottom Sheet 1 of 6

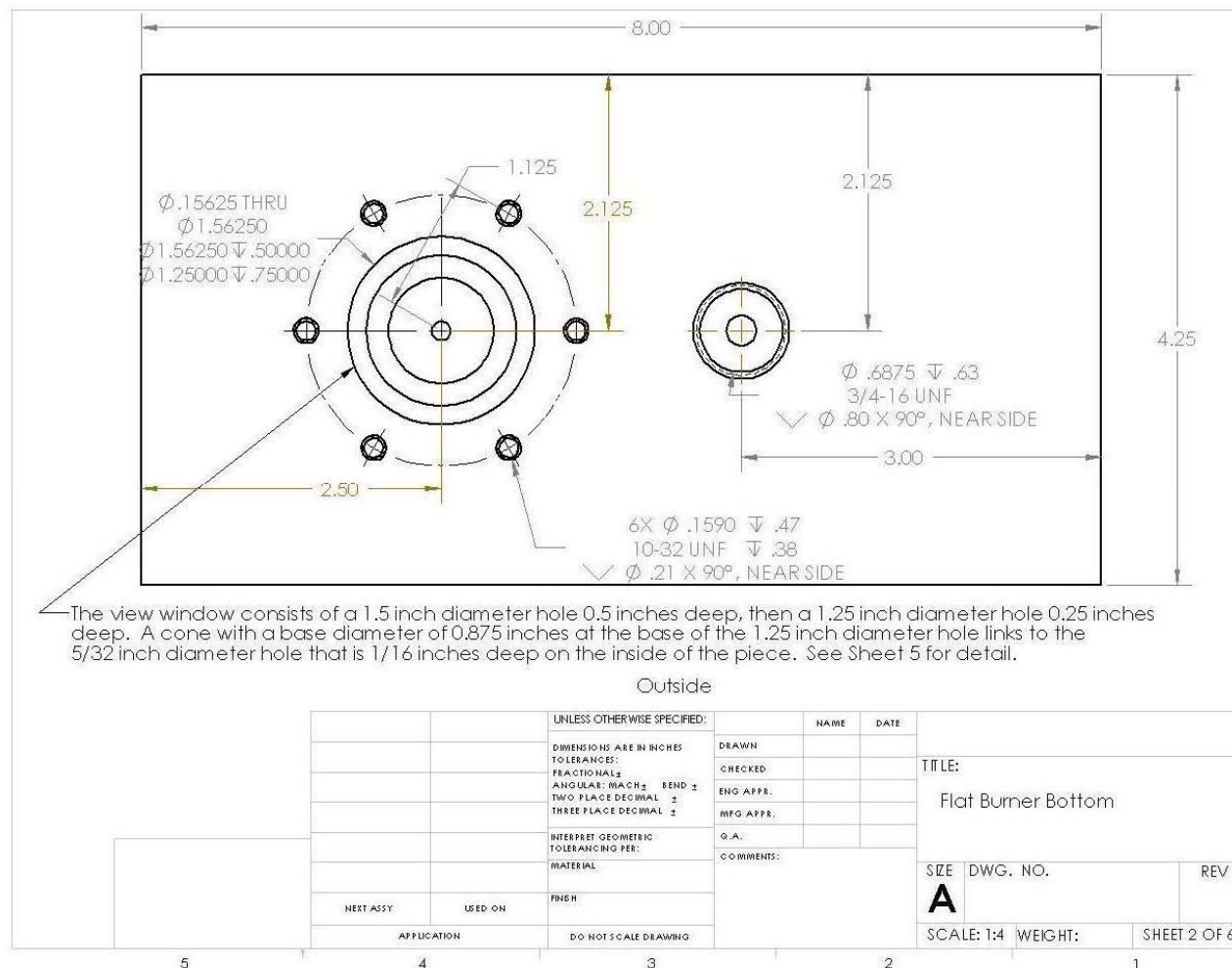


Figure 30. Flat Burner Bottom Sheet 2 of 6

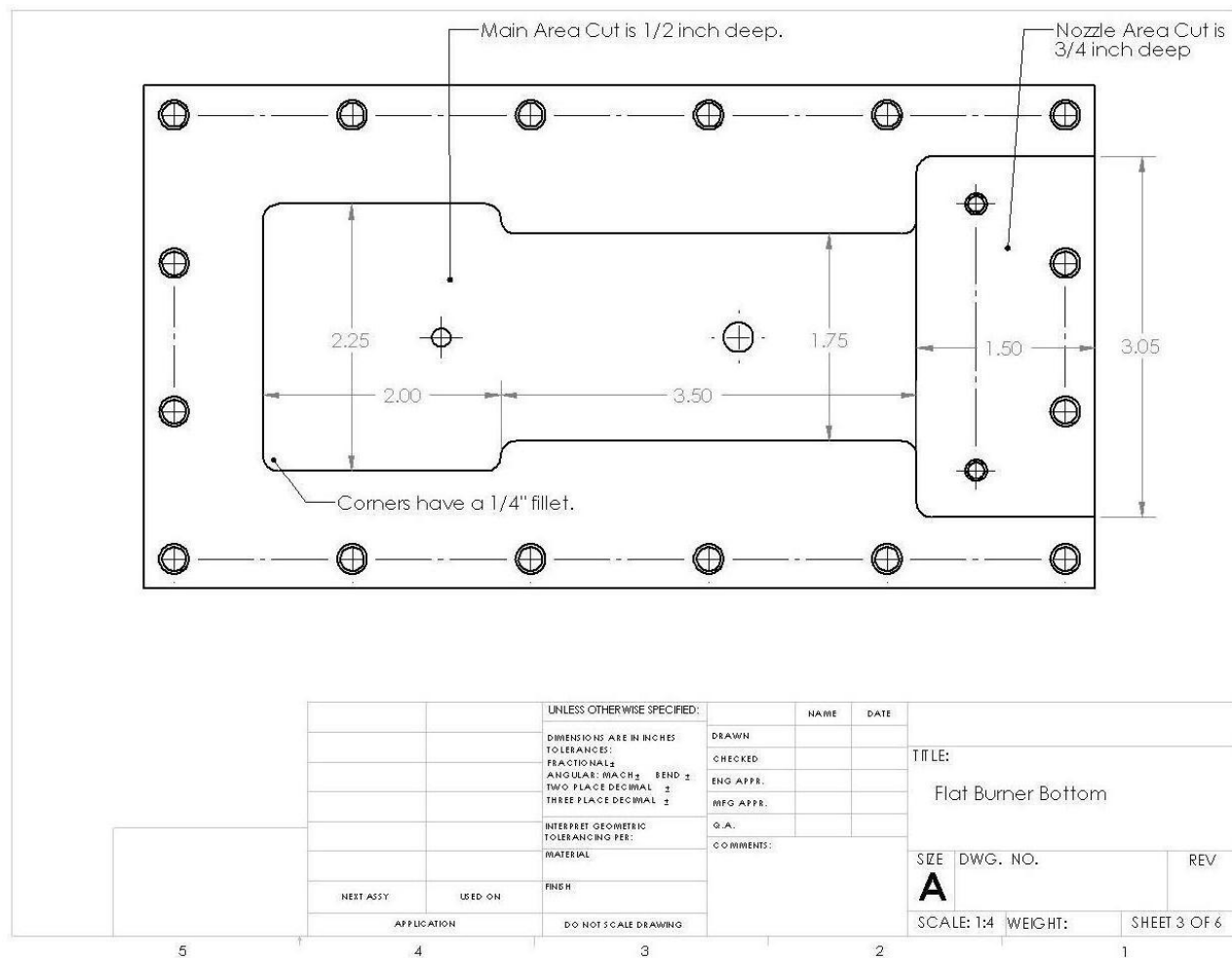


Figure 31. Flat Burner Bottom Sheet 3 of 6

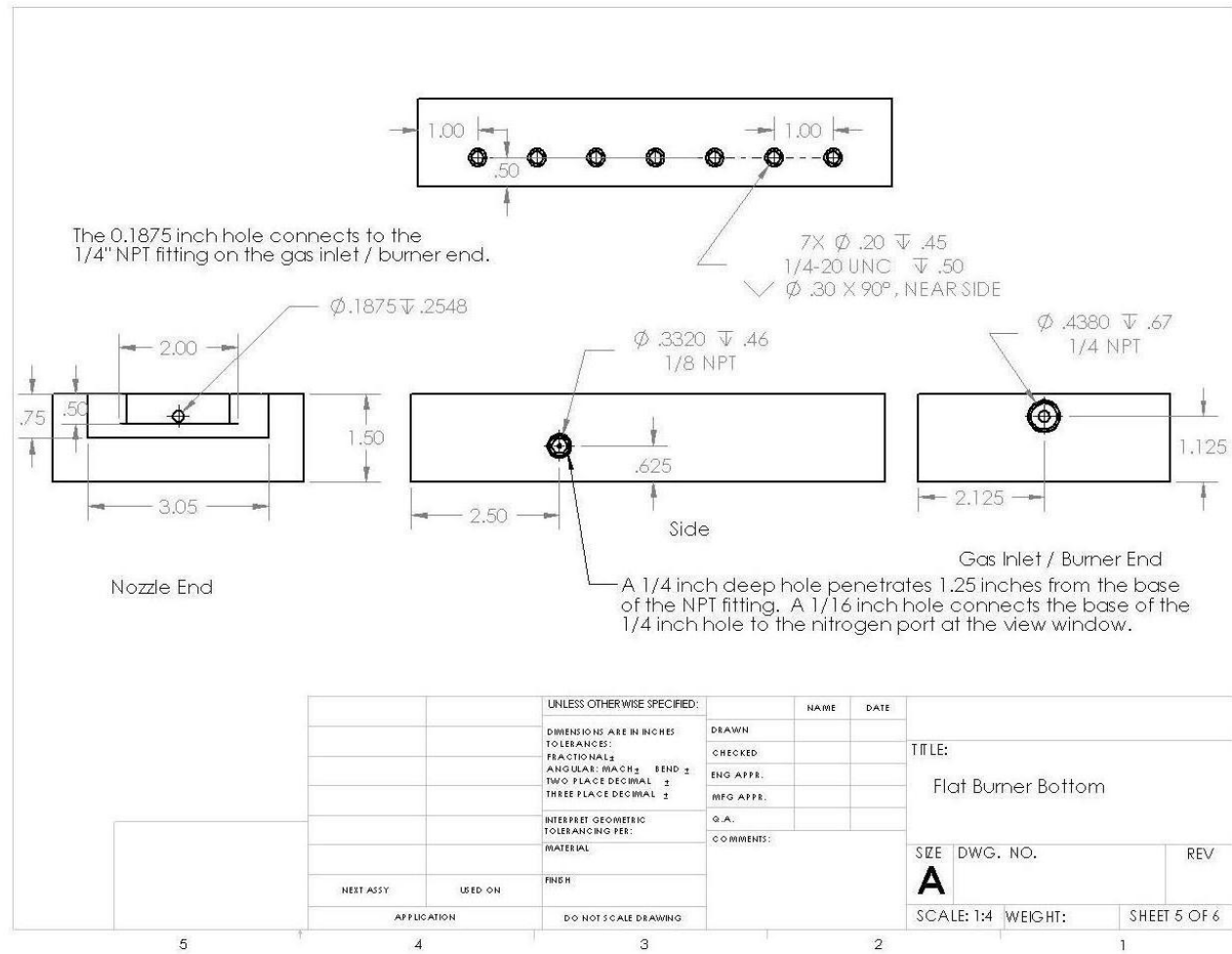


Figure 33. Flat Burner Bottom Sheet 5 of 6

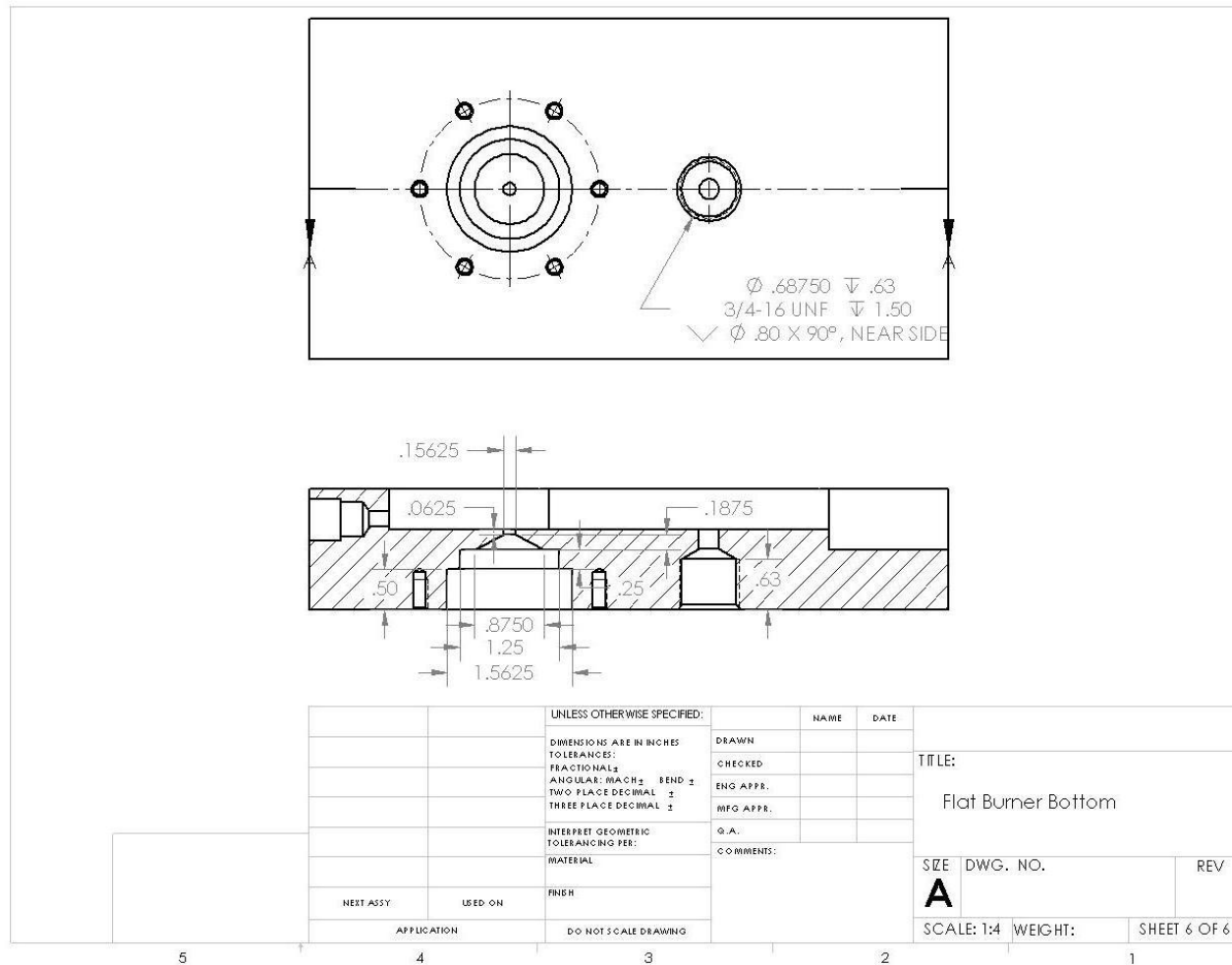


Figure 34. Flat Burner Bottom Sheet 6 of 6

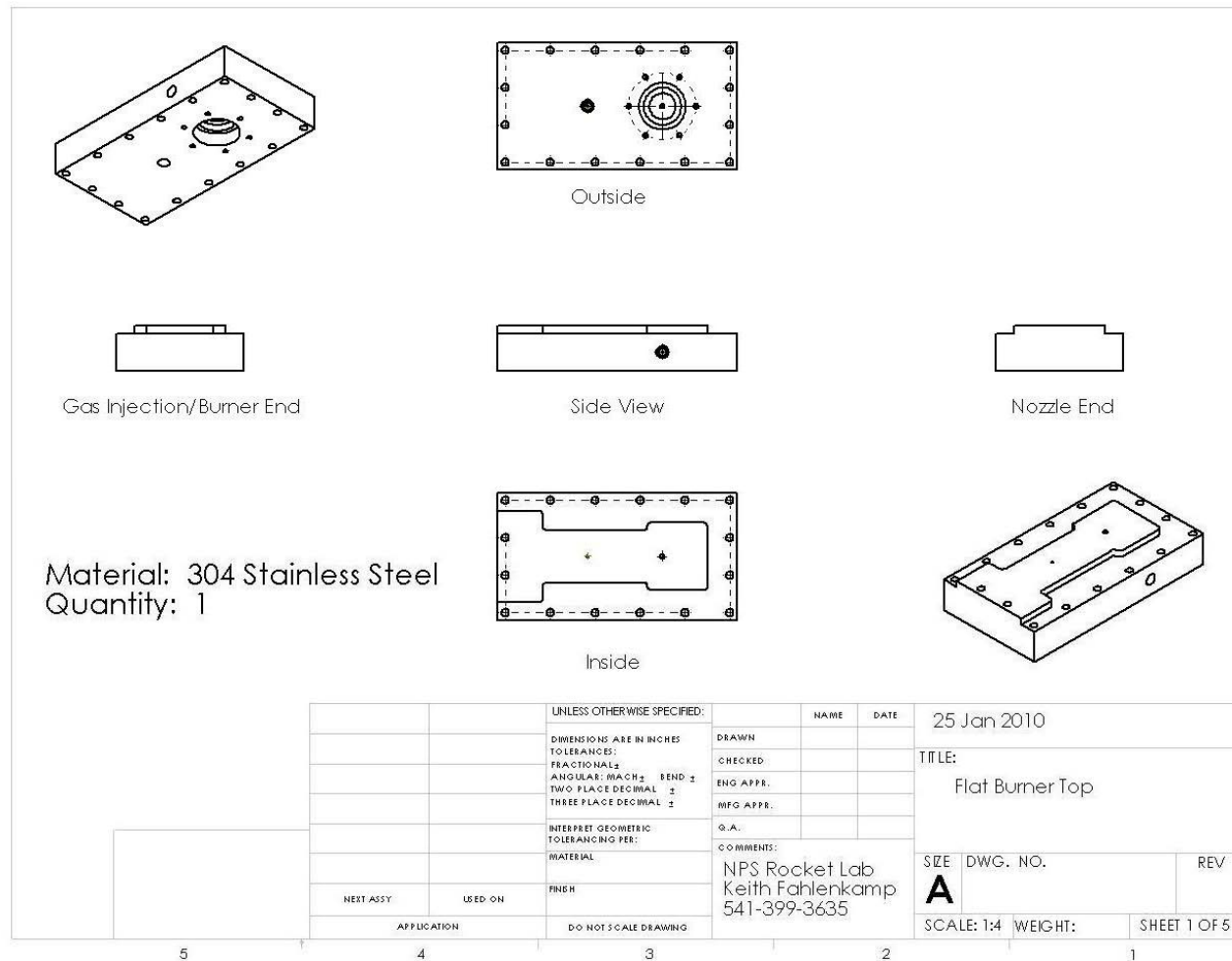


Figure 35. Flat Burner Top Sheet 1 of 5

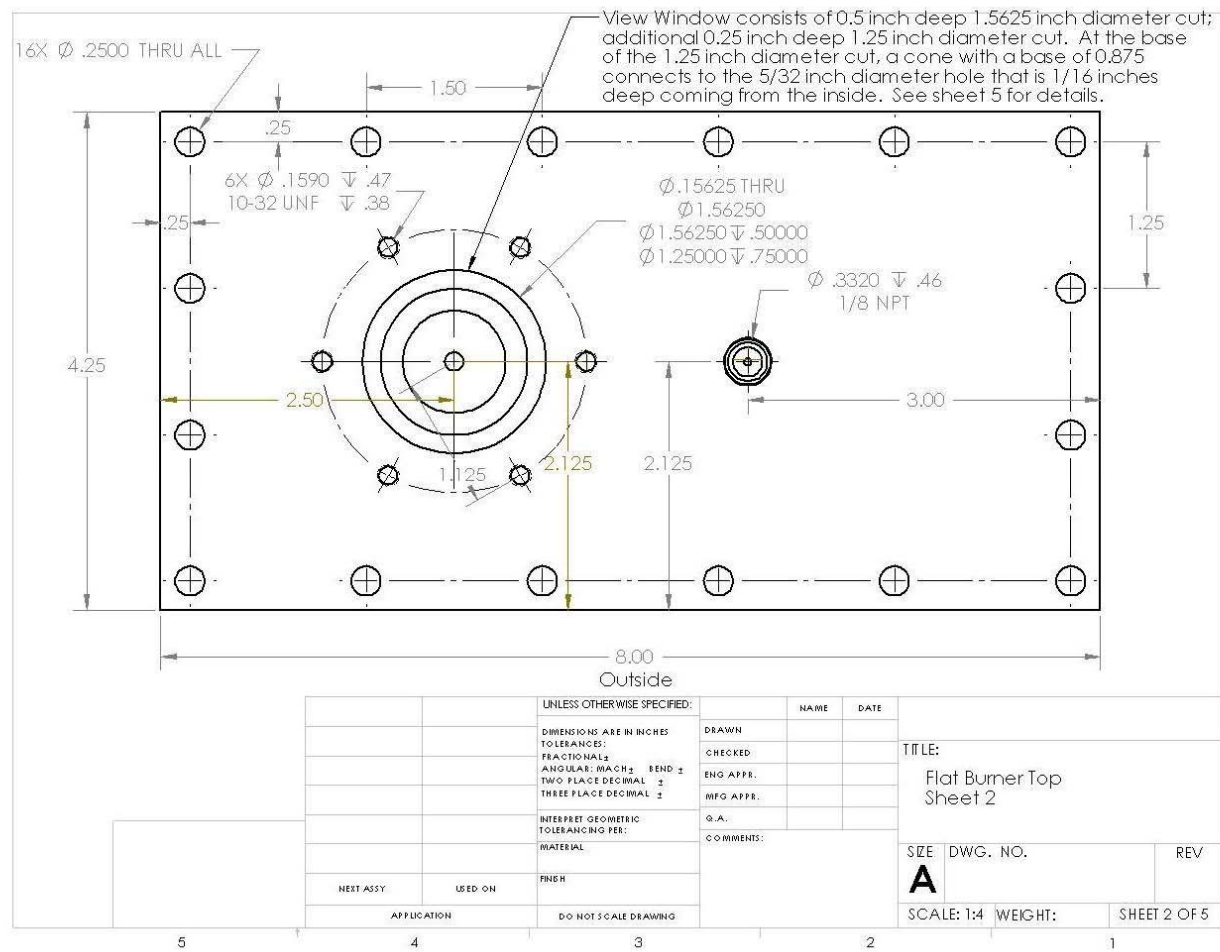


Figure 36. Flat Burner Top Sheet 2 of 5

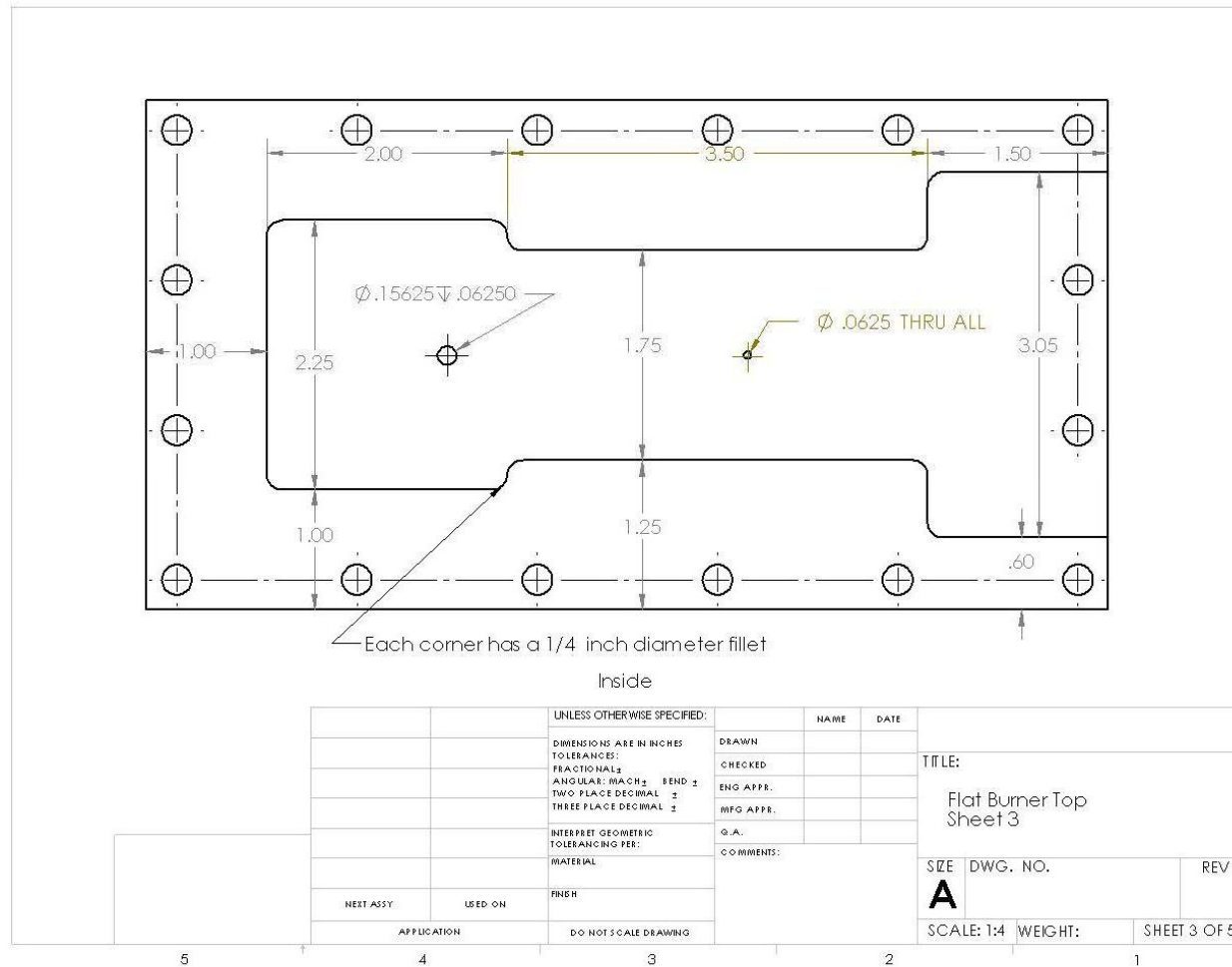


Figure 37. Flat Burner Top Sheet 3 of 5

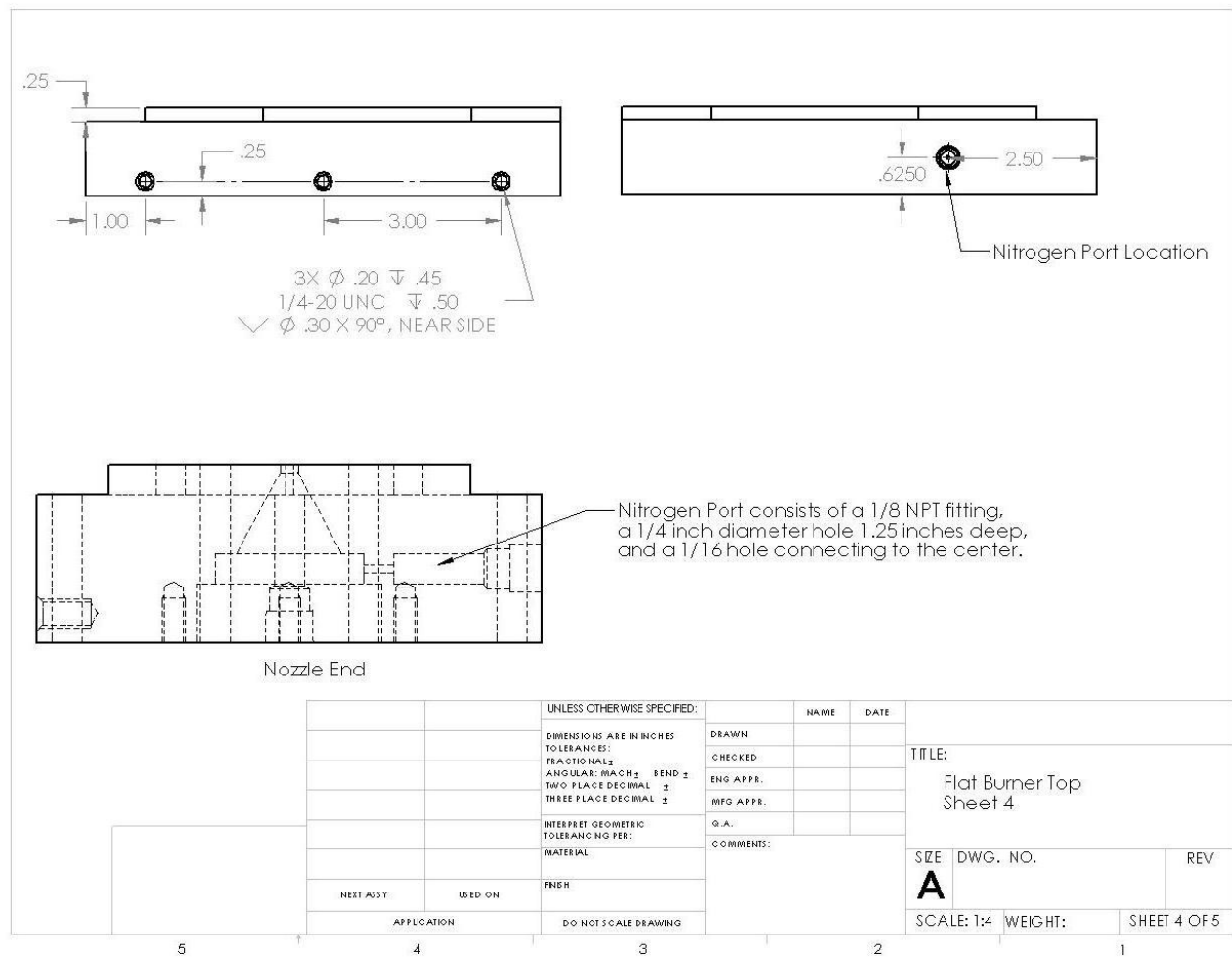


Figure 38. Flat Burner Top Sheet 4 of 5

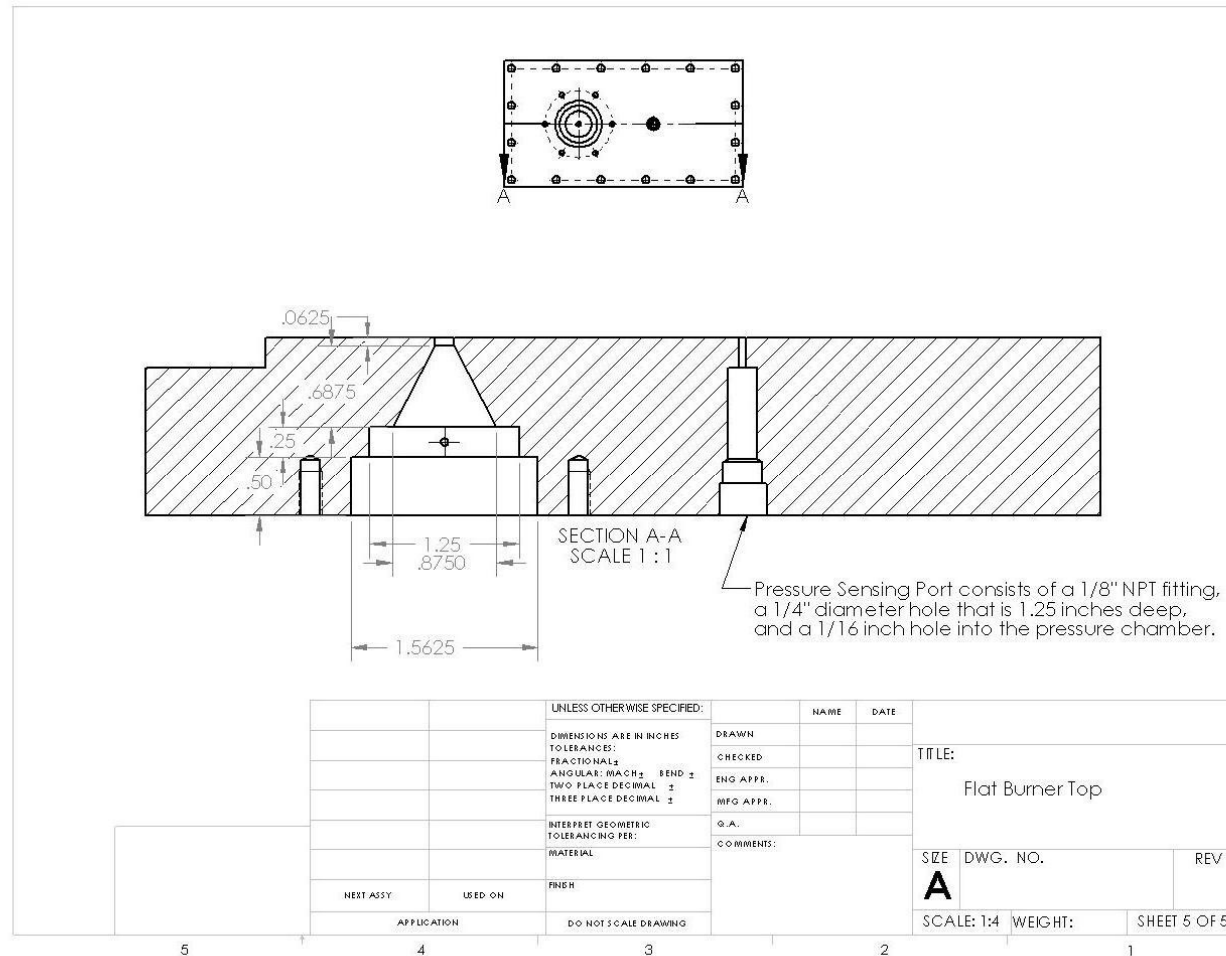
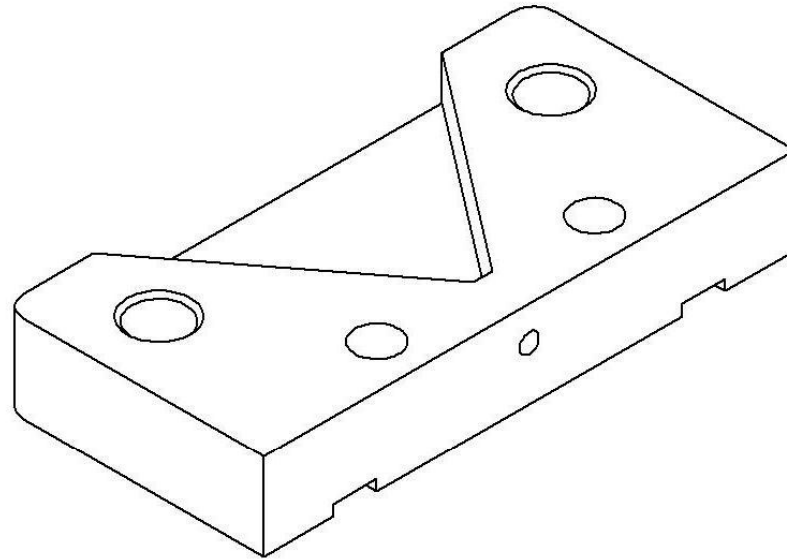


Figure 39. Flat Burner Top Sheet 5 of 5



Material: 304 Stainless Steel
Quantity: 2 (One without exit hole drilled)

		UNLESS OTHERWISE SPECIFIED:		NAME	DATE	25 Feb 2010
		DIMENSIONS ARE IN INCHES TOLERANCES:		DRAWN		
		FRACTIONAL \pm		CHECKED		
		ANGULAR: MACH \pm BEND \pm		ENG APPR.		
		TWO PLACE DECIMAL \pm		MFG APPR.		
		THREE PLACE DECIMAL \pm		G.A.		
		INTERPRET GEOMETRIC TOLERANCING PER:		COMMENTS:		
		MATERIAL		NPS Rocket Lab Keith Fahlenkamp 541-399-3635		
		FINISH		SIZE	DWG. NO.	REV
NEXT ASSY	USED ON			A		
APPLICATION		DO NOT SCALE DRAWING		SCALE: 1:1	WEIGHT:	SHEET 1 OF 2

Figure 40. Flat Burner Nozzle Sheet 1 of 2

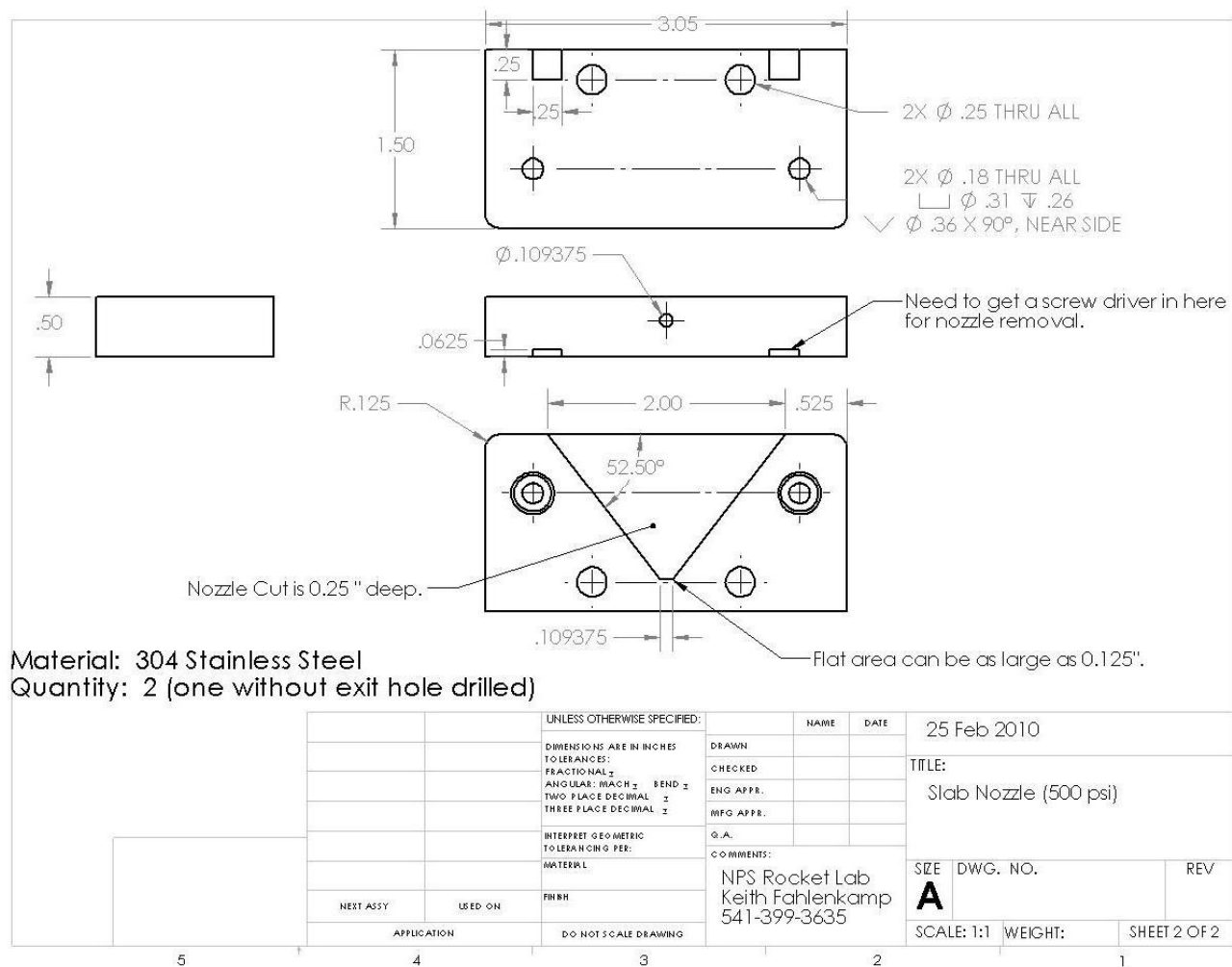


Figure 41. Flat Burner Nozzle Sheet 2 of 2

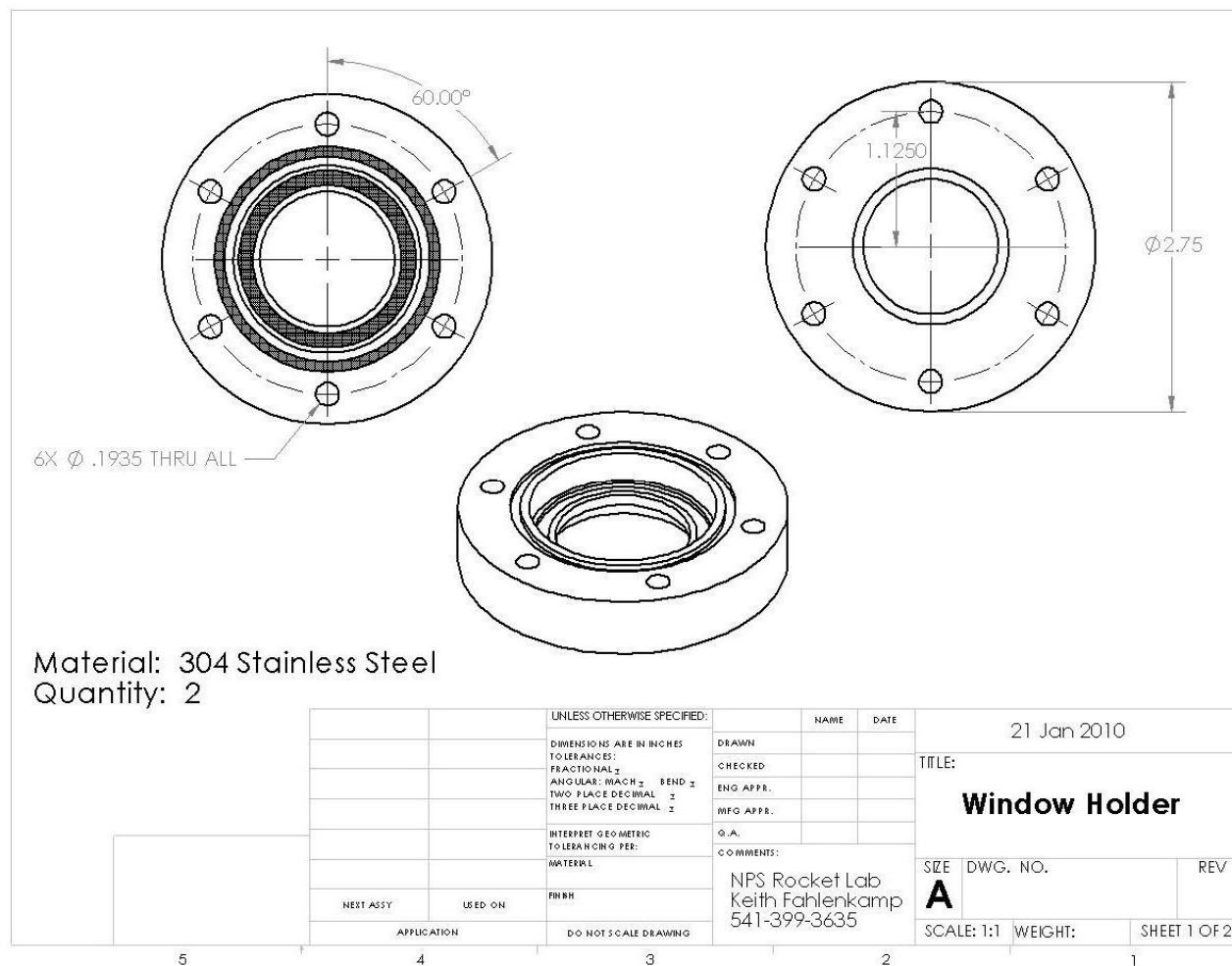


Figure 42. Window Holder Sheet 1 of 2

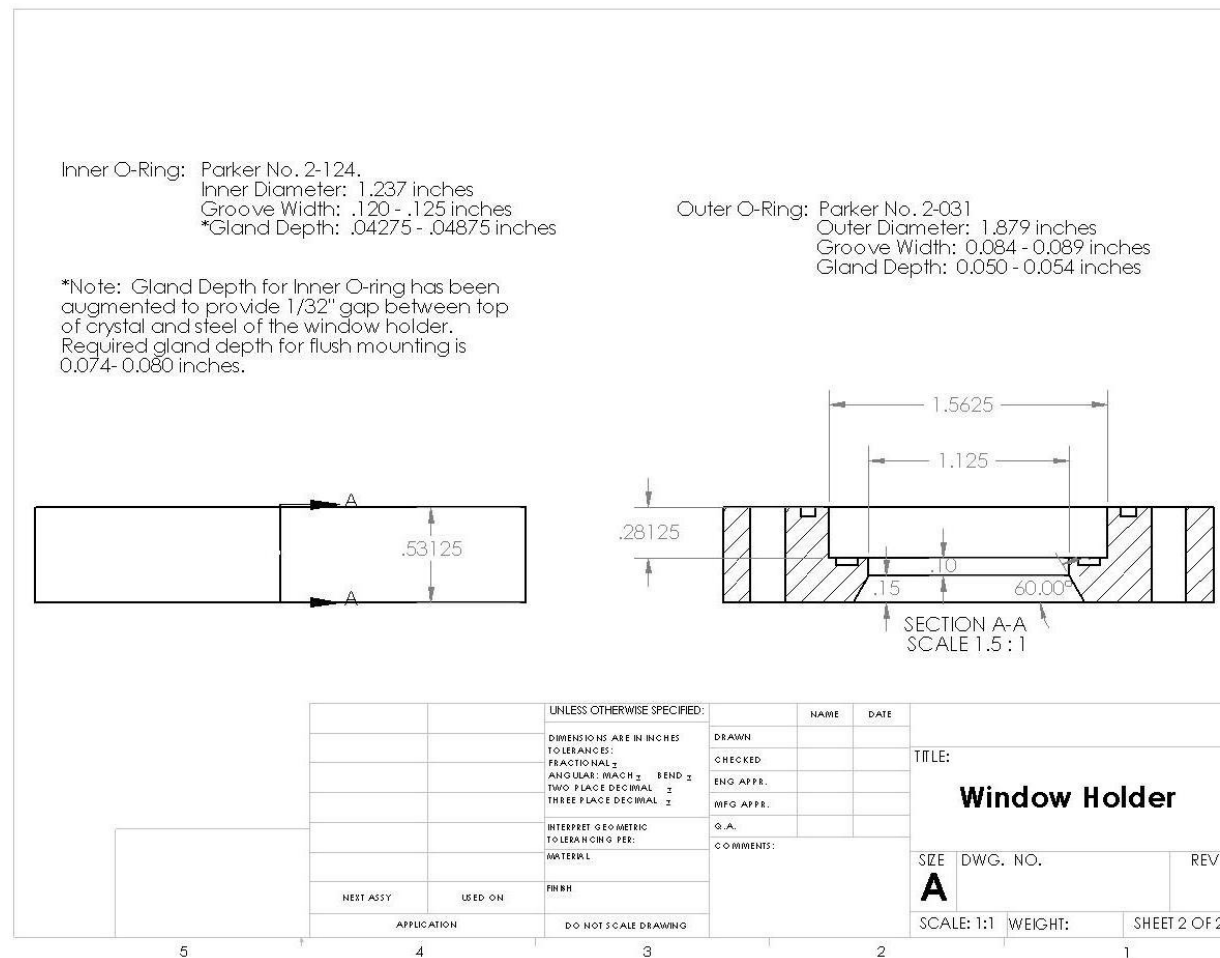


Figure 43. Window Holder Sheet 2 of 2

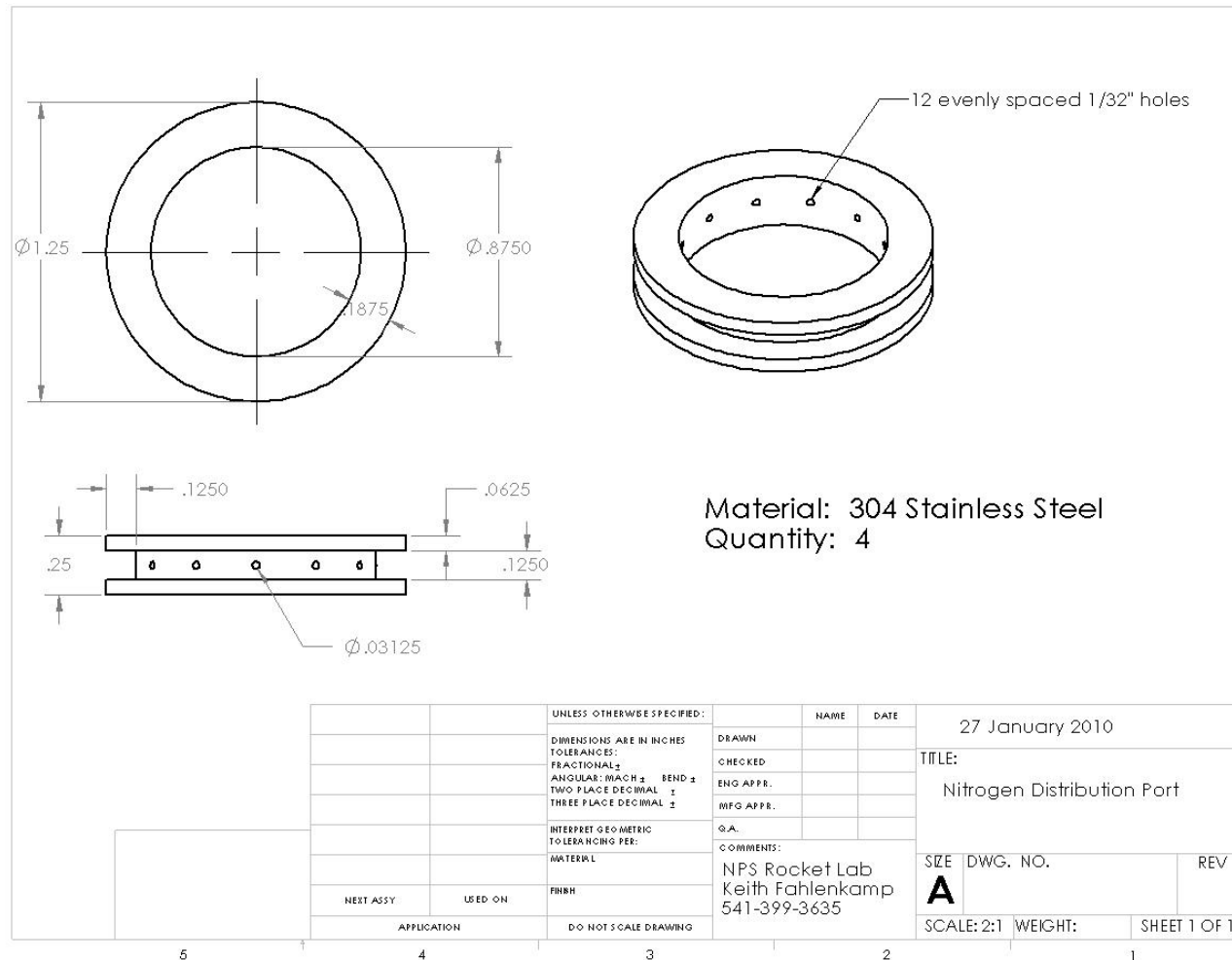


Figure 44. Nitrogen Distribution Port Sheet 1 of 1

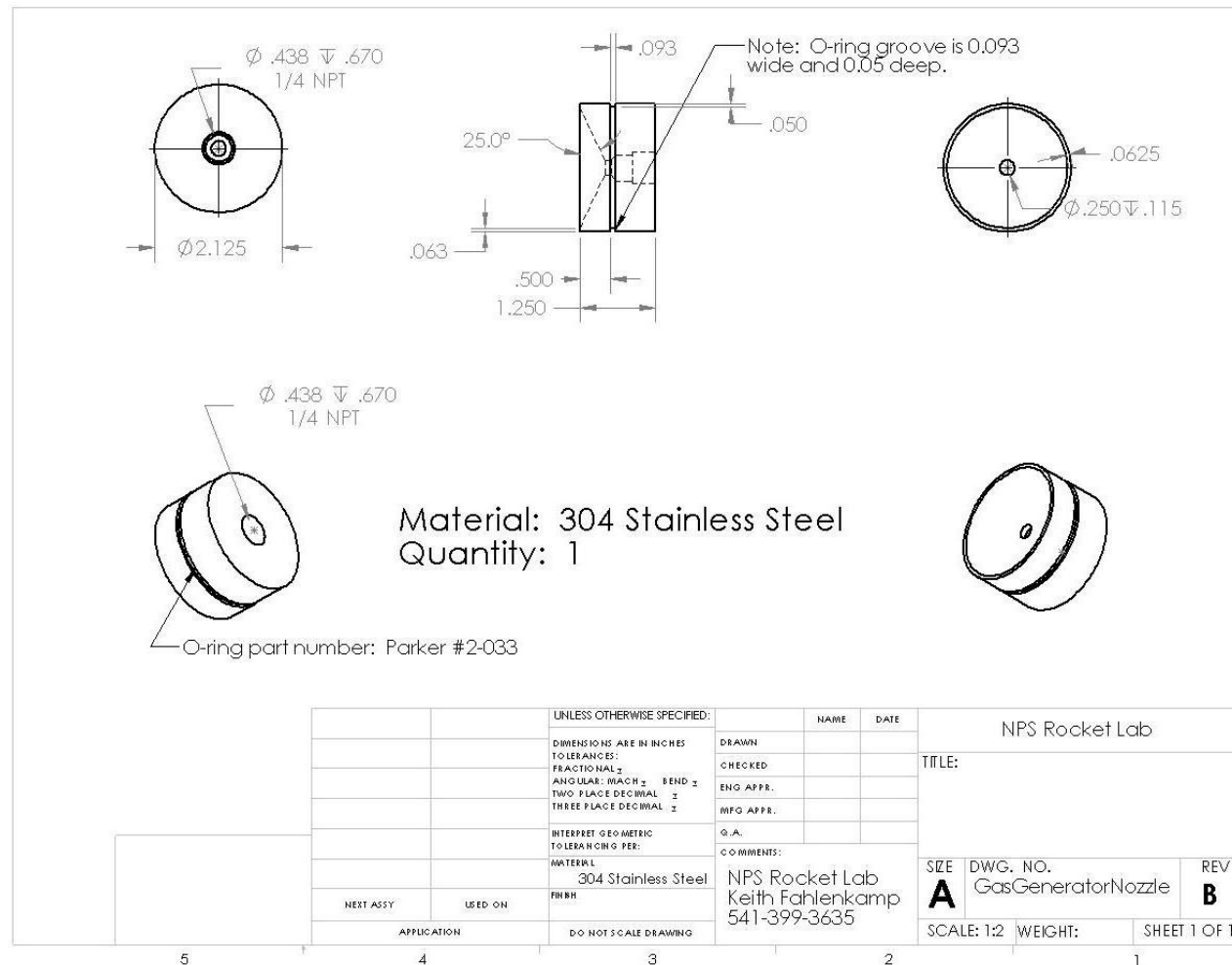


Figure 45. Gas Generator Nozzle Sheet 1 of 1

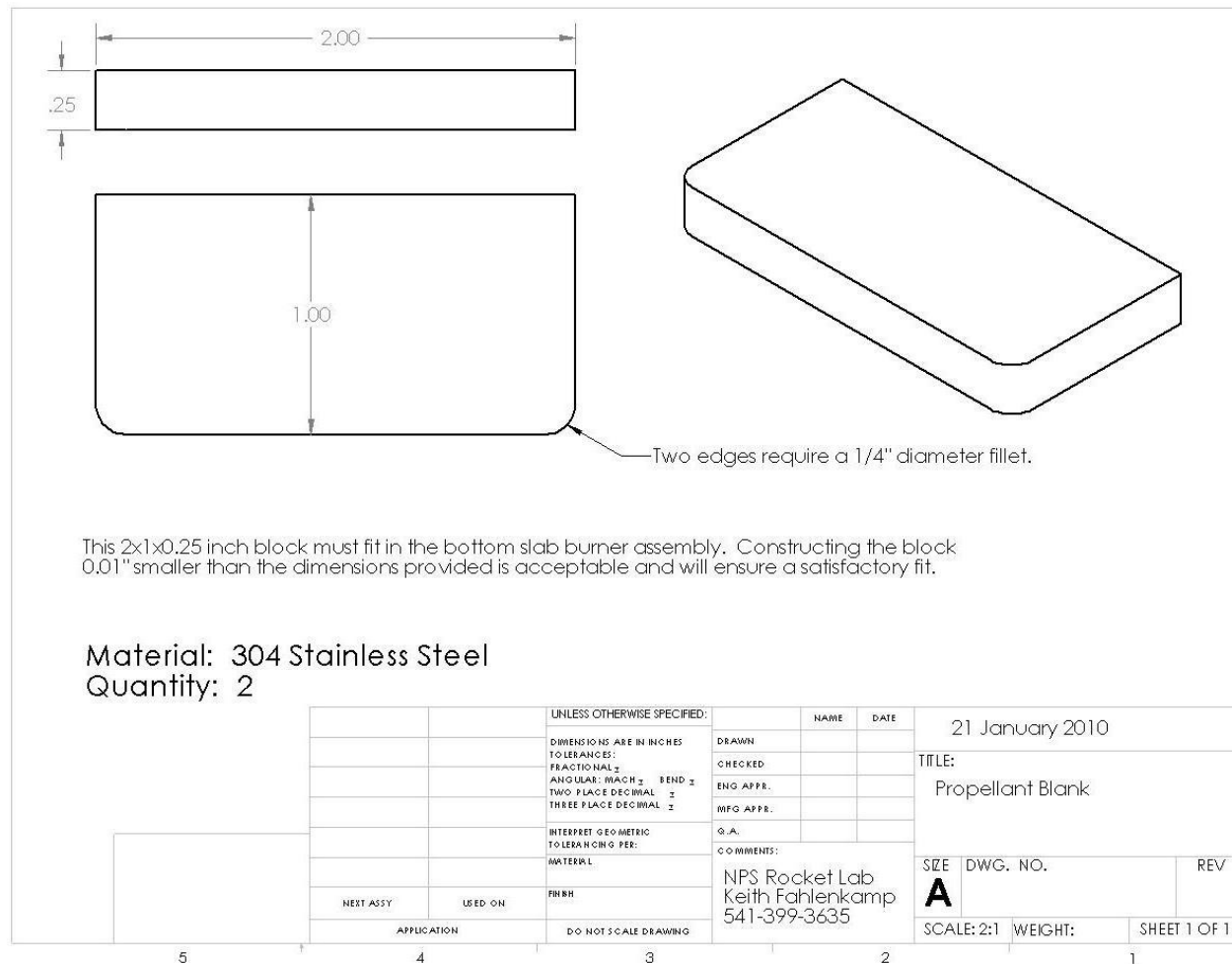


Figure 46. Propellant Blank Sheet 1 of 1

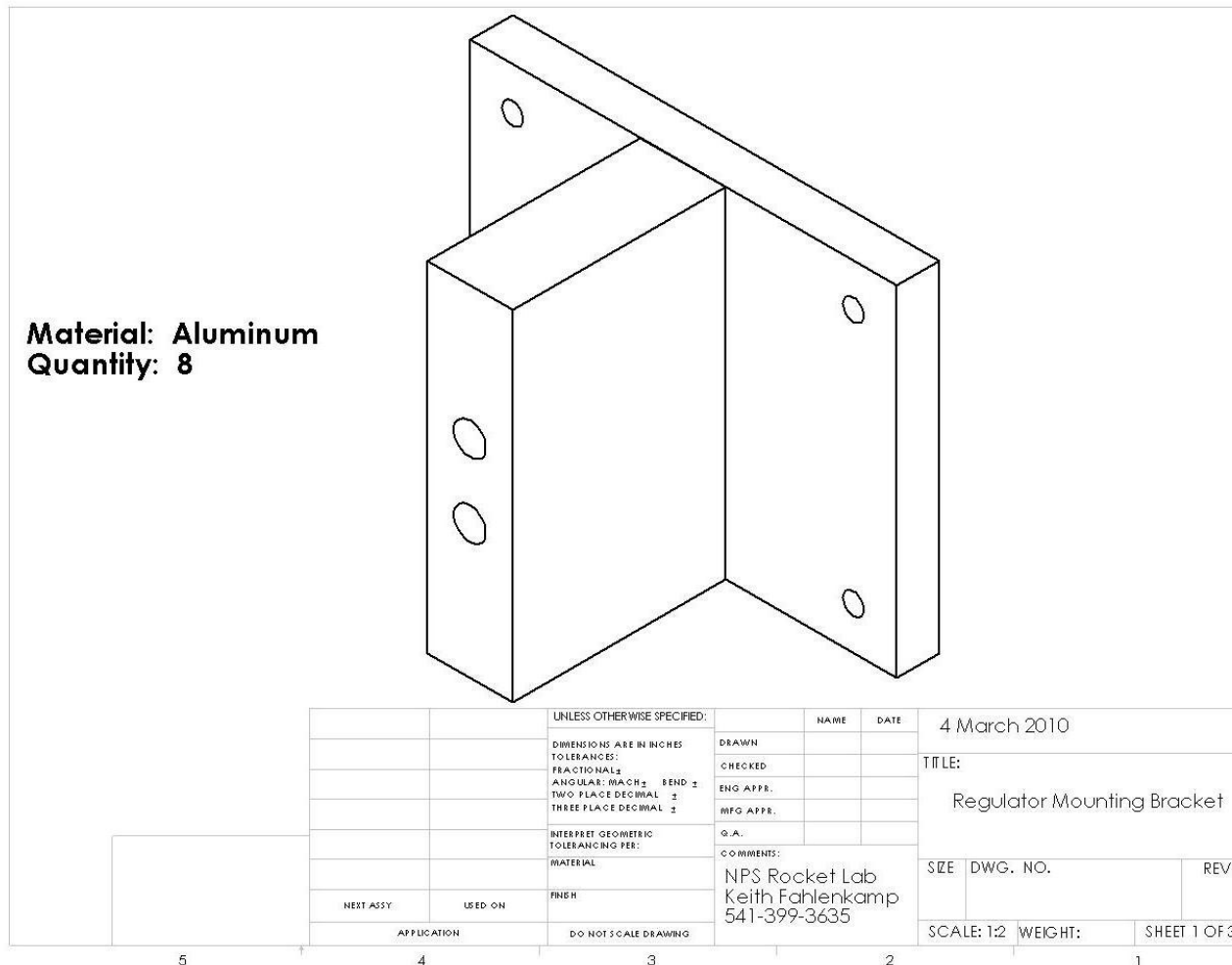


Figure 47. Regulator Mounting Bracket Sheet 1 of 3

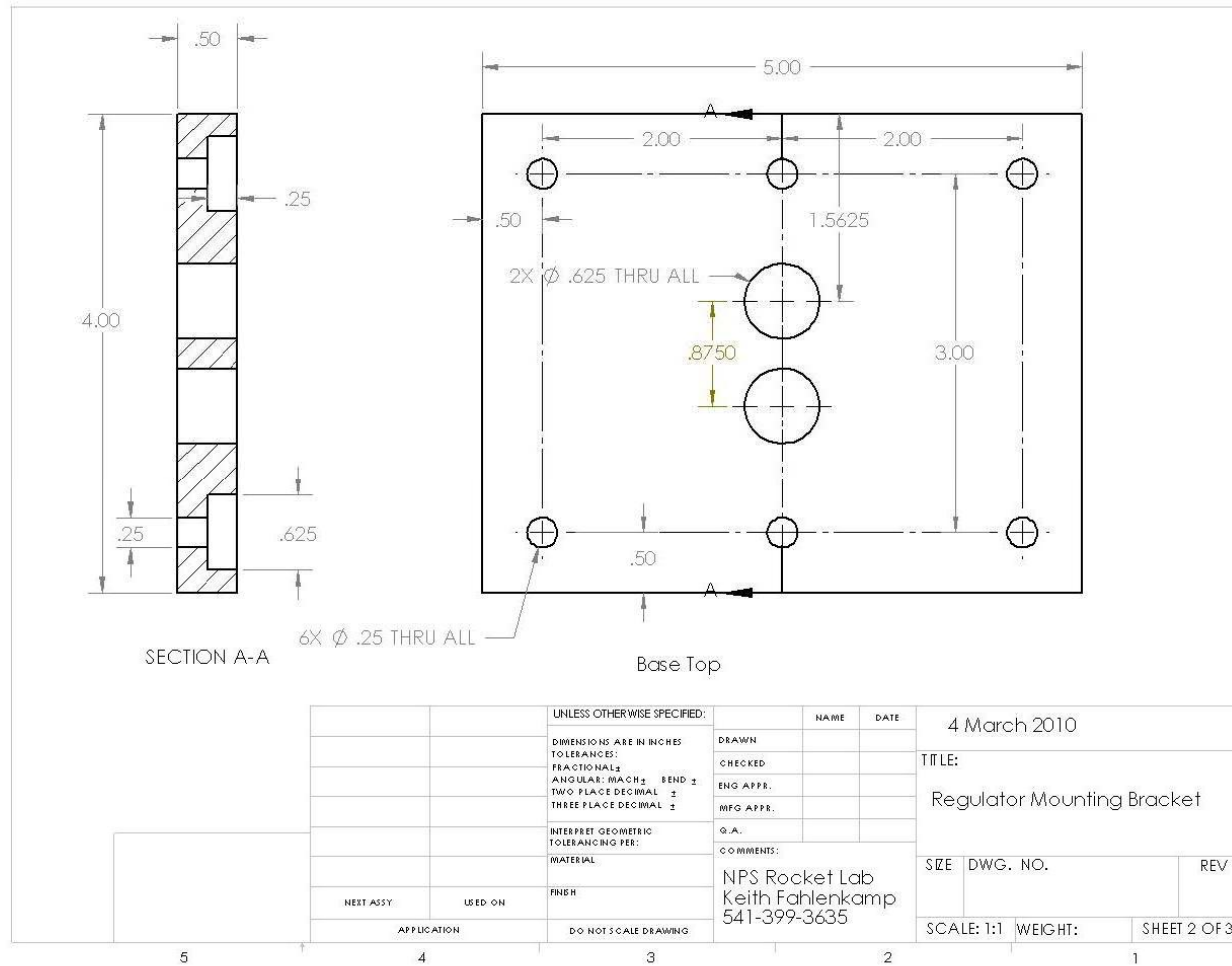


Figure 48. Regulator Mounting Bracket Sheet 2 of 3 (Base)

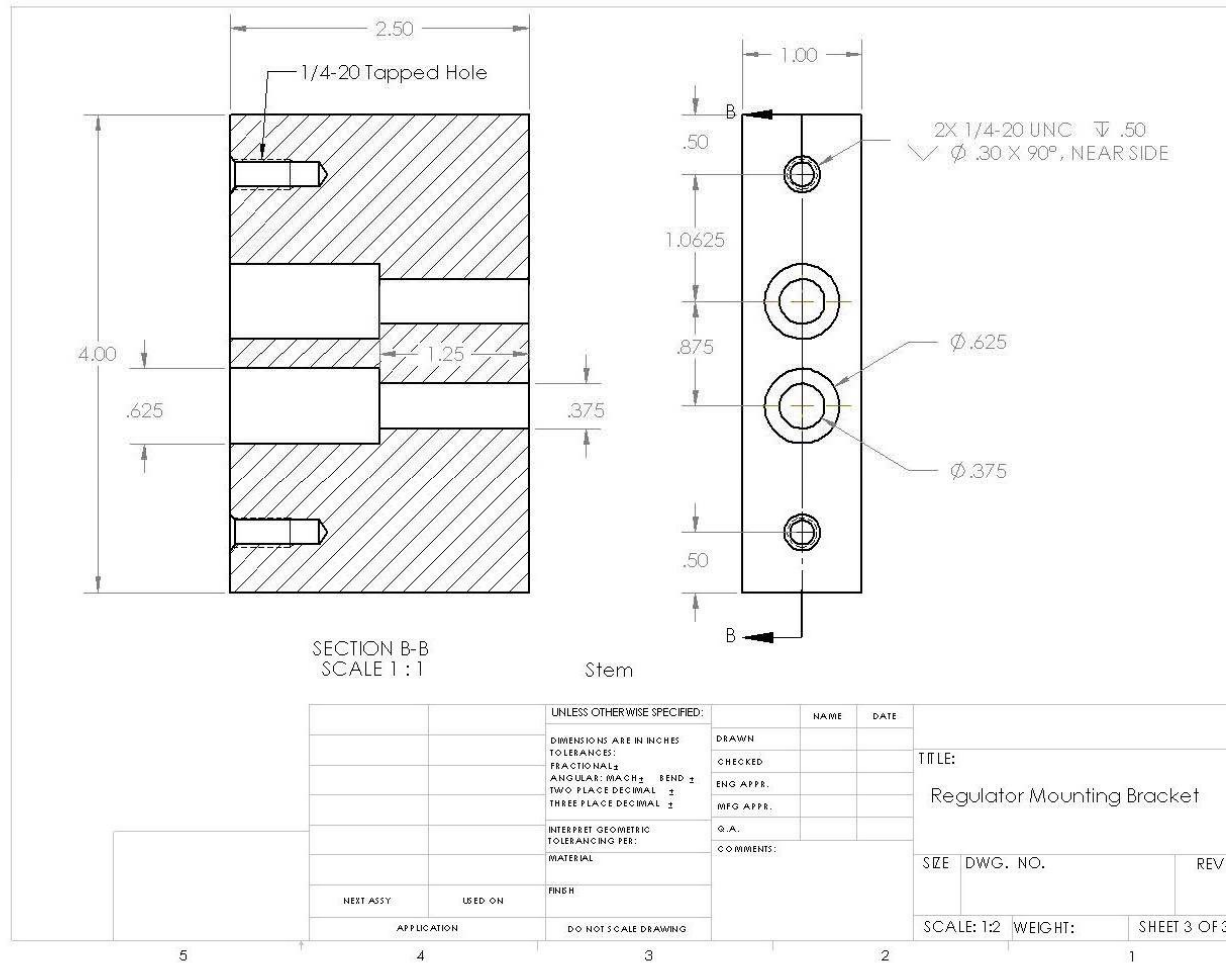


Figure 49. Regulator Mounting Bracket Sheet 3 of 3 (Stem)

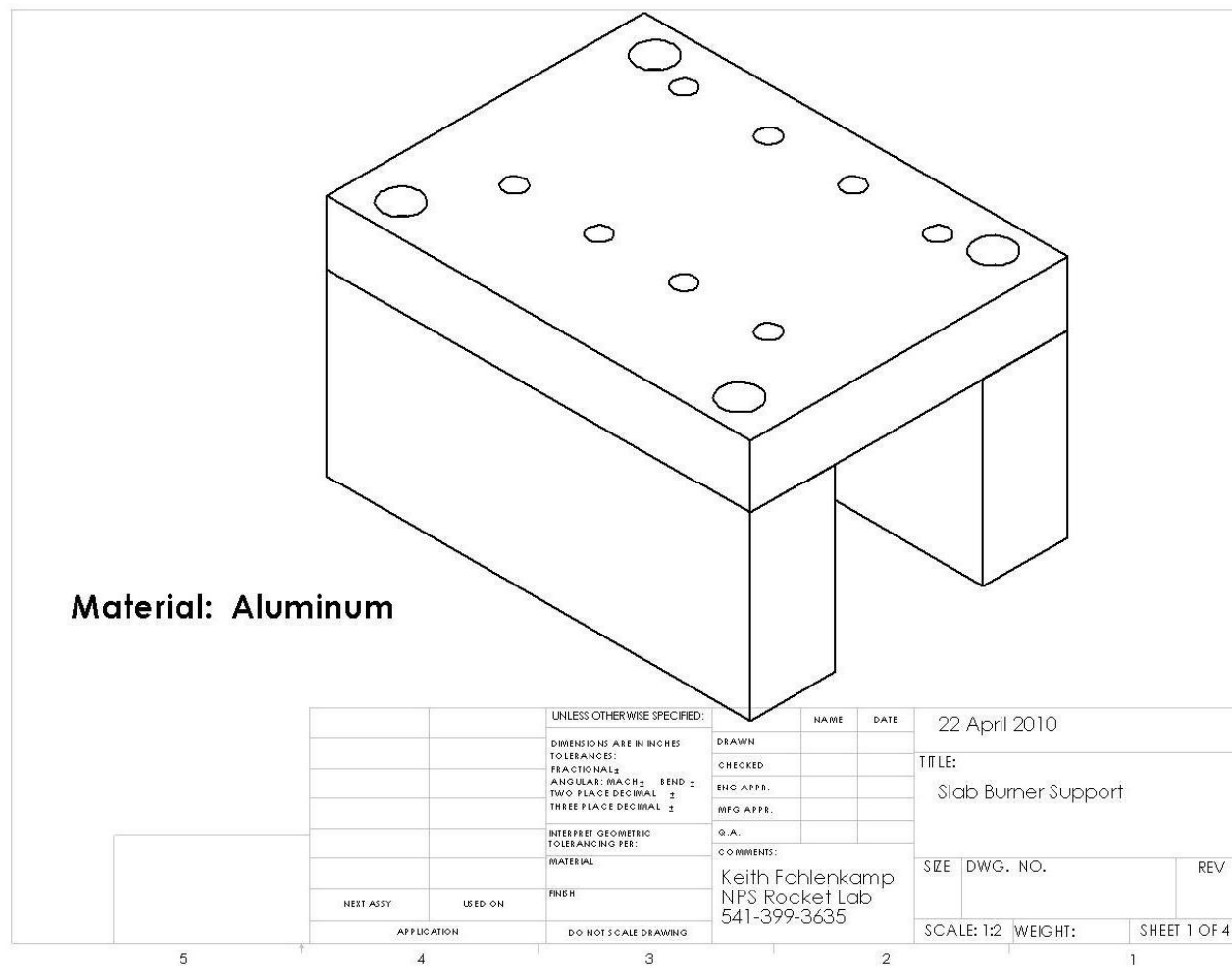


Figure 50. Slab Burner Support Sheet 1 of 4

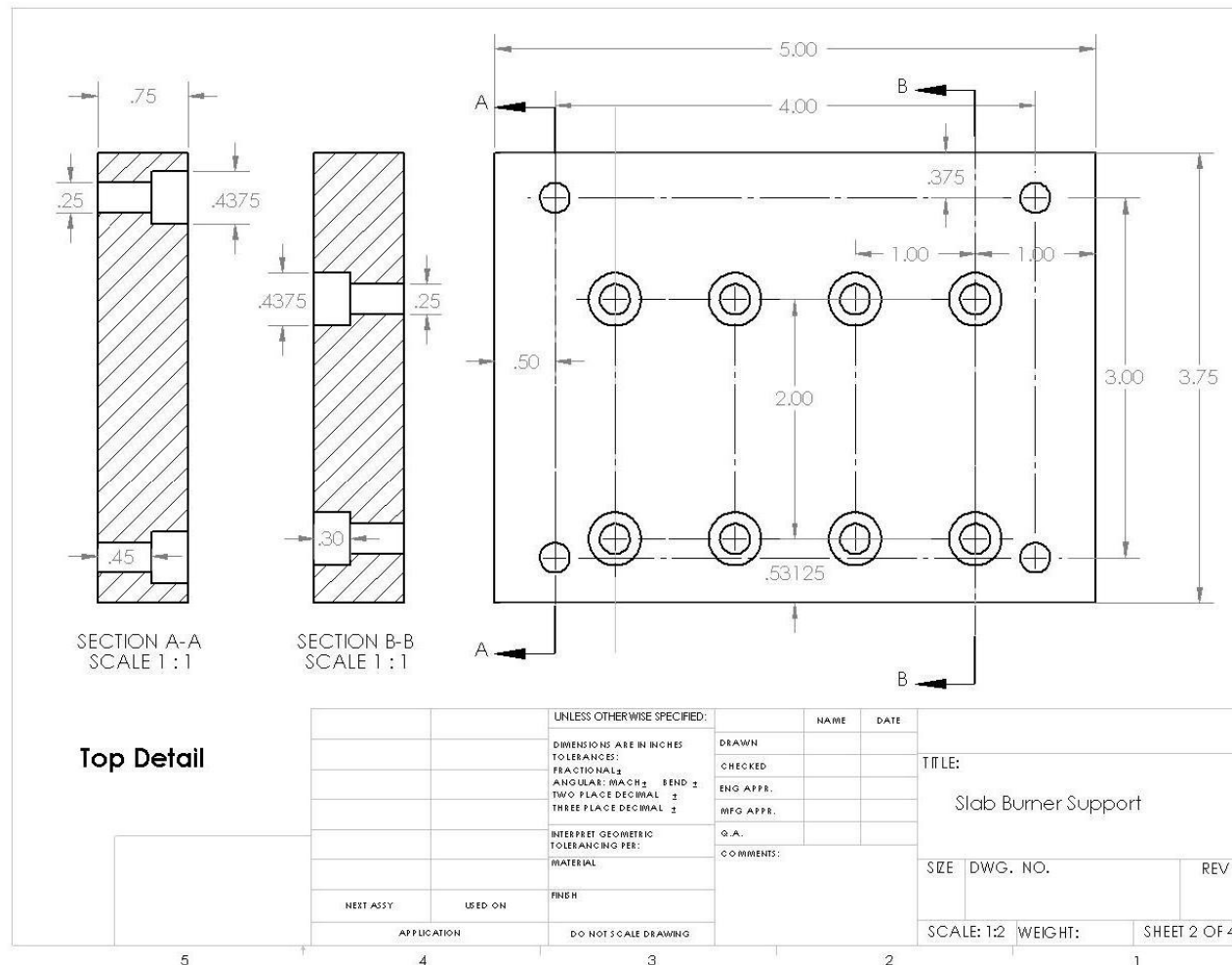


Figure 51. Slab Burner Support Sheet 2 of 4 (Top)

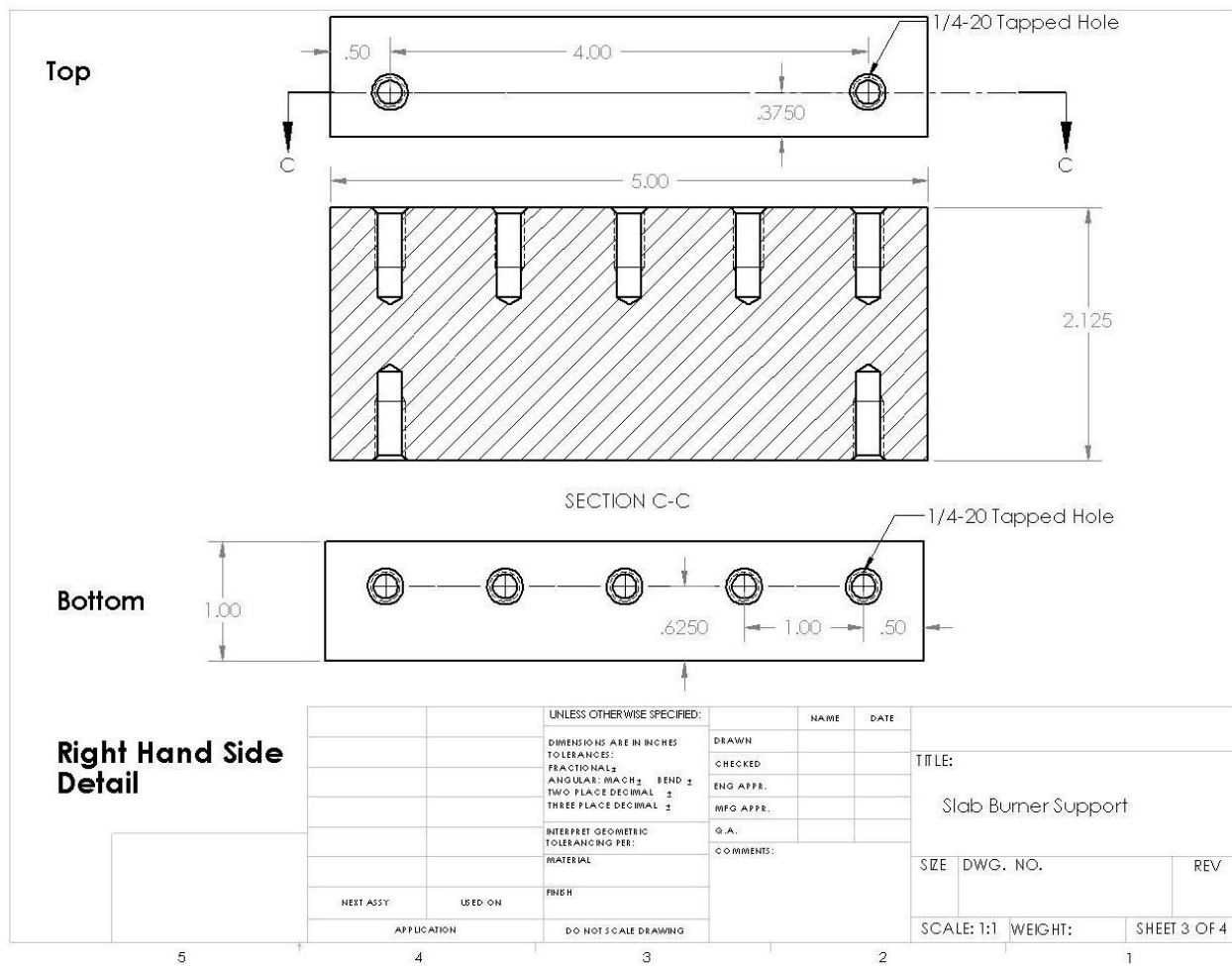


Figure 52. Slab Burner Support Sheet 3 of 4 (Right Leg)

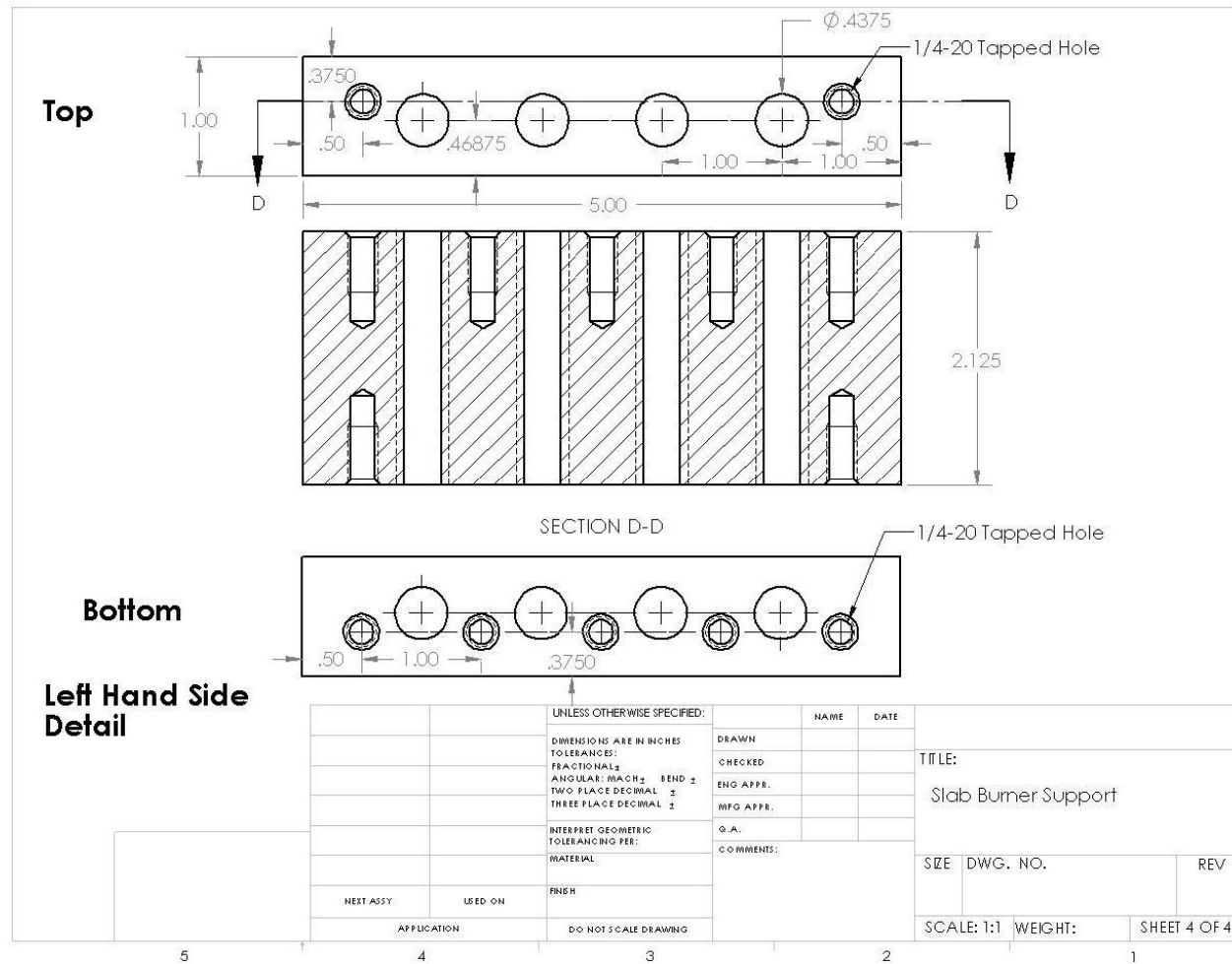


Figure 53. Slab Burner Support Sheet 4 of 4 (Left Leg)

THIS PAGE INTENTIONALLY LEFT BLANK

APPENDIX C: LABVIEW SOFTWARE CODE

A. ER 3000 CONTROL

1. Block Diagram

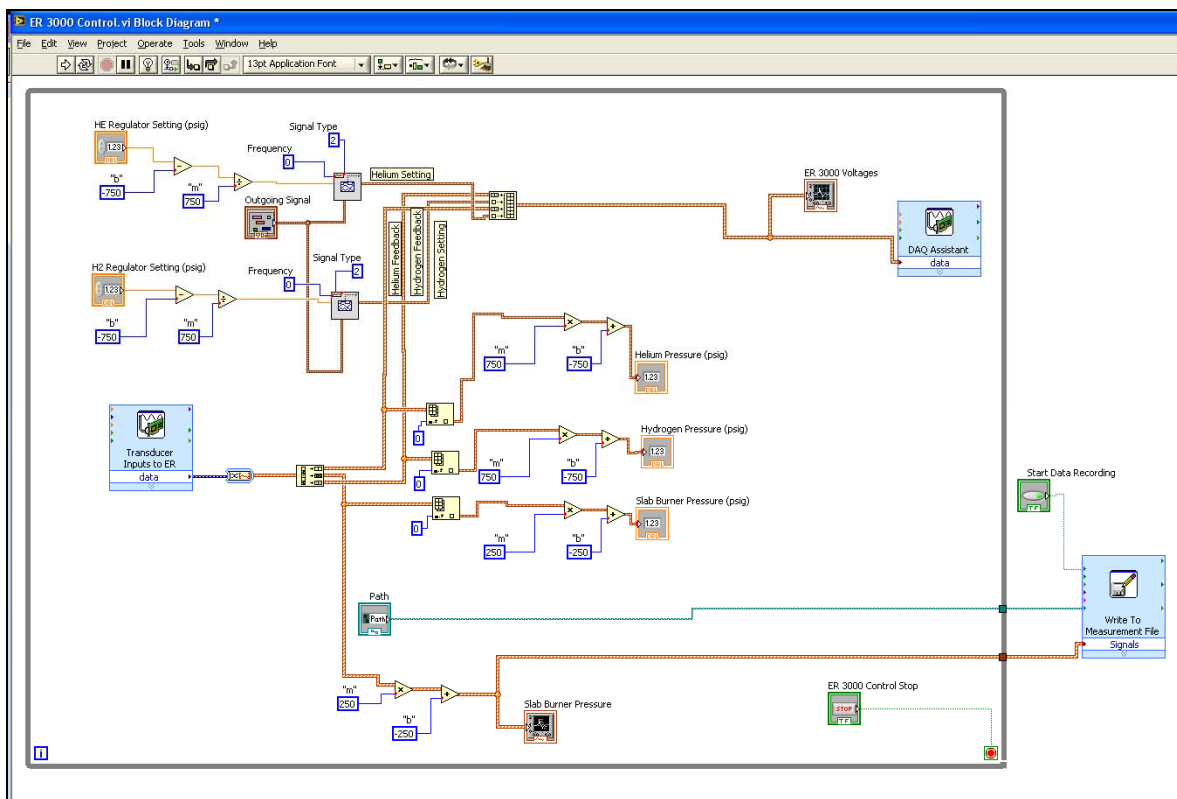


Figure 54. ER 3000 Control.vi Block Diagram

2. ER 3000 Control.vi Explanation

Data is gathered from three pressure transducers using an Input DAQ assistant. The pressure transducers send a signal ranging from 1 to 5 volts that linearly maps to a pressure range of 0 to 3000 psig for the hydrogen and nitrogen/helium transducers and 0 to 1000 psig for the slab burner transducer. All three signals are gathered by the same input DAQ using a national instruments PXI-6133 high speed data acquisition card. All three signals must be gathered by the same DAQ because the card has only one analog to digital converter and must use multiplexing to process each signal. The processed signals leave the DAQ in a single array, which has to be “decimated” into three separate arrays corresponding to the three individual signals.

The slab burner signal is mathematically converted from a voltage value into a pressure value and then fed into a waveform chart to display instantaneous pressure on the front panel. This signal is also written to file using a Write to File DAQ. The write begins when the Start Data Recording button is pressed. This feature needs improvement as it currently only records one buffer size of data. One buffer size is 100 samples. Since samples are taken at 10,000 Hz, the data recorded in the file only represents 0.01 seconds of the event.

In order to regulate the pressures using the TESCO ER 3000 regulators, both a setpoint value specified by the user and a feedback signal from the pressure transducers are required. The user input on the front panel, in psig, is mathematically converted into a voltage signal in the block diagram. Next, the two user input signals and the two transducer feedback signals are multiplexed back into a single array and fed into a Write DAQ assistant. It is essential that the order of the multiplexed signals entering the array is identical to the order of the signals specified within the Write DAQ assistant. The Write DAQ assistant sends two signals to the each ER 3000 pressure regulator through a National Instruments PXI-6722 card. The signals that are sent are also plotted on the front panel using a waveform graph.

After some trial and error, it was discovered that a sample frequency of 10,000 Hz and a buffer size of 100 samples worked well for ER 3000 control. Therefore all signals are processed at this speed. This includes the data collection and signal transmission described above as well as the user input signal generation.

B. VALVE CONTROL

1. Block Diagram

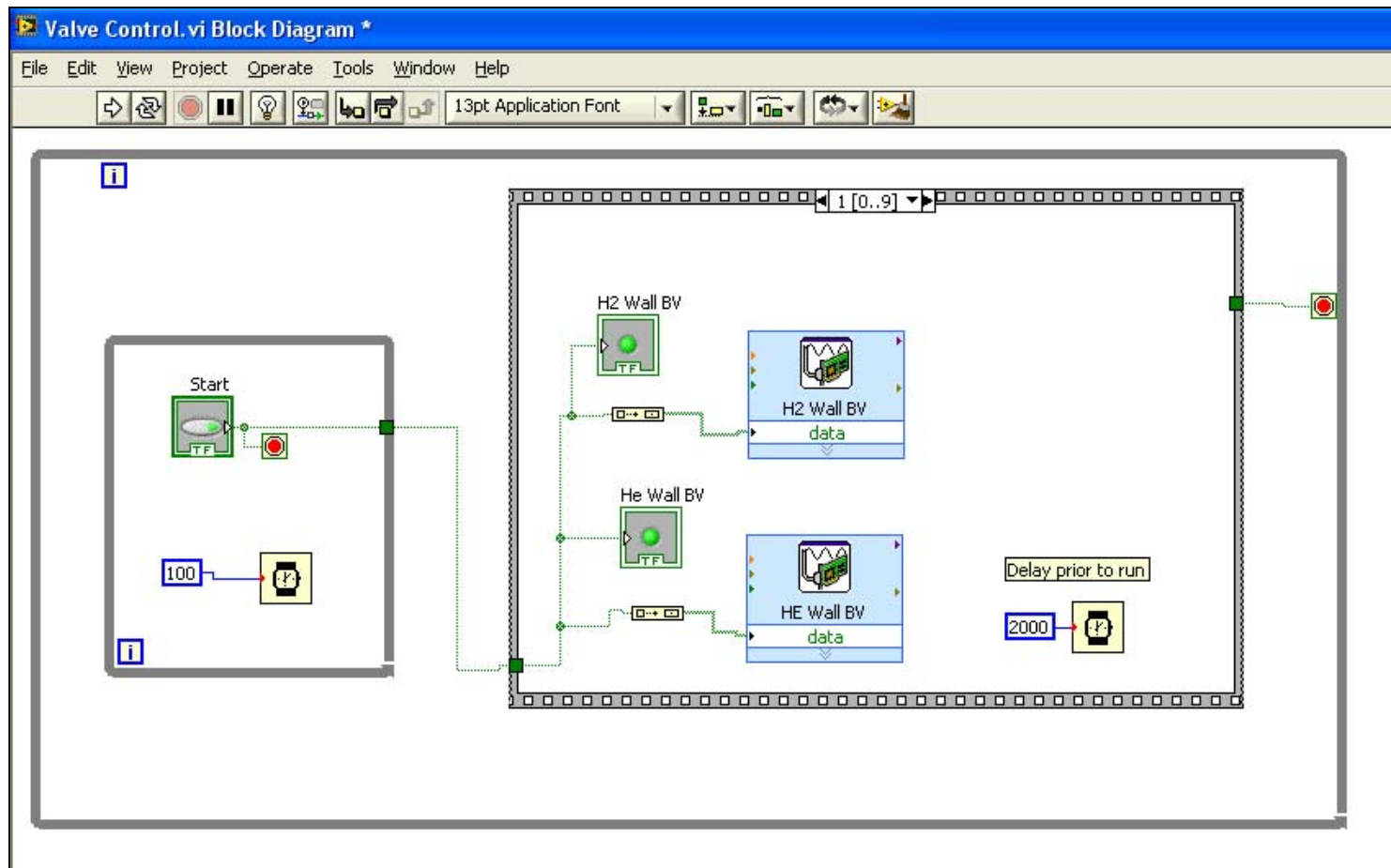


Figure 55. Valve Control.vi Block Diagram

2. Valve Control.vi Explanation

A total of six valves and the spark plug for ignition torch lightoff is controlled using the valve control vi. The national Instruments PXI-6509 card is used for all digital output signals to the valves. A sequence structure begins when the start button is pressed. After the start button is pressed there is a two-second delay. Next the ½ inch hydrogen and nitrogen/helium ball valves are opened and another two-second delay is used to ensure the regulators are able to properly pressurize the newly open pipeline. The ¼ inch ball valves are opened next followed by a one-second delay. The ¼ inch solenoid valves and the ignition torch are then simultaneously opened and lit off. User input from the front panel determines the ignition torch burn duration. The torch is secured by shutting the ¼ inch solenoid valves, then the ¼ inch ball valves are shut one second later, and finally the ½ inch ball valves are after one more second. The program automatically stops when the sequence is complete.

THIS PAGE INTENTIONALLY LEFT BLANK

APPENDIX D: TEST CELL PHOTOGRAPHS

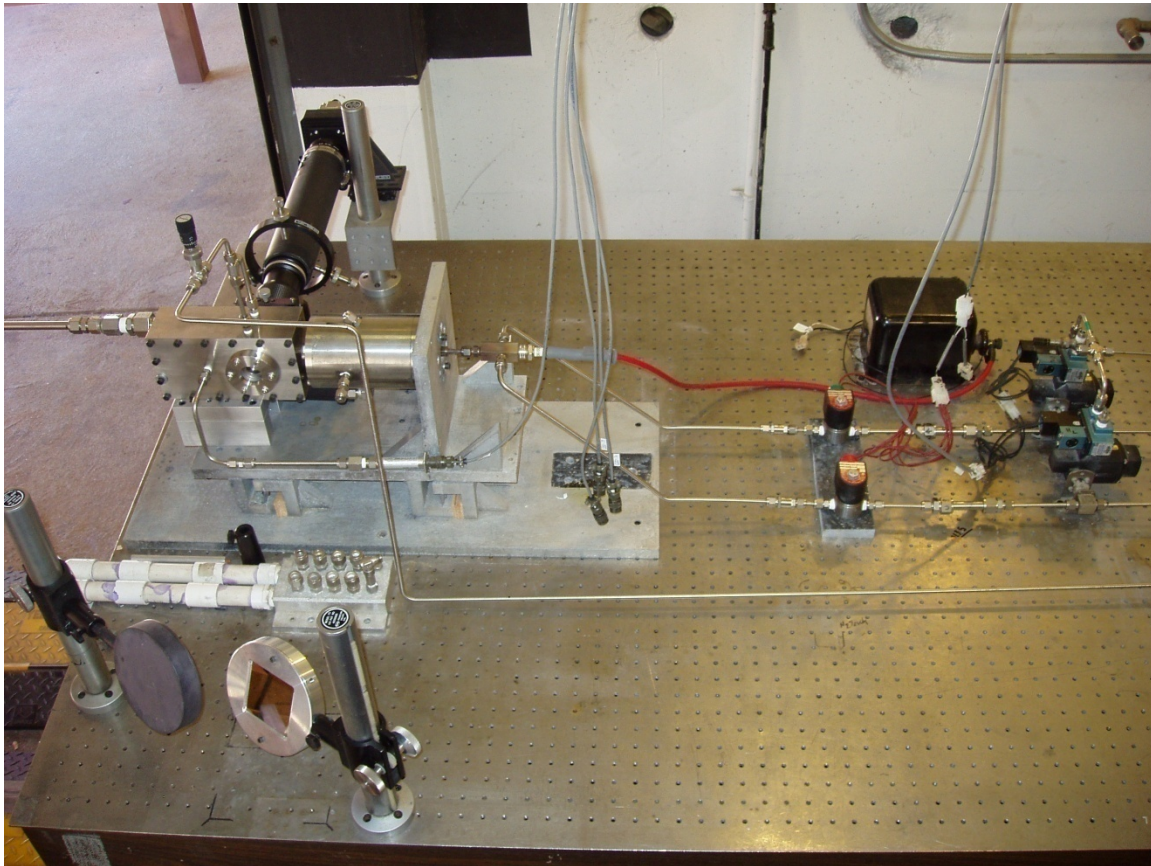


Figure 56. Experimental Setup



Figure 57. Oxford Copper Vapor Laser



Figure 58. National Instruments Control Cabinet

THIS PAGE INTENTIONALLY LEFT BLANK

LIST OF REFERENCES

- [1] G. Sutton and O. Biblarz, *Rocket Propulsion Elements*. Hoboken, NJ: John Wiley and Sons, 2001.
- [2] A. Bandera, F. Maggi and L. T. DeLuca, “Agglomeration of Aluminized Solid Rocket Propellants,” *AIAA Paper* 2009-5439, 45th AIAA/ASME/SAE/ASEE Joint Propulsion Conference & Exhibit, Denver, Colorado, 2–5 August 2009.
- [3] N. S. Cohen, “A Pocket Model for Aluminum Agglomeration in Composite Propellants,” *AIAA Paper* 1981-1585, 17th SAE and ASME Joint Propulsion Conference, Colorado Springs, CO, 27–29 July 1981.
- [4] Oleg B. Kovalev, “Motor and Plume Particle Size Prediction in Solid-Propellant Rocket Motors,” *Journal of Propulsion and Power*, vol. 18, no. 6, pp. 1199–1210, November–December 2002.
- [5] T. L. Jackson, F. Najjar and J. Buckmaster, “New Aluminum Agglomeration Models and Their Use in Solid Propellant-Rocket Simulation,” *Journal of Propulsion and Power*, vol. 21, no. 5, pp. 925–936, September–October 2005.
- [6] R. A. Reed and V. S. Calia, “Review of Aluminum Oxide Rocket Exhaust Particles,” *AIAA Paper* 92-2819, 28th Thermophysics Conference, Orlando, Florida, 6–9 July 1993.
- [7] C. J. Smithells, *Metal Reference Book* (5th ed.). London: Butterworth & Co., 1976.
- [8] C. R. DeSena, “Characterization of Initial Particle Size Distributions of Aluminized Composite Propellants,” M.S. thesis, Naval Postgraduate School, Monterey, California, December 2006.
- [9] AK Steel Corporation, “304/304L Stainless Steel Product Data Bulletin,” 2007.
- [10] A. C. Ugural and S. K. Fenster, *Advanced Strength and Applied Elasticity* (4th ed.). Upper Saddle, NJ: Prentice Hall PTR, 2003.
- [11] F. P. Incropera and D. P. DeWitt, *Introduction to Heat Transfer* (3rd ed.). John Hoboken, NJ: Wiley & Sons, 1996.
- [12] L. H. Caveny and A. Gany, “Breakup of Al/Al₂O₃ in accelerating flowfields,” *AIAA Paper* 1979–300, 17th Aerospace Sciences Meeting, New Orleans, LA, 15–17 January 1979.

THIS PAGE INTENTIONALLY LEFT BLANK

INITIAL DISTRIBUTION LIST

1. Defense Technical Information Center
Ft. Belvoir, VA
2. Dudley Knox Library
Naval Postgraduate School
Monterey, CA
3. Professor Christopher Brophy
Department of Mechanical and Aerospace Engineering
Monterey, CA
4. Professor Anthony Gannon
Department of Mechanical and Aerospace Engineering
Monterey, CA